REDOX REGULATION OF CYCLIC ELECTRON FLOW AROUND PHOTOSYSTEM I

By

Deserah Dawn Strand

A DISSERTATION

Submitted to
Michigan State University
in partial fulfillment of the requirements
for the degree of

Plant Biology—Doctor of Philosophy

2014

ABSTRACT

REDOX REGULATION OF CYCLIC ELECTRON FLOW AROUND PHOTOSYSTEM I

By

Deserah Dawn Strand

The proton coupled electron transfer of the light reactions of photosynthesis supply ATP and reducing power to metabolic processes within the chloroplast and, ultimately, the organism. The textbook pathway of electron transfer or 'Z-scheme' of photosynthesis supplies a fixed ratio of ATP and reducing power (i.e. reduced ferredoxin and NAD(P)H), however, the downstream metabolic demands require a highly dynamic ratio. This poses a problem when downstream metabolic demands lead to a deficit of ATP, a buildup of reducing equivalents may occur in the stroma, which may then lead to the buildup of reactive oxygen species (ROS). To balance the output of the light reactions, the chloroplast employs several mechanisms to either shunt electrons out of the system, or by redirecting electrons away from downstream metabolism and back into the plastoquinone pool to generate additional ATP in a process termed cyclic electron flow around photosystem I (CEF).

CEF has been proposed to be catalyzed by multiple pathways. In plants, this includes the antimycin A sensitive ferredoxin quinone reductase (FQR) and the respiratory Complex I analog, the NADPH dehydrogenase complex (NDH). We found these pathways are differentially regulated by redox status, with the FQR more active in a reducing environment (E_m = -306 mV), while the NDH is activated in response to ROS. We further found that the kinetics of activation for the two pathways were different, with the FQR rapidly activated (seconds to minutes) and the NDH activated more slowly

(minutes). Additionally, we have evidence that the NDH is a proton pumping plastoquinone reductase. This observation indicates the two pathways contribute different levels of *pmf* to offset an ATP deficit. We propose CEF pathways are differentially regulated in response to chloroplast redox state. The FQR is rapidly activated when reducing equivalents in the stroma accumulate in response to a short-term or rapidly fluctuating ATP deficit. When the FQR fails to restore homeostasis and the ATP deficit leads to ROS formation, the NDH complex is activated as a more robust mechanism of *pmf* generation via CEF.

This dissertation is dedicated to Dr. Virginia Lee, a truly inspiring person.

ACKNOWLEDGEMENTS

I've received much academic and personal support over the course of my graduate career. I would like to thank the entirety of the Kramer lab, both at Michigan State University and Washington State University, for their unending willingness to help me through whatever I needed from them. My advisor, Dr. David Kramer, has been an amazing source of knowledge and inspiration. I have been challenged almost everyday working with the Kramer lab. I'd also like to specifically thank Dr. Jeffrey Cruz for the hours of technical (and oftentimes emotional) support he has given me. Robert Zegarac has been an enormous help by providing his technical expertise. Dr. Kaori Kohzuma was an excellent resource and the best office mate I could have asked for. Dr. Nicholas Fisher has been both inspiring and insightful throughout his time at MSU. Dr. Sean Weiss has also been very helpful and encouraging in many aspects of my more difficult projects. Dr. Ben Lucker and Chris Hall were more than willing to help me figure out how to grow and experiment on Chlamydomonas, and while none of this work made it into this dissertation, they have been of valuable assistance along the way.

In addition to Chris Hall, I've had the great opportunity to work with an excellent group of students at both MSU and WSU. At MSU, L. Ruby Carrillo has been a great sounding board for ideas and an overall joy to work with. I hope we have the opportunity to continue to work together in the future. A recent addition to the Kramer lab, Geoff Davis, has also been wonderful to work with. At WSU, Dr. Stefanie Tietz and Amelia Barhanovich helped me get through the transition to, not only graduate school, but also to a new state, and Dr. Aaron Livingston helped me (smoothly) transition into the chaos of the Kramer lab. Dr. Elisabeth Ostendorf was an

excellent roommate and friend, first as a visiting student at WSU, and currently as a post-doc at MSU.

I would also like to thank all the undergraduate research assistants I had the chance to work with throughout the years. Ben Wolf, Brendan Johnson, and Heather Enlow were particularly amazing to work with. I couldn't have done so much without them.

I would also like to thank Dr. Dale Vogelien, at Kennesaw State University, for the excellent experiences as an undergraduate that led me to trying for a career in plant research. I learned so much from, and was inspired everyday, working with her. Also at KSU, I am very grateful for the opportunities to work with Dale Zaborowski, Dr. Marina Koether and Dr. Thomas McElroy. I believe that these early experiences helped shape me as a scientist. Finally, I would like to thank my friends and family for their ongoing support in everything I do. Ariel Smith (now Rosshirt), has always been there to talk to, whether I was frustrated or homesick. My parents have been of constant support throughout my years at MSU and I am very grateful for this. I would also like to thank my brother, Jason, for being entirely positive and encouraging.

TABLE OF CONTENTS

LIST OF FIGURES

Chapter 1

Control of non-photochemical exciton quenching by the proton circuit of photosynthesis[1]

Deserah D. Strand and David M. Kramer

[1] This chapter is modified from Strand, D.D., and Kramer, D.M. (2014) Control of Non-Photochemical Quenching by the Proton Circuit of Photosynthesis. *In* Advances in Photosynthesis and Respiration, Vol. 40, Non-Photochemical Quenching and Energy Dissipation in Plants, Algae and Cyanobacteria Demmig-Adams, B., Garab, G., Adams III, W., Govindjee (*Eds*) Springer Netherlands DOI:10.1007/978-94-017-9032-1 ISBN 978-94-017-9031-4

1.1 Abstract

This review discusses our current understanding of the chloroplast proton circuit, i.e. those reactions that involve the storage and utilization of light energy in the transfer of protons, and its importance for regulating photosynthetic light-capture/electron-transfer reactions. The photosynthetic machinery of plants is finely tuned to balance the needs for efficient light capture with an avoidance of photodamage by regulating the capture of light energy, via thermal dissipation of excess excitation energy (assessed from non-photochemical quenching, NPQ, of chlorophyll *a* fluorescence) by regulating light-driven electron transfer processes. In addition to driving ATP synthesis at the chloroplast ATP synthase, the thylakoid electrochemical gradient of protons or proton-motive force (*pmf*) plays a central role in regulating NPQ. The transthylakoid proton concentration gradient (ΔpH) component of *pmf* triggers the "energy-dependent", or q_E component of NPQ, which protects photosystem II from photodamage and regulates electron transfer through the cytochrome b_6f complex, thereby preventing damage to photosystem I. The extent and mode of storage in ΔpH and Δψ of *pmf* are regulated by several processes that respond to the metabolic, or physiological, state of the organism. The extent of *pmf* is determined by proton influx (via linear and alternative electron flows) into the thylakoid lumen, and proton efflux through the chloroplast ATP synthase. Both processes are modulated by, or responsive to, environmental conditions and resulting metabolic fluctuations. Proton influx is controlled by linear electron flow and a series of alternative electron flow pathways, possibly including cyclic electron flow around photosystem I, the Mehler peroxidase reaction (or water-water cycle), and oxidation of plastoquinol by the plastid terminal oxidase. The fraction of *pmf* stored as ΔpH is also regulated by plastidic ionic strength or luminal buffering capacity, altering the sensitivity of

pH-dependent processes to *pmf*. The integrated regulation of these processes is an open, active area of research.

1.2 Introduction

Sunlight, harnessed in photosynthesis, is the energy source for most life on our planet. Energy from absorbed sunlight presents a challenge for photosynthetic organisms because within the light reactions of photosynthesis, highly reactive redox intermediates are formed that can generate harmful reactive oxygen species (ROS). Thus, plants must regulate photosynthetic light harvesting and electron transfer to avoid photodamage, especially when light input exceeds the capacity of photosynthesis to safely process it (1). To meet this need, essentially every process in photosynthesis is regulated to balance minimization of deleterious side reactions with the need for efficient capture of solar energy (2, 3). This regulation is critical for efficient energy conversion, since most of the energy captured by an ecosystem is lost within the light reactions of photosynthesis, much of it dissipated in photoprotective processes, the level of which can be estimated from the non-photochemical quenching (NPQ) of chlorophyll *a* fluorescence (4–7). This is a critical point: even though the rate-limiting steps in photosynthesis occur in biochemical processes that follow the initial storage of energy by the light reactions, these limitations inevitably result in the loss of energy by one of two mechanisms: backup of electrons and protons resulting in long-lived excitation states (and potential ROS formation), or activation of processes that "dump" or dissipate energy in excess of that needed to sustain the downstream processes. As discussed below, the former mechanism can result in the buildup of deleterious intermediates while the second prevents their generation, but, if not tightly regulated, could lead to excessive energy loss.

Over developmental time scales, this regulation can occur by altering such processes as gene expression, protein accumulation, and the synthesis of pigments and antioxidants (3, 8). However, plants must also respond to rapid fluctuations in environmental conditions such as light and temperature, requiring equally rapid regulation at the level of the photosynthetic machinery itself (1, 9).

One of the major mechanisms for this regulation is NPQ of antenna excitation energy, a key component of which, q_E ("energy dependent" quenching), is triggered by acidification of the thylakoid lumen caused by the transthylakoid proton concentration gradient, or ΔpH component of thylakoid proton-motive force (*pmf*) (9, 10). The *pmf* is generated by the light-induced electron transfer reactions and, in turn, drives photophosphorylation of ADP to ATP. In this paper, we review our understanding of how the process of activating q_E is intimately integrated into the entire energy storage system to balance energy capture and storage.

1.2.A The electron and proton circuits of photosynthesis

The light reactions of oxygenic photosynthesis consist of two highly integrated energy-storing circuits. The "electron circuit" stores energy through a series of light-driven electron transfer reactions, via the linear electron flow (LEF) pathway (Figure 1.1) (3). Light energy is captured by pigments in light-harvesting complexes and shunted to a special subset of chlorophylls in photosystem I (PS I) and photosystem II (PS II) (11–13). The photochemically excited chlorophylls in PS II extract electrons from water and transfer them through an electron transfer chain, reducing plastoquinone (PQ) to plastoquinol (PQH_2), then to the cytochrome b_6f complex (b_6f), plastocyanin, and finally to PS I. An additional photon of light energy is

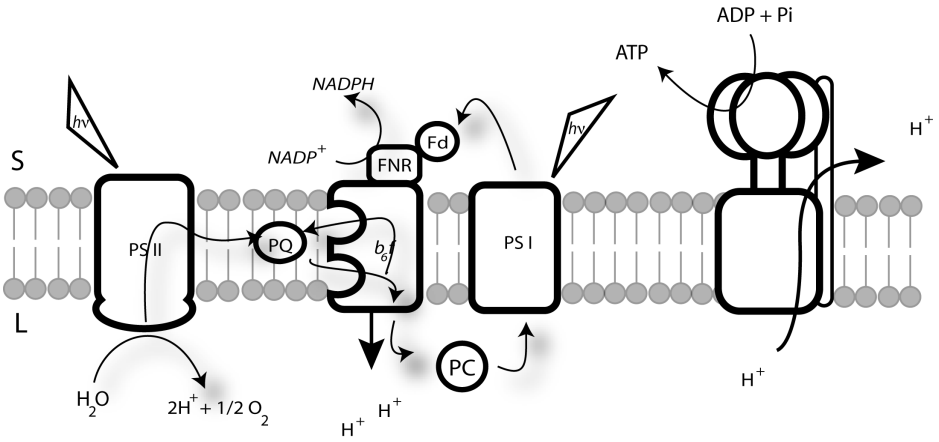

Figure 1.1 The light-dependent electron and proton transfer reactions of photosynthesis. Electrons are extracted from water and passed through an electron transport chain. Protons are translocated into the lumen generating a *pmf* to drive ATP synthesis. Stroma (S), Lumen (L), Photosystem I (PS I), Photosystem II (PS II), Plastoquinone (PQ), Ferredoxin-$NADP^+$ reductase (FNR), Ferredoxin (Fd), Plastocyanin (PC), the cytochrome b_6f complex (b_6f).

introduced at PS I, driving electron transfer to ferredoxin (Fd) and $NADP^+$, which are then used to drive reductive processes in the cell.

The "proton circuit" is energetically and mechanistically coupled to the electron circuit to store energy in an electrochemical gradient of protons between the stroma and thylakoid lumen across the thylakoid membrane, or *pmf*, which drives the synthesis of ATP through the ATP synthase that spans the thylakoid membrane. Protons are released into the thylakoid lumen during water oxidation at PS II. Additional protons are translocated via the Q-cycle, an enzymatic redox loop catalyzed by the b_6f complex and related complexes involving the oxidation and reduction of plastoquinones and subsequent electron and proton transfer reactions that results in proton translocation across the thylakoid membrane (14, 15).

1.2.B The proton circuit is a central regulator of photosynthesis

When light absorption exceeds the capacity of the downstream reactions of photosynthesis, reactive intermediates may accumulate potentially leading to photoinhibition and photodamage, although the relationship between reactive intermediates and photoinhibition is still controversial [reviewed in (16)]. Plants have multiple mechanisms of avoidance and dissipation of excess light, including activation of processes underlying NPQ, changes in leaf orientation, chloroplast movement, rearrangement of the photosynthetic machinery, and changes in photosynthetic gene expression (8, 17–19).

This chapter focuses on how the activation of a process reflected in NPQ and other processes that regulate light capture and electron flow interact with the proton circuit of photosynthesis. We concentrate mainly on these processes in higher plants and, where appropriate, in algae. The case of cyanobacteria is not covered here because, in these organisms, NPQ is controlled by factors not directly related to *pmf* (20, 21).

Much of the dynamic regulation of photosynthesis directly involves the thylakoid proton circuit, which modulates light capture, photoprotection, and electron transfer allowing the light reactions to respond to changes in the physiology of the organism. Chloroplasts are thought to protect themselves from photodamage by dissipating excess light energy, as reflected in NPQ (1, 22). The major, rapidly reversible component of NPQ in plants is termed q_E (for energy-dependent quenching), and is triggered by the ΔpH component of *pmf*, which acidifies the lumen, thereby activating violaxanthin deepoxidase, catalyzing the conversion of violaxanthin to antheraxanthin and zeaxanthin (23), and protonating the antenna-associated protein PsbS (10, 22, 24).

Photosynthetic electron flow is regulated at the b_6f complex by acidification of the lumen. As a result of the buildup of the ΔpH component of *pmf,* plastoquinol oxidation is slowed at the Q_o site (quinol oxidation) (25, 26). This prevents accumulation of electrons on highly reducing components of the acceptor side of PS I, which can lead to generation of reactive oxygen species (ROS) and/or affect redox regulation of metabolism.

In extreme cases, lumen acidification can sensitize PS II to light-induced destabilization (27, 28). There is evidence that this can occur *in vivo* under low CO_2 or environmental stresses, such as drought (26). This is often called photoinhibition. Because it produces inactive PS II, which quenches excitation energy and decreases electron transfer, photoinhibition may represent a regulatory “tactical retreat" to prevent overexcitation and damage to DNA or other cellular components (29–31).

The proton circuit is, in turn, modulated by secondary regulatory mechanisms, particularly at the ATP synthase, allowing the light reactions to respond to changes in the

physiology of the organism. The activity of the ATP synthase is downregulated to retard proton efflux from the thylakoid lumen, increasing *pmf* and leading to down-regulation of light capture by q_E and regulation of electron transfer reactions at the b_6f complex (9, 25, 32–35). The fraction of *pmf* stored as ΔpH and electric field (Δψ) affects the relationship between *pmf* and lumen acidification, further adjusting the pH-dependent responses underlying NPQ (33, 36). In addition, the responses of q_E to lumen pH can be modulated by altering the expression of q_E-related proteins (10, 37, 38).

These "flexibility mechanisms", which may adjust *pmf*-dependent NPQ responses to physiological and metabolic changes, fall into two categories (2, 25). "Type I" mechanisms adjust the "q_E response" (defined as the activation state of q_E as a function of LEF) by altering light-driven proton-transfer reactions via activation of alternative cyclic electron transfer processes and, because proton efflux from the lumen is generally coupled to ATP synthesis, affect the ratio of ATP/NADPH arising from photosynthetic electron transport. "Type II" flexibility mechanisms, on the other hand, adjust the q_E response without altering the ATP/NADPH balance. The distinction between Type I and Type II mechanisms is critical because, despite both having an effect on q_E, they have very different consequences for downstream metabolism, i.e., the requirement for the ATP/NADPH ratio to precisely match that required by downstream reactions may pose substantial constraints on the activation of Type I mechanisms.

1.3 Type I flexibility mechanisms: NPQ and balancing of the chloroplast energy budget

Proton and electron transfer reactions in photosynthetic complexes are tightly coupled and consumption of photosynthetic products must thus match production to prevent buildup of

reactive intermediates (2, 3, 39). The ratio of ATP/NADPH from LEF is thought to be fixed at 1.3, approximately 13% less than the 1.5 required for the Calvin-Benson-Bassham (CBB) cycle and other metabolic processes in the chloroplast [reviewed in (2)]. The ATP and NADPH consumption within the chloroplast is also dynamic and dependent on the activation of multiple processes and thus requires rapidly adjustable plasticity in the relative output of ATP and NADPH. At least five processes have been proposed to remedy a deficit of ATP in the chloroplast (2, 3, 40, 41), as discussed in the following sections.

1.3.A Malate valve

The "malate valve" (Figure 1.2) (41) involves shuttling of reducing equivalents from the chloroplast to other cellular compartments. NADP-malic enzyme (MDH) uses NADPH to reduce oxaloacetate to malate. The malate can then be exported from the chloroplast to the mitochondria to generate ATP from respiration. In this process, ATP production is maintained while NADPH is only transiently reduced, allowing it to help balance the chloroplast ATP/NADPH ratio. MDH is inhibited by $NADP^+$, suggesting a control mechanism involving NADPH levels, which would be consistent with an involvement in balancing production of ATP and NADPH in the chloroplast. On the other hand, it has been argued that the activity of the malate valve is too low to account for substantial ATP/NADPH rebalancing under permissive conditions, i.e., conditions like those in the laboratory, where loss of productivity to environmental stress is minimal (42, 43), although there is also evidence that malate valve activity is increased under prolonged stress where the ratio of ATP/NADPH consumption may be higher (41). Supporting this evidence, Hebbelman et al. (44) found upregulation of antioxidant pathways in mutants lacking MDH when exposed to high light, suggesting that the malate valve may play expanded roles under non-laboratory conditions.

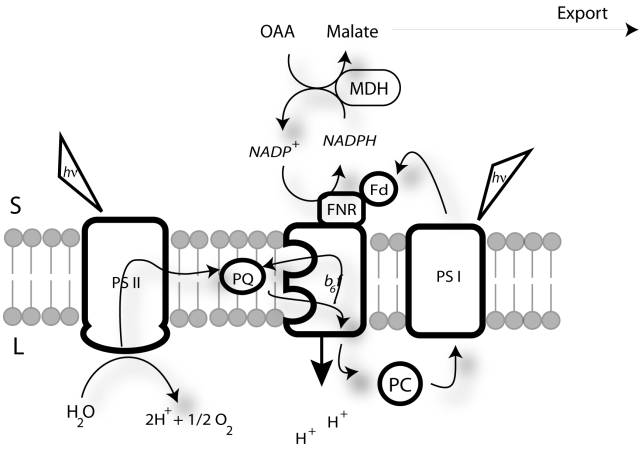

Figure 1.2 The malate valve. NADPH is consumed in the production of malate from oxaloacetate (OAA) via NADP-malate dehydrogenase (MDH). The malate is then exported from the chloroplast.

1.3.B Mehler peroxidase reaction (MPR)

In the MPR, also referred to as the water-water cycle (Figure 1.3), electrons from LEF are shunted away from $NADP^+$ reduction and instead reduce O_2 to superoxide at PS I (45–47). Superoxide is then dismutated to H_2O_2 and O_2 via superoxide dismutase and then H_2O_2 is reduced to H_2O via ascorbate peroxidase. This leads to production of ATP via LEF-coupled accumulation of protons in the thylakoid lumen, without net reduction of $NADP^+$ (48). The MPR appears to contribute significantly to ATP synthesis and photoprotection in cyanobacteria and bryophytes, but appears to have limited *in vivo* capacity in vascular plants and algae under permissive steady state conditions (42, 49–54). It has been reported that MPR may have an important role during activation of photosynthesis to prevent over-reduction of the electron transport chain under excess light (46, 55, 56).

1.3.C Plastid terminal oxidase (PTOX)

Chloroplasts also contain an alternate oxidase (PTOX) that oxidizes PQH_2 and reduces O_2 to H_2O (Figure 1.4) (57). Electron flow from PS II through PTOX could generate ATP from proton accumulation at PS II; however, its capacity would be limited by the fact that only one proton is expected to be deposited into the lumen per electron transferred from PS II through PTOX. In vascular plants, PTOX is important in developing plastids (58) and some alpine plants (59, 60), although its contribution to ATP/NADPH balance in steady-state photosynthesis in most species is probably small (2, 3). It has recently been proposed that PTOX works in conjunction with the chloroplast NADPH:plastoquinone oxidoreductase (NDH, see below) to

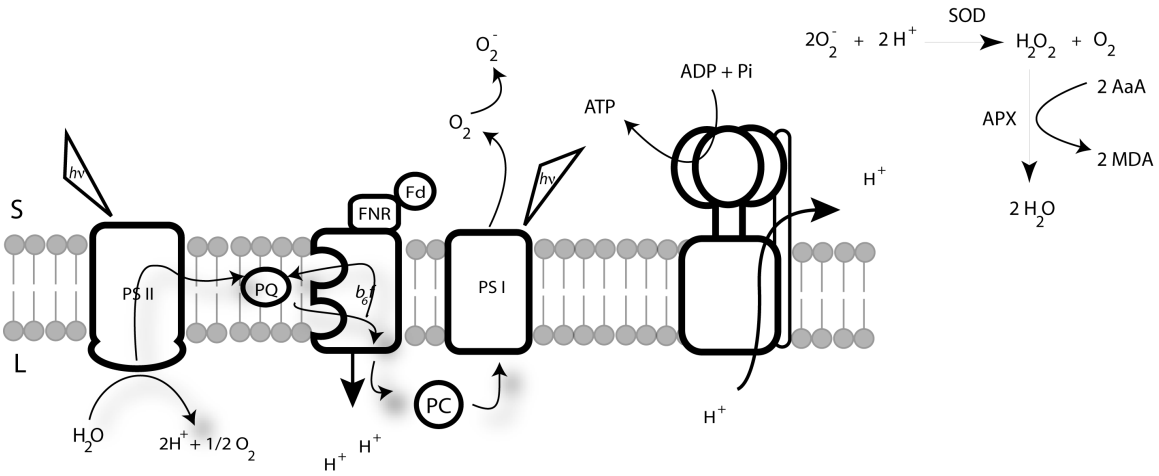

Figure 1.3 The Mehler peroxidase reaction. Electrons from PS I reduce O_2 to superoxide (O_2^-), which is dismutated to H_2O_2 via superoxide dismutase (SOD), and then reduced to H_2O and O_2 via ascorbate peroxidase (APX), oxidizing ascorbate, or ascorbic acid (AsA), to monodehydroascorbate (MDA).

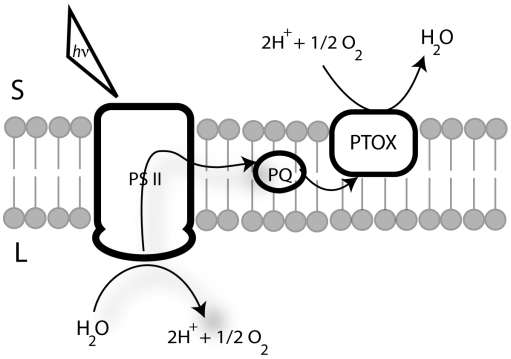

Figure 1.4 The plastid terminal oxidase (PTOX). Electrons from PS II reduce plastoquinone (PQ), which is then oxidized via PTOX, bypassing the Q-cycle. Proton translocation into the lumen is only possible via the plastoquinone reductases (PS II in this figure).

tune the redox state of the photosynthetic electron transport chain, and possibly acts as an electron sink under high-light conditions in tomato (60, 61).

1.3.D Exchange of ATP and ADP+P_i between the stroma and cytosol

The ATP budget could also be balanced by direct exchange of ATP and ADP + inorganic phosphate (P_i) among chloroplast, cytosol, and mitochondria. Early suggestions that chloroplasts directly exchange ATP and ADP+P_i with the cytosol were questioned by observations of slow ATP and ADP exchange in isolated chloroplasts (62, 63), leading to the generally accepted view that the chloroplast ATP budget is "self-contained". However, this has not been rigorously tested under physiologically relevant conditions, opening up the possibility that ATP and ADP+P_i exchange may, in fact, be sufficiently rapid to allow highly flexible energy balancing.

1.3.E Cyclic electron flow (CEF) around PS I

CEF is strongly implicated in the ATP/NADPH balance (2, 3, 64–66). CEF involves photochemistry in PS I, but not PS II, resulting in oxidation of plastocyanin and reduction of Fd. Electrons from PS I are transferred back into the PQ pool in a ferredoxin-dependent process involving a plastoquinone reductase (PQR). Following its formation by PQR, PQH_2 is oxidized by the b_6f complex via the Q-cycle (14, 15), resulting in proton translocation into the thylakoid lumen that generates *pmf*. This *pmf* is then used to drive ATP synthesis. The electrons are passed back to PS I via plastocyanin. This process results in ATP formation, with no net NADPH production, altering the ATP/NADPH stoichiometry formed by the light reactions.

CEF appears to be minimally activated under non-stressed conditions in C_3 plants, when LEF nearly meets the ATP required for chloroplast metabolism (9, 35, 67–70). However, CEF is upregulated when high ATP demand is greater, e.g., under environmental stress (52, 59, 71, 72), when carbon-concentrating mechanisms or C_4 photosynthesis are engaged (73, 74), or during

induction of photosynthesis when dark-adapted plants are suddenly exposed to light (75, 76). CEF may also play a regulatory role via acidification of the thylakoid lumen (25, 66, 77). These ATP/NADPH balancing and regulatory roles for CEF are not independent, since ATP/NADPH balance is critical for maintaining *pmf*, and thereby regulating q_E or electron flux through the b_6f complex. However, CEF is clearly not essential for q_E since q_E can be observed in the absence of CEF (35), when other processes, including the regulation of the ATP synthase and partitioning of *pmf* into ΔpH and Δψ components, can account for regulation of q_E responses (25, 32, 33, 78).

Several labs have isolated mutants, in *Arabidopsis* and tobacco, exhibiting high rates of CEF (*hcef*). Characterization of these mutants has established that CEF can run at high rates even in C_3 plants, but must also be highly regulated in the wild type to prevent over-acidification of the thylakoid lumen. The high rates of CEF in *hcef* mutants has allowed more facile probing of key CEF processes to explore its regulation and biochemical pathways. The genetic loci of some of these *hcef* mutants have been identified (69, 79), yielding hints about the mechanism and regulation of this process.

One high CEF plant (*hcef1*) was found with a mutation in the CBB cycle enzyme fructose-1,6-bisphosphatase (69). Despite similar effects on overall photosynthesis, suppressing the expression of glyceraldehyde phosphate dehydrogenase (70) and fructose bisphosphate aldolase (79) led to increased CEF, while suppression of others enzymes, including Rubisco small subunit (70), ATP synthase, and the Rieske protein of the b_6f complex (80), or the triose-phosphate/phosphate translocator (81), did not lead to an apparent increase in CEF. These contrasting effects suggest that CEF, as discussed in more detail below, may be regulated by specific intermediates or byproducts, rather than simply by slowing overall photosynthesis.

1.3.E.1 CEF pathways

The pathway(s) and regulatory mechanisms of CEF are currently the subject of debate. The identity of the PQR is as yet unresolved and several protein complexes have been proposed, but have yet to be fully characterized. Several putative PQRs, and many additional associated proteins have been proposed (Figure 1.5), such as Proton Gradient Regulation 5 (PGR5) and the PGR5-Like protein (PGRL1) (82, 83). Some of these are plant-specific, such as the NADPH dehydrogenase complex (NDH) (84, 85) or algae-specific, such as type II (non-proton pumping) NADH:plastoquinone oxidoreductase, NDA2 (86). It should be noted that these pathways are not necessarily mutually exclusive, and may either operate in parallel (87–90) or differentially under specific conditions (79, 91, 92).

1.3.E.1.A Chloroplast NDH pathway

One proposed route of CEF is through the thylakoid NAD(P)H dehydrogenase complex (NDH) (84, 85). The NDH complex is highly conserved in cyanobacteria and green plants across all phyla (93). The ~550 kDa (84) plant complex consists of >24 subunits, 11 of which are chloroplast encoded (94) and are (with a few notable exceptions) highly homologous to mitochondrial and bacterial respiratory Complex I (85). The identification of novel plant-specific NDH-associated proteins suggests that the plastid NDH has diverged in structure and regulation from Complex I and cyanobacterial NDH-1 (94, 95). Complex I contains an integral membrane hydrophobic arm with at least 3 proton channels (85); the genes coding for these channels are conserved in NDH (94, 96).

In Complex I, proton pumping is attributed to conformational changes in conserved lysine and glutamate residues that are also conserved in chloroplast NDH (96–98). The specific and generally high level of conservation of the NDH complex in vascular plants suggests that the

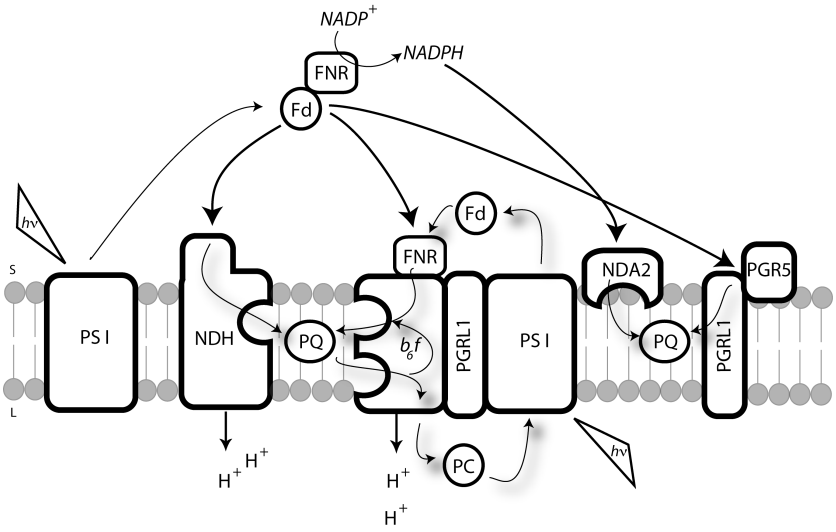

Figure 1.5 Proposed routes of cyclic electron flow around photosystem I. 1) The thylakoid NAD(P)H dehydrogenase complex (NDH). 2) A PS I-b_6f supercomplex. 3) A Type II (non-proton pumping) NAD(P)H dehydrogenase complex (NDA2). 4) A ferredoxin plastoquinone reductase thought to be comprised of a complex containing PGRL1 and PGR5.

same mechanism operates in plant chloroplasts. The occurrence of proton pumping in NDH would make CEF a very efficient ATP-generating process and imply an important role for the NDH complex in maintaining the thylakoid ATP budget.

In support of involvement of NDH in CEF, the *hcef1* mutant shows constitutively high CEF that requires the NDH complex (but not PGR5, which is involved in an alternative pathway; see below). These results suggest that NDH can catalyze high rates of CEF, at least under certain conditions (69). Direct participation of NDH in photosynthesis is further supported by a report that NDH is activated by formation of a supercomplex with PS I, implying a direct participation in photosynthesis rather than a function in non-photosynthetic plastids (95).

Because chloroplast NDH levels are relatively low (NDH:PS I ~1:20) (95), it is not clear whether this enzyme is able to catalyze high rates of CEF under all conditions. However, NDH subunits accumulated at much higher levels under environmental stresses (99–101) and in *hcef1* (69). Increased expression is also seen in C_4 bundle-sheath chloroplasts, where the required ratio of ATP/NADPH is higher (91). It has also been observed that CEF and NDH activity increase *in vitro* and *in vivo* upon exposure to H_2O_2, which is expected to increase during environmental stress (99, 102–104) (discussed further in Chapter 3). Thus, NDH may be activated, both by increased expression and at the enzyme level, to catalyze CEF that is highly efficient in ATP synthesis under environmental stresses. On the other hand, it is almost certain that other CEF pathways operate in other systems and under different environmental conditions, as discussed in the following sections.

1.3.E.1.B Supercomplex pathways

While *Chlamydomonas reinhardtii* lacks genes for chloroplast NDH (105), a CEF competent supercomplex comprised of PS I, LHCI, LHCII, the b_6f complex, ferredoxin $NADP^+$

reductase (FNR), and PGRL1 has been isolated (92). In *C. reinhardtii*, it has been observed that CEF activation correlates with an antenna state transition to PS I (106). State transitions modulate partitioning of photosynthetic antenna complexes between PS I and PS II (39). State 1 is induced when PS I is preferentially excited, resulting in the continued association of LHCII with PS II, and under these conditions LEF is operating (107). When light conditions favor PS II, the redox state of the PQ pool activates phosphorylation of LHCII by the STT7/STN7 kinase and LHCII associates with PS I in state 2 (108). It is under these state 2 conditions that the supercomplex was isolated (92). Similar supercomplex formation has been suggested to facilitate CEF in higher plants (3, 109), but has not been fully characterized. In addition, NDH is proposed to require formation of a supercomplex with PS I (95).

Overall, it appears that rearrangement of thylakoid protein complexes into super-complexes associated with processes like state transitions may regulate CEF and other photosynthetic functions. It may therefore be important that *C. reinhardtii* appears to have a much larger capacity for state transitions than higher plants: up to 80% vs ~15% (39, 108), respectively, consistent with the reported higher capacity for CEF in *C. reinhardtii*.

The specific electron-transfer pathway for supercomplex CEF is not known, although it has been proposed that heme c_i of the b_6f complex may act as a conduit for electrons from the stroma to the plastoquinone reductase (Q_i) site (110). It is also intriguing that the CEF supercomplex shows relatively high rates of electron transfer from the b_6f complex to P700 despite the fact that the experiments were performed in isolated complexes with plastocyanin concentrations much lower than those expected in thylakoids (92). The channeling of electron transfer by close association in super-complexes could be important for controlling the fraction

of electrons sent into LEF or CEF, as discussed in Breyton et al. (111), Peng et al. (95), and Johnson (65).

1.3.E.1.C The ferredoxin-plastoquinone reductase (FQR) pathways

CEF has also been proposed to be facilitated by an antimycin A-sensitive PQR termed ferredoxin:quinone reductase (FQR) (112). While its identity has yet to be fully elucidated, this complex has been proposed to be a complex comprised of PGRL1 and PGR5 (82, 83, 113).

Shikanai and coworkers (82, 87) identified a mutant (*pgr5*) lacking the ability to maintain *pmf*-dependent NPQ and deficient in the small membrane-associated protein PGR5. This mutant was determined to be lacking the ability to perform FQR-mediated PQ reduction, based on *in vitro* reduction assay kinetics similar to antimycin A inhibition. Avenson et al. (35) calculated that the PGR5 pathways could contribute up to 13% of proton flux *in vivo* under steady-state conditions in *A. thaliana*. However, they also showed that many of the phenotypes associated with *pgr5* can be attributed, not to CEF, but to effects on ATP-synthase activity, calling into question the physiological importance of PGR5-catalyzed CEF. Similarly, Aro and coworkers (114) have presented evidence that the main function of PGR5 is in the regulation of PS I redox state, perhaps via effects on ATP synthase, and PGR5 is not involved in CEF.

Work on the *hcef1* mutant likewise implied that PGR5 is dispensable for CEF (69). The *hcef1 pgr5* double mutant retained the same elevated rates of CEF as *hcef1*, implying that, at least in this high CEF mutant, PGR5 is not needed. In contrast, elevated CEF was completely lost in the *hcef1 crr2-2* double mutant that lacks NDH (69), implying that NDH is required for elevated CEF, either directly as a PQ reductase or indirectly via regulatory or developmental effects. Elevated CEF in tobacco plants with anti-sense-suppressed glyceraldehyde phosphate dehydrogenase (*gapR*) showed no sensitivity to antimycin A, an inhibitor of the FQR pathway

(70). This is in agreement with the proposed role of PGR5 in regulation of LEF but not CEF (114). Similar observations were made with another high CEF mutant, *fba3-1* deficient in fructose-1,6-bisphosphate aldolase (79). In this mutant, however, it has been proposed that the PGR5-dependent pathway may compensate for the absence of NDH. Overall, these results do not support PGR5 as the primary route of CEF, but rather suggest multiple roles for PGR5 in maintaining photosynthetic processes (92).

In addition to its proposed role in the *C. reinhardtii* super-complex, PGRL1 has recently been suggested to act as a PQR (113). PGRL1 is an integral thylakoid-membrane protein (83) that associates with PGR5 and PS I in higher plants, and associates with the CEF supercomplex in *C. reinhardtii* (92). Loss of PGRL1 leads to a decrease in Fd-dependent dark PQ reduction as assayed by chlorophyll *a* fluorescence, similar to the loss seen in PGR5 (82). Identification of conserved cysteine residues, binding of a metal cofactor, and the ability of recombinant PGRL1 to reduce dimethyl-*p*-benzoquinone (DMBQ) (dependent on the presence of PGR5) suggests that PGRL1 is a quinone reductase (113). However, some caution with regard to this interpretation is warranted. Inhibition of the observed FQR activity, performed with artificial quinones, required antimycin A concentrations 3 orders of magnitude higher than are effective in thylakoids (82, 112, 115).

1.3.E.1.D NDA2 pathway

For *C. reinhardtii*, it has been proposed that CEF is catalyzed by a type II NADH:plastoquinone oxidoreductase, termed NDA2, related to those found in bacteria, fungi, plants, and protists (86). NADH, which is reduced during metabolism but not directly by PS I, appears to be the preferred substrate for NDA2, suggesting a primary role in metabolism-related PQ reduction (i.e., not directly related to the light-driven CEF) (86). Consistent with this role,

NDA2 appears to be important for redox poising of the plastoquinone pool (116) and hydrogen production under sulfur deficiency (117), i.e., functionalities not directly associated with CEF. However, NDA2 also shows partial (10%) activity with NADPH (86), perhaps allowing it to operate in CEF, although a contribution to photosynthetic ATP production has yet to be demonstrated.

1.3.E.2 Regulation of CEF

Several signals for CEF regulation have been proposed, including CBB cycle intermediates, state transitions, ATP/ADP ratios, NADPH or Fd redox states, and/or ROS (68, 70, 99, 102, 103, 106, 109, 111). Given the numerous pathways that may be involved, it is likely that multiple regulatory processes are employed, and each pathway may have different signals for activation. This is thus an active area of research, albeit with little resolution to date. A few important advances are discussed in the following.

Livingston et al. (70) assayed major photosynthetic metabolites from mutants affected in photosynthesis with elevated (*hcef1* and *gapR*) and unchanged (anti-sense Rubisco small subunit tobacco mutant; *ssuR*) CEF, respectively. None of the metabolites measured (fructose-6-phosphate, dihydroxyacetone phosphate, fructose bisphosphate, phosphoglycerate, ribulose-5-phosphate, glucose-5-phosphate, phosphoenolpyruvate) correlated with the activation of CEF, indicating that these metabolites are unlikely to be simple regulators of CEF.

It has been proposed that CEF in *C. reinhardtii* is regulated by state transitions (discussed above). The transition to state 2 has been shown to correlate with activation of CEF in algal systems under specific conditions (92, 106). It has been shown, however, that state 2 is not absolutely required for CEF in *C. reinhardtii* (118) and more recent work has shown that CEF

can proceed in the absence of state transitions, leading to suggestions that redox status, and not phosphorylation state, controls CEF (119, 120).

Consistent with a role in balancing the chloroplast's energy budget, it has been suggested that ATP/ADP or NADPH/$NADP^+$ ratios can regulate CEF (109). CEF has been proposed to be activated during photosynthetic induction, thus increasing ATP supply when this supply is limiting the CBB cycle (64, 109). However, this conclusion is not consistent with previous spectroscopic findings (121). Furthermore, metabolic profiling of *hcef* mutants showed no significant differences in ATP/ADP or NADPH/$NADP^+$ ratios in wild type versus mutant lines with elevated CEF (70), suggesting that regulation of CEF may instead involve ROS.

ROS have been implicated in a number of signaling processes, such as growth and environmental stress response (122–124). The *hcef1* mutant accumulates significantly higher levels of H_2O_2 compared to wild-type *A. thaliana* (104) (Chapter 3). With the discovery of the role of H_2O_2 in the activation of the NDH complex by phosphorylation (102), CEF was established as a target of ROS. Indeed, infiltration with H_2O_2 also leads to increased CEF, the level of which correlates with the concentration of H_2O_2 (104) (discussed in Chapter 3). However, H_2O_2 has also been shown to inhibit several steps in the CBB cycle, knockdown/knockout mutants of which show an *hcef* phenotype (70, 125). CEF in the *hcef1* and *gapR* mutants is independent of the antimycin A-sensitive pathway (69, 70). In *hcef1*, and possibly also in *gapR*, ROS accumulation, or another signal downstream of CBB cycle inactivation, may lead to phosphorylation and activation of NDH. Therefore, it is possible that FQR or other paths of CEF are also regulated by additional factors independent of ROS.

1.4 Type II flexibility mechanisms: regulation of *pmf* partitioning and ATP synthase activity and the consequences for NPQ

While Type I flexibility mechanisms alter the ATP/NADPH ratio available for downstream metabolism, Type II mechanisms alter *pmf* without changing this ratio. Included in the latter category is regulation of the ATP synthase and changes in *pmf* partitioning between ΔpH and $\Delta\psi$. Downregulation of the ATP synthase increases *pmf*, and subsequently the q_E response, while alterations in *pmf* partitioning may alter q_E response to total *pmf*.

1.4.A The chloroplast ATP synthase is a central regulator of photosynthesis

The enzymatic activity of the chloroplast ATP synthase is rapidly modulated in response to metabolic or physiological conditions, allowing it to regulate both the light reactions, via effects on the proton circuit, and the assimilatory reactions, via effects on chloroplast ATP and P_i levels (25, 34). Under low CO_2, environmental stresses, and feedback-limiting conditions at high CO_2, ATP synthase activity is rapidly and reversibly downregulated, slowing proton efflux from the lumen (32, 34). The resulting buildup of *pmf* activates downregulation of the antennae via processes underlying q_E, and slows electron transfer at the b_6f complex, thus downregulating the light reactions (25).

Because many of the assimilatory enzymes of photosynthesis are controlled by stromal ATP, ADP, and P_i levels, changes in the activity of the ATP synthase should act to co-regulate or coordinate the light and assimilatory reactions (126). Decreasing ATP synthase activity should result in decreased ATP and increased ADP and P_i, regulating assimilatory and metabolic reactions.

Several possible mechanisms can be proposed for metabolism related ATP synthase regulation. It has been well documented that chloroplast ATP synthase is regulated by redox modulation of γ-subunit thiols (127). Recently, Kohzuma et al. (128) further tested this hypothesis by modifying the conserved acidic residues on the γ-subunit. This manipulation modified the redox potential of the thiols, but the mutant complex still maintained wild-type responses to metabolic limitations. Thus, redox switching and metabolic regulation of ATP synthases have different mechanisms and physiological roles. Redox regulation appears to act as a sensitive on-off switch, activating ATP synthase even in very low light (129, 130), possibly to prevent "wasteful" ATP hydrolysis in the dark (131).

In one possible model for metabolic regulation of ATP synthase, the availability of stromal P_i can be drawn down to below its K_M at the ATP synthase, e.g., under limiting internal CO_2 (32) or under feedback limitation resulting from accumulation of photosynthetic products under high CO_2 levels (132, 133). In agreement with these models, Takizawa et al. (126) found that lowering P_i levels decreases the activity of ATP synthase, leading to downregulation of photosynthesis. It has also been observed that downregulation of the ATP synthase occurs at high CO_2 levels, when P_i availability is thought to limit photosynthesis (134). These results are consistent with, but do not establish, a direct causal relationship between P_i levels and ATP synthase activity.

It has also been proposed that ATP synthase can be regulated by phosphorylation and subsequent binding of a 14-3-3 protein (135, 136). Although the phosphorylation state of the ATP synthase appears to change in response to light exposure of dark-adapted plants (137), no measurements of phosphorylation in response to metabolic status have been reported. The 14-3-

3-protein family is known to interact with enzymes involved in chloroplast metabolism (138), but a direct role in phosphorylation of the ATP synthase has yet to be shown, and 14-3-3 proteins may be nonspecific.

1.4.B Regulation of *pmf* partitioning

Chemiosmotic coupling can be driven by *pmf* via either of its two components, proton diffusion potential, ΔpH, and transthylakoid electric field, Δψ. Early work on isolated thylakoids suggested that the contribution of Δψ to thylakoid *pmf* was low, but more recent work showed that Δψ can make significant contributions to *pmf* (139). Although the two components of *pmf* are thermodynamically equivalent, they have very different consequences for the regulation of photosynthesis (25). Buildup of the ΔpH component decreases the pH of the thylakoid lumen, activating q_E and slowing electron transfer at the b_6f complex (26). Modulation of the fraction of ΔpH and Δψ to total *pmf* can change the sensitivity of q_E to the *pmf*, and thus act as an additional level of photoprotective regulation at limiting CO_2, elevated temperatures, or other environmental stresses (26, 33, 37, 140). While the mechanism of this modulation partitioning is currently not understood, it is clear that several factors determine the storage of Δψ, i.e., membrane capacitance, ionic strength, and buffering capacity of the lumen (139). It is unlikely that thylakoid membrane capacitance would change sufficiently rapidly to account for the observed changes in Δψ/ΔpH. On the other hand, ion channels in the plasma membrane, chloroplast inner envelope and thylakoid membranes can control ion movements across the thylakoid. In the absence of counter-ion movement across the membrane, we would expect the buffering capacity of the lumen to maintain a higher fraction of ΔpH than Δψ (Figure 1.6*A*). Active ion channels for Mg^{2+}, Ca^{2+}, Cl^-, and K^+ have been confirmed to occur in thylakoids

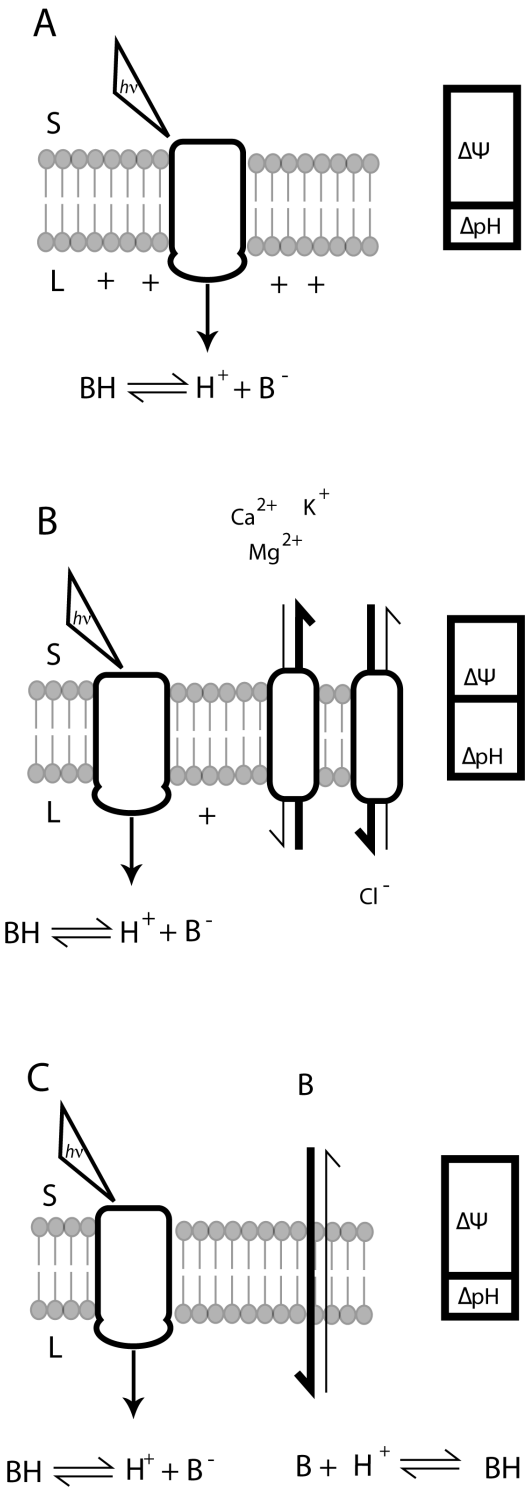

Figure 1.6 Proposed mechanisms of changes in *pmf* partitioning.

Figure 1.6 (Cont'd) A) In the absence of counter ion movement, $\Delta\psi$ should predominate. B) Counter ion movement (i.e. lumenal cation efflux/anion influx) would allow increased ΔpH. C) A membrane permeable weak base would increase the buffering capacity of the lumen, collapsing the ΔpH. Inspired by Nicholls and Ferguson (141).

(142–144), and Cruz et al. (139) proposed the regulation of chloroplast ion balance as the major mechanism of adjusting $\Delta pH/\Delta\psi$ (Figure 1.6*B*). In accord with this proposal, a gated K^+ channel was found to be required for maintaining ΔpH in cyanobacteria (145, 146). Consistent with the view that *pmf* partitioning is controlled by ion movements, it was recently found that disruption of a thylakoid K^+ channel in plants resulted in higher partitioning of *pmf* into $\Delta\psi$, with consequences for the regulation of photosynthesis by the proton circuit (147).

An additional regulatory mechanism was proposed by Ioannidis et al. (148) who showed that putrescine, a polyamine acting as a weak base and involved in plant stress responses, can regulate $\Delta\psi/\Delta pH$ by modulating the effective proton buffering capacity of the lumen. This work supports a "biological weak base" model (Figure 1.6*C*), in which molecules like polyamines may allow for rapid modulation of *pmf* partitioning.

1.5 Concluding remarks

The proton circuit plays a central role in governing the responses of processes underlying NPQ, predominantly by activating the q_E response, but also by governing the rate of electron transfer through the b_6f complex and thus modulating the PQ-pool redox state. The proton circuit also provides a very flexible means by, which metabolic or physiological states of the chloroplast influence NPQ responses, e.g., via regulating CEF or ATP synthase. It is obvious that, although we are beginning to delineate the interacting processes, a large number of important questions remain open.

One way to assess whether our understanding of the proton circuit and its influence on NPQ is complete, and to identify additional important open questions, is to compare physiological responses with numerical simulations. There have been several attempts to model

pmf and the q_E response to *pmf* (26, 139, 149). These models are based on broad simplifications, but show qualitatively reasonable *pmf* and responses that reflect the general trends seen *in vivo*. The recent model of Zaks et al. (149) is noteworthy in that it incorporates several possible regulatory mechanisms for q_E, and provides a solid framework for future inclusions of more complex processes. However, these models also highlight the fact that we know little about several regulatory mechanisms, especially CEF and *pmf* partitioning that are clearly important for balancing the proton circuit (150).

1.6 Acknowledgements

We would like to thank Dr. Jeffrey Cruz and Dr. Nick Fisher for helpful discussions. The authors are funded by Grant DE-FG02-11ER16220 from the Division of Chemical Sciences, Geosciences, and Biosciences, Office of Basic Energy Sciences of the US Department of Energy.

Chapter 2

Redox regulation of the antimycin A sensitive pathway of cyclic electron flow around photosystem I in higher plant thylakoids

Deserah D. Strand, Nicholas Fisher, Geoffry A. Davis, L. Ruby Carrillo, and David M. Kramer

2.1 Abstract

The chloroplast must rapidly regulate supply of reducing equivalents and ATP to meet downstream metabolic demands. Cyclic electron flow around photosystem I (CEF) is proposed to help balance the ATP/NADPH budget by using reducing equivalents to drive plastoquinone reduction, leading to the generation of proton motive force and subsequent ATP synthesis. While high rates of CEF have been observed *in vivo*, isolated thylakoids show only very slow rates, suggesting that the activity of a key complex is lost or down-regulated upon isolation. We performed a systematic investigation to discover the factors responsible for this loss of activity. We show that isolation of thylakloids while in the continuous presence of thiol reductant dithiothreitol (DTT) maintains high CEF activity through the ferredoxin-dependent antimycin A-sensitive pathway. Maintaining low concentrations (~2 mM) of reduced DTT while modulating the concentration of oxidized DTT leads to reversible activation/inactivation of CEF with an apparent midpoint potential of –306 mV and n = 2, consistent with redox modulation of a thiol/disulphide couple.

We propose the 2 most widely studied routes of CEF in plants, the FQR and NDH, are both regulated by redox status of the chloroplast, but have different roles in energy balance. In our model, FQR is activated under reducing conditions as a 'first response' and the NDH activated later when the FQR fails to restore balance and ROS (and likely an oxidizing conditions) is produced.

2.2 Introduction

The light reactions provide the ATP and reducing equivalents required for metabolic processes within the chloroplast. Most photosynthetic energy is stored by the linear electron flow (LEF) pathway, which involves activation of both photosystem II (PS II) and photosystem I (PS

I). Excitation of photosystem II (PS II) with photons results in the oxidation of water at the oxygen evolving complex and the reduction of plastoquinone to plastoquinol (PQ/PQH_2). PQH_2 is oxidized at the Q_o (quinol oxidation) site of the cytochrome b_6f complex (b_6f) in which one electron is passed to plastocyanin in the lumen, and the other electron participates in the Q-cycle, reducing a PQ bound at the Q_i (plastoquinone reductase) site. Light energy is also captured by the photosystem I (PS I) reaction center, resulting in oxidation of PC and reduction of ferredoxin (Fd), which is used as a donor for downstream metabolism, including reduction of $NADP^+$ to NADPH. Proton deposition into the lumen is coupled to electron transfer reactions during water oxidation and the Q-cycle, establishing an electrochemical gradient of protons, or proton motive force (*pmf*) across the thylakoids. The *pmf* is, in turn, used by the ATP synthase to drive the photophosphorylation of ADP to ATP. LEF in its unmodified form should provide a fixed stoichiometry of reducing equivalents (i.e. reduced FD, NADPH) and ATP, therefore any changes in the metabolic demands of the chloroplast must be met by rapid changes in alternative electron flow to prevent formation of reactive intermediates (2, 3, 78). Multiple alternative electron pathways have been identified including the water-water cycle (44, 45), the malate shunt (41), the plastid terminal oxidase (59, 61, 151), and cyclic electron flow around photosystem I (CEF) (112).

CEF can alleviate an ATP deficit by passing electrons from the acceptor side of PS I back to PQ, driving the translocation of protons into the lumen without net reduction of NADP+. The mechanism and role of CEF is intensely debated, partly because it is difficult to measure, and partly because multiple proposed pathways may participate under different species and under different conditions [see review in (2)]. Proposed pathways of CEF, in higher plants, include the

multi-subunit type I NADPH dehydrogenase complex (NDH) which is homologous to respiratory Complex I (84, 85), the PGR5-PGRL1 dependent antimycin A-sensitive Fd dependent quinone reductase (FQR) (82, 112, 113), and PQ reduction through the Q_i site of the b_6f complex (110). In algae, CEF involves the formation of a b_6f-PSI supercomplex (92), and/or the FQR related PGR5 (152, 153) and PGRL1 (92, 154), or NDA2, a type II NADPH dehydrogenase (86).

The regulation of CEF is also enigmatic, with multiple mechanisms proposed that may impact different pathways , including ROS, state transitions, chloroplast redox state, ATP/ADP, and NADPH/$NADP^+$ (64, 70, 76, 92, 99, 102, 106, 111, 154, 155). Past work linking CEF activation to antenna state transitions in Chlamydomonas has recently been challenged (120, 155).

A possible clue to the open questions surrounding CEF is that, while high rates of CEF are readily measured *in vivo* (69, 70, 72, 79) (Chapters 3 and 4), this activity is severely diminished in thylakoid preparations, suggesting that the a key component of the process is lost or down-regulated upon isolation. We thus aimed in this work to systematically explore the relationship between thylakoid *in vitro* conditions and CEF activity, revealing redox requirements that may be involved in the regulation of CEF *in vivo*.

2.3 Results

2.3.A Effect of reductant on CEF activity *in vitro*

Freshly isolated thylakoids were assayed for their ability to generate a light driven proton gradient (Figure 2.1). Assays were repeated under two conditions, one in the presence of methyl viologen, allowing exclusively LEF, and the other in the presence of presence of NADPH and Fd

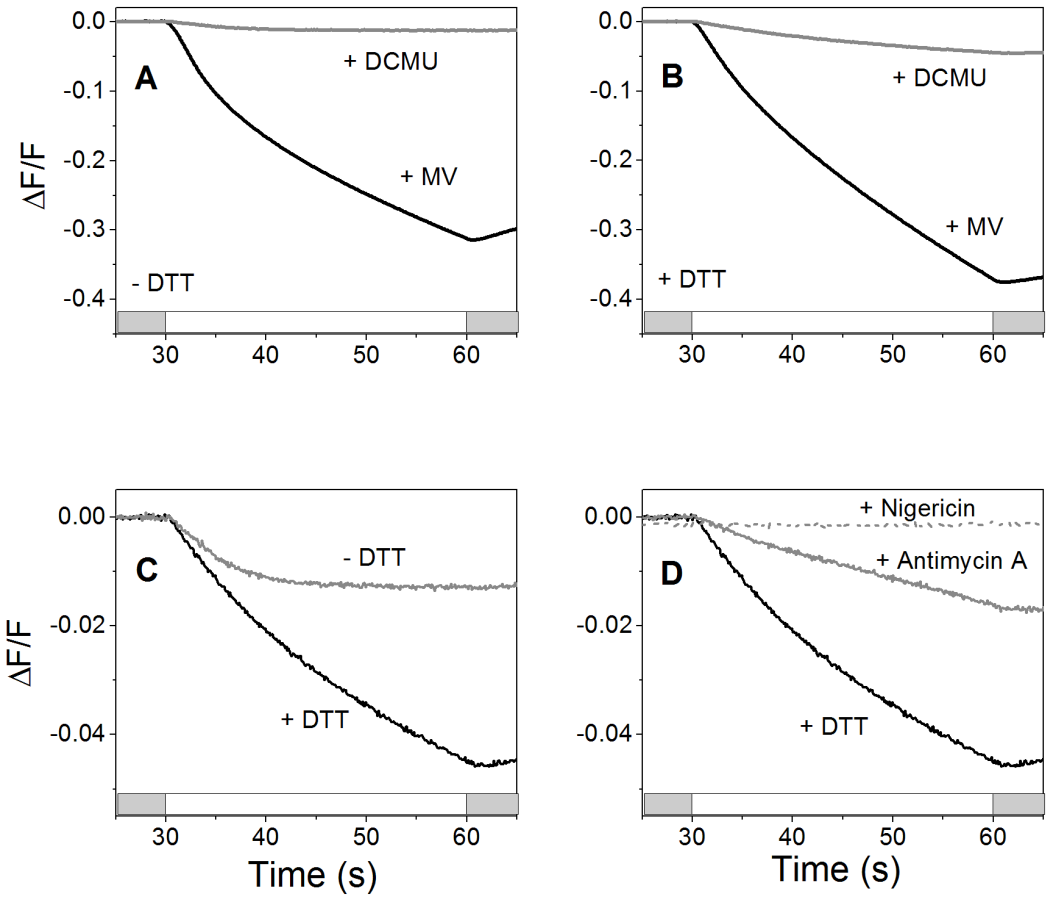

Figure 2.1 Light induced formation of *pmf* monitored by acridine fluorescence quenching upon illumination with 200 μmol photons m^{-2} s^{-1} photosynthetically active radiation. A) Linear electron flow, with methyl viologen (MV) as a final electron acceptor, black line, and CEF, in the presence of DCMU, grey line, in chloroplasts isolated without any reductant B) Linear electron flow, black line, and CEF, grey line, in chloroplasts isolated with 2 mM reduced DTT C) CEF in chloroplast isolated with 2 mM reduced DTT, black line, and without DTT, grey line D) Sensitivity of chloroplasts isolated with 2 mM reduced DTT, black line, to 5 μM Antimycin A, grey line, and 20 μM nigericin, dashed grey line.

and dichloromethyl urea (DCMU), allowing CEF exclusively. Proton translocation activity was determined by acridine fluorescence quenching under illumination, which indicates the generation of the ΔpH component of *pmf* (156). This method of assessing CEF has the advantage of being sensitive to true *pmf*-storing processes and not to recombination reactions within PS I that can appear as CEF but do not result in net proton translocation. A 5:1 ratio of 9-amino acridine (9AA) and 9-amino-6-6-chloro-2-methoxy-acridine (ACMA) was used to obtain a more linear response of acridine fluorescence quenching to ΔpH (156). Valinomycin and KCl were added to each reaction to dissipate the transthylakoid electric field component of *pmf* (Δψ) so that all *pmf* was in the form of ΔpH, which is detectable by acridine fluorescence quenching.

In Figure 2.1*A* thylakoids were isolated without reductant in the isolation buffers. While onset rate and extent of ΔpH generated in the presence of MV was substantial, that for CEF was only 8.2% (estimated from the initial slope) that of LEF, indicating a low CEF rate of proton translocation. The final steady-state amplitude of acridine quenching for CEF was only 3.8% that of LEF. The relaxation of the ΔpH under the different conditions was similar, indicating that the difference in ΔpH accumulation could not be attributed to changes in the proton efflux rates or ATP synthase activities.

When chloroplasts were isolated in the presence of 2 mM reduced DTT, the relative capacity for CEF increased substantially (Figure 2.1*B*) to 13.3% (initial slope) and 12.1% (amplitude) of LEF. This increase translates to an increase in the initial rate of proton influx via CEF of 63% when chloroplasts are isolated in the presence of reduced DTT and an increase in the total amplitude of CEF generated CEF by 275% (Figure 2.1*C*). The similarity in slow acridine fluorescence dark recovery kinetics across treatments indicates that the rate of proton

efflux was affected by the presence of DTT, and is consistent with a lack of substrate (ADP or P_i) for the chloroplast ATP synthase.

CEF in the chloroplast preparation containing reduced DTT was sensitive to 5 μM Antimycin A (75% decrease in initial slope, 64% decrease in the amplitude of quenching, Figure 2.1*D*), indicating involvement of the FQR (115), and was completely dissipated by the addition of nigericin, which leads to complete uncoupling when used in the presence of valinomycin and excess KCl (Figure 2.1*D*).

To confirm the activity of CEF we measured light-induced absorbance changes at 703 nm to monitor the redox state of P700 (Figure 2.2). As oxidized $P700^+$ absorbs less at this wavelength than reduced P700, in the presence of DCMU, the monitoring of 703 nm absorbance changes allows the comparison of both the reduction state of the PQ pool, and rates of electron transfer through PS I. Figure 2.2 shows light induced changes in ΔA_{703nm} in chloroplasts isolated with 2 mM DTT and those isolated without. The light induced absorbance changes show a slower oxidation of P700 in the chloroplasts isolated with 2 mM DTT_{RED} than those without ($t_{1/2}$ = 2 s and $t_{1/2}$ < 10 ms, respectively), indicating a more reduced PQ pool in the thylakoids isolated with reductant. We also see a faster reduction of P700 in the dark interval following the actinic flash in the presence of 2 mM DTT_{RED}.

While all results were obtained with NADH, similar observations were seen with NADPH (data not shown).

Interestingly, after isolation, 2 mM DTT_{RED} was not able to restore full activity of CEF in thylakoids isolated without reductant (Figure 2.3). Even when assayed with DTT_{RED}, CEF

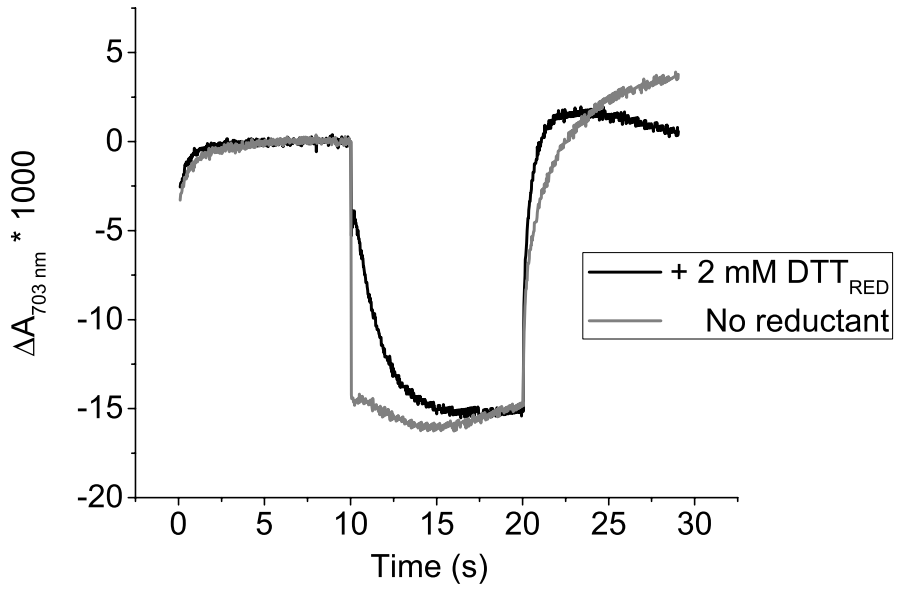

Figure 2.2 Light induced P700 redox changes. Chloroplasts were isolated and assayed with 2 mM reduced DTT, black line, and without reductant, grey line, in the presence of DCMU[2].

[2] Data for this figure were kindly provided by Dr. Nicholas Fisher.

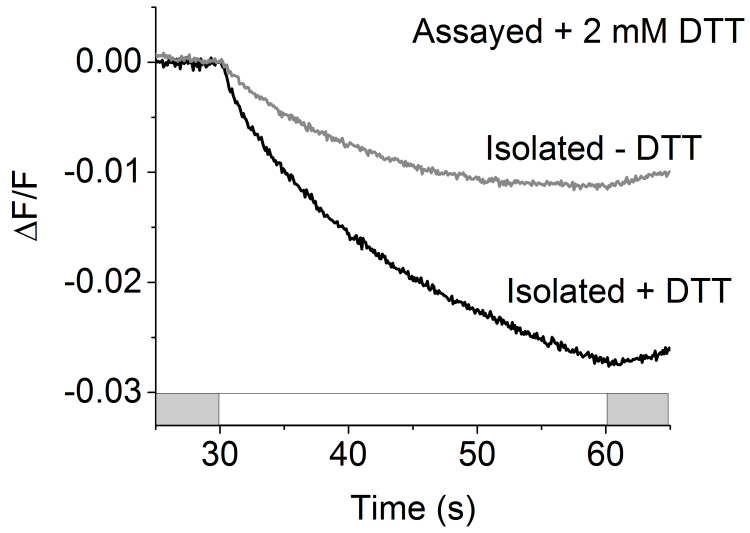

Figure 2.3 Irreversible loss of CEF in thylakoids isolated in the absence of DTT. Light induced acridine fluorescence quenching in DCMU treated thylakoids isolated with 2 mM DTT_{RED} (black line) or without reductant (grey line). Activity was assayed in the presence of 2 mM DTT_{RED}.

activity of the thylakoids isolated without DTT_{RED} was only half that of the thylakoids isolated with DTT_{RED} (53.5% from initial slope, 57% from amplitude of acridine fluorescence quenching), suggesting irreversible loss or damage to an FQR component.

2.3.B Dependency of Fd on CEF activity

The extent of formation of ΔpH in the presence of DCMU was sensitive to the addition of Fd, with an 81% decrease in proton influx via CEF (initial slope) and a 71% decrease in total *pmf* generated by CEF (amplitude) when Fd is omitted (Figure 2.4), indicating the DTT_{RED} did not reduce the PQ pool directly, but was dependent on Fd, further supporting involvement of the FQR; these results are consistent with previous work (82, 112). In contrast, in 'highly active chloroplasts' addition or absence of NADH had less effect on the extent of light driven acridine fluorescence quenching in the presence of DCMU (34% decrease in proton influx and 19% decrease in *pmf*, from initial slope and amplitude of fluorescence quenching, respectively) (Figure 2.4).

As thylakoids were prepared from a crude preparation of broken and intact chloroplasts, and ruptured within the reaction cuvette, it is likely there was a small amount of Fd and $NAD(P)^+$/NAD(P)H remaining in the cuvette. This may explain residual activity without addition of Fd.

2.3.C The redox dependence of CEF activation by DTT

In order to determine the redox potential in which CEF is active or inactive, we assayed activity in a range of DTT_{OX}/$2DTT_{RED}$ concentrations in thylakoids isolated with 2 mM DTT to maintain activity (see above, Figure 2.3). The concentration of DTT_{RED} was held constant at

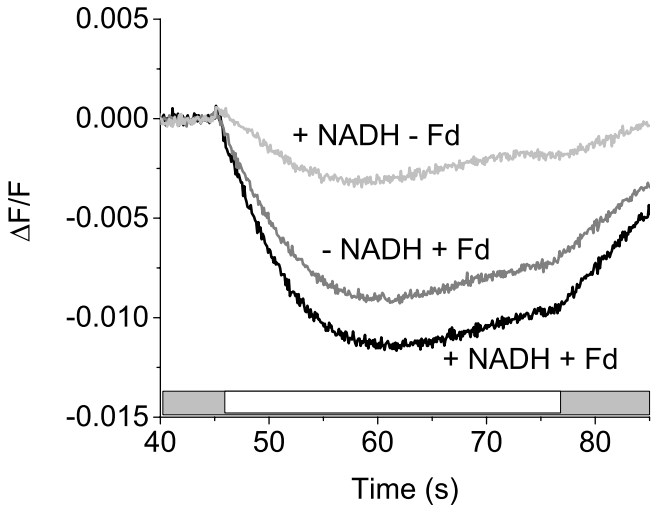

Figure 2.4 Dependence of CEF on Fd *in vitro*. Acridine fluorescence quenching as an indicator of *pmf* formation in the presence of DCMU. Total extent of *pmf* was greatly diminished without addition of Fd, but was not largely changed when NADH was omitted from the reaction.

4 mM and incremental addition of DTT_{OX} was added to obtain Figure 2.5. Figure 2.5 shows the fractional activity of CEF determined by the total amplitude of acridine fluorescence quenching as a function of the ratio of the [DTT_{OX}/2DTT_{RED}]. Half maximal CEF activity was observe at a calculated redox potential of -306 mV versus standard hydrogen electrode when the data was fit to a modified form of the Nernst equation. The fit is consistent with a slope of n = 2.

We tested this reversibility by rupturing 'highly active' chloroplasts in a concentration of DTT_{OX}/2DTT_{RED} predicted to poise the redox potential at -300 mV, which should be near half activity. This was followed by subsequent addition of 9 mM DTT_{RED}, which should bring the redox potential down to -380 mV, and strongly activate or restore CEF activity. Activity of CEF was increased after addition of DTT_{RED} (Figure 2.6).

This does not address whether CEF is reversibly lost during preparation as we have seen previously (Figure 2.3), but shows that the regulatory component is rapidly reversible *in vitro*.

2.4 Discussion

There is a multitude of research conducted on CEF *in vitro* using isolated thylakoids from mutants, or under varying conditions. A reduction in already low rates of CEF in thylakoids *in vitro* have been used to infer large physiological effects *in vivo* (82, 87, 157). We have demonstrated that the nature of isolation and assay conditions are vital for the conservation of CEF *in vitro*.

2.4.A FQR-mediated CEF is active under reducing conditions *in vitro*

It has been previously described in algae that the redox state is the determining factor for formation of a CEF competent supercomplex (92, 155). However, in plants, this is the first demonstration that CEF is dependent on chloroplast redox state *in vitro*. While activation of the

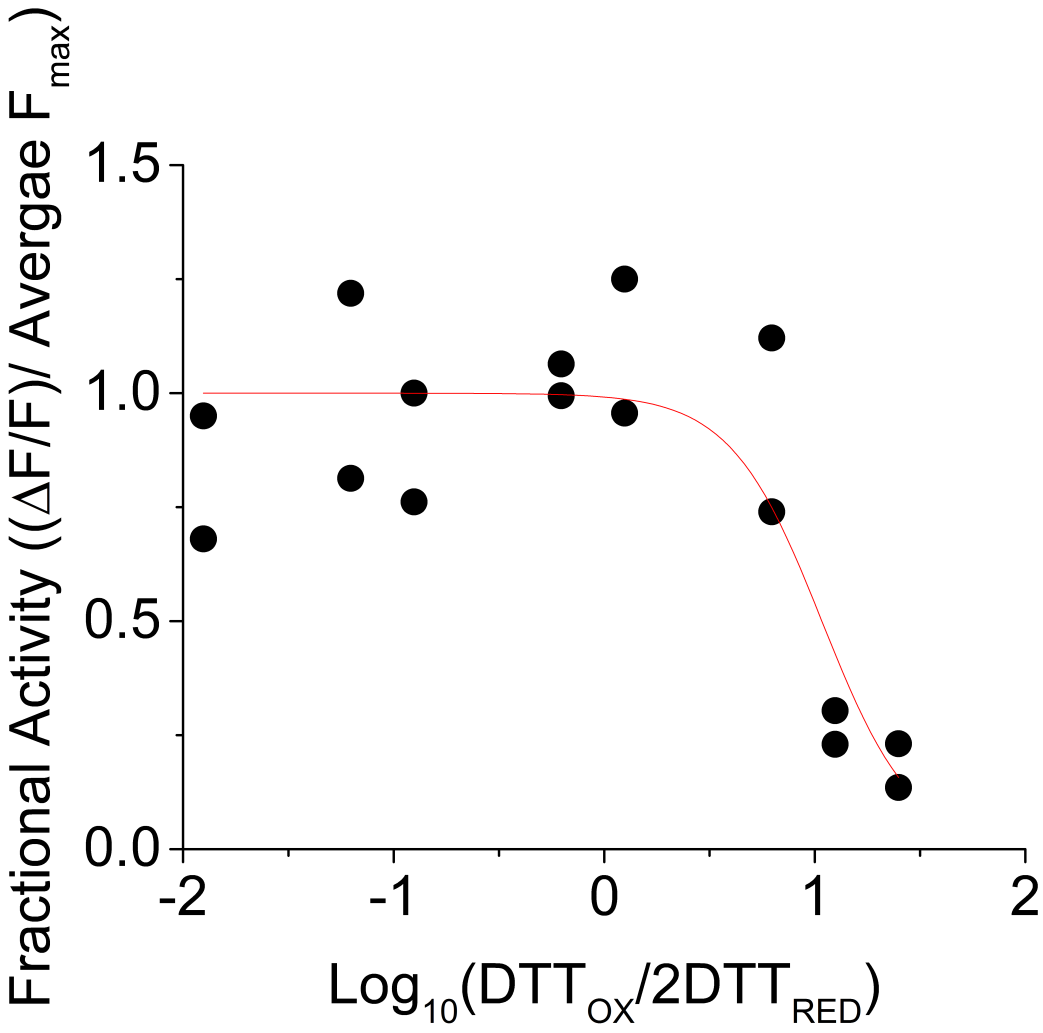

Figure 2.5 Redox titration of CEF activity under varying concentrations of $DTT_{OX}/2DTT_{RED}$. The E_m of CEF activation is calculated to be around -306 mV.

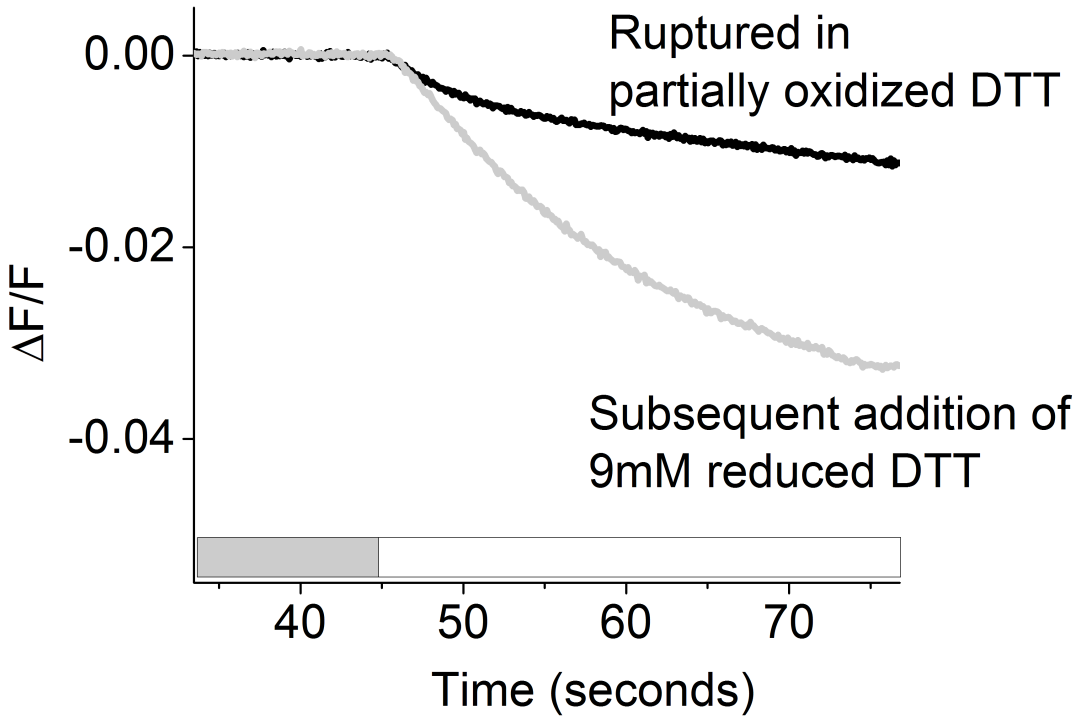

Figure 2.6 Rapid reversibility of CEF. 'Highly active' chloroplasts were assayed for CEF activity in partially oxidized DTT (black line), and then assayed for CEF activity after subsequent addition of 9 mM DTT_{RED} (grey line).

NDH complex has been suggested to be activated in the presence of ROS (99, 102) (discussed in Chapter 3), we have demonstrated that the 'elusive' antimycin A sensitive FQR, possibly involving a PGR5/PGRL1 complex, is more active under reducing conditions (Figure 2.1D, and 2.4). This lends support to two separate and independently regulated CEF pathways.

2.4.B FQR-mediated CEF may involve a regulatory thiol

The activity of CEF in isolated chloroplasts is dependent on the redox potential of the reaction buffer (Figures 2.1*A-C*, 2.2, and 2.6) and the midpoint potential of activity is -306 mV when fit with n = 2 (Figure 2.5). This range is in agreement with involvement of a thiol, which have been described as having midpoint potentials ranging from as high as -124 mV to -330 mV and may be shifted further with pH (158–160).

Assignment of CEF activity in our assays to the FQR is supported by both the sensitivity of activity to antimycin A (Figure 2.1*D*) and the dependency of Fd (Figure 2.4). Based on this identification of the FQR pathway, if a thiol is involved, it is possible the thiol is directly located on the FQR related PGRL1. Keeping in mind the effect of pH on redox potential, this would be in tentative agreement with recent work (113), in which a reversible thiol/disulfide pair (E_m = ~-280 mV) was identified within PGRL1, which may be involved in formation and disassociation of the PGRL1-PGR5 complex.

There is extensive precedence for regulatory thiols in photosynthesis controlling both the electron transport chain and carbon fixation reactions in response to chloroplast redox state. The observation that CEF is also regulated in response to chloroplast redox state adds an additional level of regulation to the proton circuit of photosynthesis.

Among the regulatory thiols associated with the electron transport chain is one with a E_m ~-360 mV associated with activity of the b_6f complex (161). It is possible the regulation of this

thiol could interfere with our measurements of *in vitro* CEF, however, as activity of the b_6f complex is apparently downregulated with a more reducing redox potential, the effect would cause our apparent CEF activity to be underestimated. Another point of redox regulation of the proton circuit is at the ATP synthase (131, 162). Again, with any interference at this regulatory point, we would expect an underestimation of CEF in our active state or overestimation of CEF in our inactive state.

The observation that FQR-mediated CEF is more active in a reduced state is in agreement with the involvement of a regulatory thioredoxin recently described by Courteille et al. (163), but the exact interactions are unclear as this enzyme has been proposed to be a CEF suppressor.

2.4. C FQR-mediated CEF is sensitive to thylakoid isolation conditions

The large increase in CEF when thylakoids are isolated with DTT_{RED} is not seen when DTT_{RED} is added to thylakoids isolated without reductant. This suggests the irreversible loss or damage of an FQR component. This lability of a complex has been seen in multiple instances of redox active proteins such as ascorbate peroxidase, which is irreversible damaged when isolated without ascorbate (164). This is important to note as rates of CEF may be underestimated if complex activity is partially lost during isolation.

2.4. D Implication for regulation *in vivo*, two pathways of CEF

While addition of reduced DTT is not physiological, the conditions in the above experiments may be reflective of conditions in which changes in downstream metabolism leads to a more reduced $NAD(P)^+$/NAD(P)H pool and lead to rapid reduction of a regulatory thiol and in turn, rapid activation of CEF (Figures 2.6 and 2.7*A*). This rapid activation would allow for a much faster response to redox state than that shown for activation of NDH in response to H_2O_2

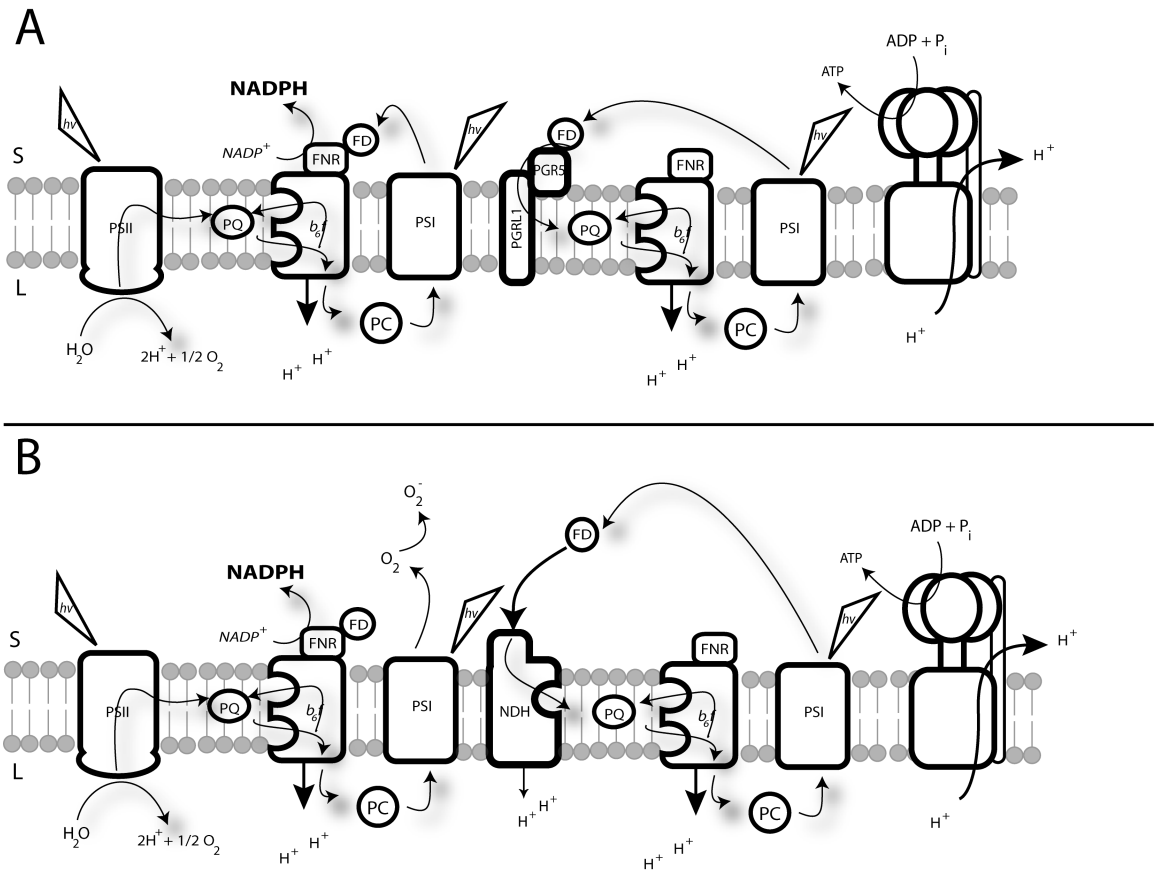

Figure 2.7 A comprehensive model of CEF activation *in vivo*. A) An ATP deficit leads to the buildup of reducing power in the stroma which leads to the activation of the antimycin A sensitive FQR pathway of CEF B) If FQR mediated CEF is unable to provide enough ATP to supply downstream metabolism, the acceptor side of PS I becomes closed and electron transfer to O_2 results in ROS formation and activation of the NDH complex.

(99, 102) (Chapter 3). This more rapidly activation of CEF may be a 'first response' to balance the ATP/NADPH output of the light reactions before the buildup of reducing equivalents leads to ROS production. This 'first response' by the FQR would also likely have a lower ATP output than the NDH complex, which may be capable of proton pumping. This may be beneficial to rapidly modulate CEF with a lower ATP output when the reduction state of the chloroplast indicates an imbalance forming. If this route of CEF is unable to augment the ATP deficit, the formation of ROS may then signal for a slightly slower, but more efficient ATP producing route of CEF, the NDH complex (Figure 2.7*B*), (discussed in Chapter 5).

2.5 Methods

2.5.A Chloroplast isolation

A crude mixture of broken and intact chloroplasts was isolated from market fresh spinach, purchased the morning of experiments, using a protocol modified from (165). Leaves were kept in the dark at 4°C until use. Leaves were ground in buffer (350 mM sorbitol, 50 mM HEPES, 5 mM $MgCL_2$, 2.5 mM EDTA, 0.1% w/v bovine serum albumin, pH 7.6), at a concentration of 1g/mL, 3 times for 3 seconds each in a standard kitchen blender, then filtered through 3 layers cheesecloth and 1 layer Miracloth. The filtrate was centrifuged for 10 minutes at 3000 X *g*. The supernatant was poured off and the pellet was resuspended in a small volume of buffer (350 mM sorbitol, 50 mM HEPES, 5 mM $MgCL_2$, 2.5 mM EDTA, pH 7.6) using a soft bristle paintbrush and used immediately. All steps were carried out on ice. Reductant was added to all isolation buffers at concentrations described in the results during assays, unless otherwise noted. While extents of activity varied from each isolation, the experimental effects remained constant. Therefore, we present representative results and comparisons are made between chloroplast isolated simultaneously.

2.5.B Oxidation and reduction of dithiothreitol (DTT)

To obtain oxidized DTT, a solution at concentration was left at room temperature for a week. The solution was monitored for oxidation by the appearance of the 283 nm peak in the absorbance spectrum indicating oxidation (data not shown).

DTT was reduced by addition of 400 mM borohydride to a 200 mM DTT solution on ice for 1 hour with occasional gentle swirling. Then HCl was added to a 400 mM concentration to convert the borohydride to boric acid. This was allowed to incubate on ice for 30 minutes. The solution was brought to pH 7.6 and diluted to 100 mM DTT concentration. Reduction of DTT was confirmed by the disappearance of the 283 nm peak in the absorbance spectrum (data not shown) indicating essentially complete reduction.

2.5.C Spectroscopic measurements

For all spectroscopic measurements, chloroplasts were ruptured in the reaction cuvette prior to the experiment in low osmotic assay buffer (50 mM HEPES, 5 mM $MgCl_2$, pH 7.6). For LEF measurements the reaction buffer contained 50 μM methyl viologen as a final electron acceptor. CEF measurements contained 20 μM DCMU, 25 μM ferredoxin, and excess NADH (100 μM). Spectroscopic measurements were performed on an in-house built spectrophotometer as described in Hall et al. (166) modified with a fluorimeter cuvette chamber. For the redox titration, NADH was decreased to 25 μM to minimize the impact on redox potential.

2.5.C.1 Acridine fluorescence quenching

To monitor the accumulation of the light induced changes in the pH component of *pmf* in thylakoids, acridine (80 μM 5:1 9-aminoacridine:ACMA) (156) was excited at 430 nm and total fluorescence emission between 495 nm and 700 nm was detected by filtering with a FGL495

longpass filter and a BG18 shortpass (Schott) filter (ThorLabs). Fluorescence quenching was measured during a dark-light-dark interval, and normalized to the initial dark fluorescence level.

2.5.C.2 Absorbance changes at 703 nm

The redox state of PS I was measured using absorbance changes at 703 nm as described in (120) using a spectrophotometer modified from Hall et al. (166). Contribution of chlorophyll *a* fluorescence was limited by addition of 1 mM hydroxylamine followed by a 2 second actinic flash. Any residual chlorophyll *a* fluorescence signal contamination was monitored by repeating the experiment with a reference wavelength (730 nm) and determined to be minimal under these conditions.

2.6 Author contributions

All data presented, except where noted, were obtained by Deserah D. Strand. However, significant intellectual contribution was also made by the co-authors. Geoffry A. Davis and L. Ruby Carrillo supplied a large amount of preliminary data in collaboration, and therefore have been added as co-authors to this manuscript. L. Ruby Carrillo and Dr. Nicholas Fisher tested many different chloroplast isolation protocols and buffers. Geoffry A. Davis and Dr. Nicholas Fisher contributed significantly to the optimization of the acridine fluorescence quenching protocols and concentrations of reaction buffer components.

2.7 Acknowledgements

We would like to thank Dr. Jeffrey Cruz for helpful discussions. The authors are funded by Grant DE-FG02-11ER16220 from the Division of Chemical Sciences, Geosciences, and Biosciences, Office of Basic Energy Sciences of the US Department of Energy.

Chapter 3

Activation of cyclic electron flow around photosystem I by hydrogen peroxide *in vivo*[3]

Deserah D. Strand, Aaron K. Livingston, Mio Satoh-Cruz, John E. Froehlich,

Veronica G. Maurino, and David M. Kramer

[3] Preliminary data for this manuscript has previously appeared in Livingston (104) and this work is referenced within.

3.1 Abstract

Cyclic electron flow (CEF) around photosystem I is thought to balance the ATP/NADPH energy budget of photosynthesis, requiring that its rate be finely regulated. The mechanisms of this regulation are not well understood. We observed that mutants that exhibited constitutively high rates of CEF also showed elevated production of H_2O_2. We thus tested the hypothesis that CEF is activated by H_2O_2 *in vivo*. CEF was strongly increased by H_2O_2 both by infiltration or *in situ* production by chloroplast-localized glycolate oxidase, implying that H_2O_2 can activate CEF either directly by redox modulation of key enzymes, or indirectly by affecting other photosynthetic enzymes. CEF appeared rapidly, within 20 min of exposure to H_2O_2, suggesting activation of existing CEF complexes. H_2O_2-dependent CEF was not sensitive to antimycin A or loss of PGR5, indicating that increased CEF probably does not involve the PGR5-PGRL1 associated pathway. In contrast, the rise in CEF was greatly suppressed in a mutant deficient in the chloroplast NADPH:PQ reductase (NDH), supporting the involvement of this complex in CEF activated by H_2O_2. We propose that H_2O_2 is a missing link between environmental stress, metabolism, and redox regulation of CEF in higher plants.

3.2 Introduction

In oxygenic photosynthesis, linear electron flow (LEF) is the process by which light energy is captured to drive the extraction of electrons and protons from water and transfer them through a system of electron carriers to reduce NADPH. LEF is coupled to proton translocation into the thylakoid lumen, generating an electrochemical gradient of protons ($\Delta\tilde{\mu}_{H^+}$) or proton motive force (*pmf*). The *pmf* drives the synthesis of ATP to power the reactions of the Calvin-

Benson-Bassham (CBB) cycle and other essential metabolic processes in the chloroplast. The *pmf* is also a key regulator of photosynthesis, in that it activates the photoprotective q_E response to dissipate excess light energy, and down-regulates electron transfer by controlling the rate of oxidation of plastoquinol at the cytochrome b_6f complex (b_6f), thus preventing the buildup of reduced intermediates (1, 3).

LEF by itself results in the transfer or deposition into the lumen of three protons for each electron transferred through PS II, plastoquinone (PQ), the b_6f complex, plastocyanin and photosystem I (PS I) to ferredoxin (Fd). The synthesis of one ATP is thought to require the passage of 4.67 protons through the ATP synthase, so that LEF should produce a ratio of ATP/NADPH of about 1.3; this ratio is too low to sustain CBB cycle or supply ATP required for translation, protein synthesis transport or other processes (2). The relative demands for ATP and NADPH should dynamically change depending on environmental, developmental and other factors, so that the regulation of ATP/NADPH must be dynamically regulated.

Several alternative electron flow pathways in the chloroplast have been proposed to augment ATP production thus balancing the ATP/NADPH budget of the chloroplast (2, 3). Perhaps the least understood of these pathways is cyclic electron flow around photosystem I (CEF), in which electron flow from the acceptor side of PS I is shunted back into the PQ pool, generating additional *pmf* that can power ATP production with no net NADPH production. There are several proposed CEF pathways that may operate under different conditions or in different species (2, 3). In higher plant chloroplasts, the most studied routes of CEF are (A) the antimycin A sensitive pathway, which involves a complex of two CEF-related proteins, PGR5 and PGRL1, directly reducing the quinone pool (82, 87, 112, 113), (B) the respiratory Complex I analog, the

NADPH dehydrogenase (NDH) complex (84, 85, 94) which oxidizes Fd or NADH to reduce plastoquinone (85, 167), and (C) through the Q_i site of the b_6f complex (110, 168). Different CEF mechanisms appear to operate in other species. In Chlamydomonas, for example, CEF appears to be conducted by a supercomplex of PS I, the b_6f complex, and the PGRL1 protein (92, 155) and the involvement of PGR5 has recently been described as important for CEF under hypoxia (153).

Regardless of the mechanism of CEF, the overall process must be precisely regulated to properly balance the production of ATP to match the demands of metabolism. The mechanism of this regulation is not known, but many general models have been proposed. Perhaps the most widely cited regulatory model is the antenna state transition, which were previously shown to be correlated with activation of CEF in *C. reinhardtii* (92, 106) and favor the formation of the PS I-b_6f supercomplex (92). However, it was recently shown that state transitions are not required for CEF activation, supporting models that include redox control (118, 120, 152, 153, 155) [see also (169)]. Other possible regulatory mechanisms include sensing of ATP/ADP ratios (64, 109), the redox status of NAD(P)H or Fd (111), various CBB metabolic intermediates [reviewed in (70)], calcium signaling (102, 154), phosphorylation of CEF complexes (102) and the reactive oxygen species (ROS) H_2O_2 (70, 99, 102, 103).

In this work, we concentrate on the possible role of H_2O_2 which is produced by the light reactions of photosynthesis and are already known to regulate other cellular processes such as plant growth, development, and defense (170–172). Based on *in vitro* studies, it was previously proposed that H_2O_2 could activate CEF or chlororespiration by modifying the NDH complex (102). It has also been shown that H_2O_2 can increase the expression of the NDH complex (99)

and may further affect the accumulation of photosynthetic metabolites, indirectly activating CEF (70). Consistent with this possibility, H_2O_2 is a well-documented signaling molecule (173), possibly through its ability to oxidize thiols (174, 175). Furthermore, H_2O_2 is expected to be produced under many conditions that initiate CEF, e.g. under a deficit of ATP, when electrons should accumulate in the PS I acceptor pools leading to superoxide production which can be converted to H_2O_2 by superoxide dismutase (45).

This study aims to test the hypothesis that CEF can be initiated *in vivo* by H_2O_2 using a combination of *in vivo* spectroscopy and genetic modifications to selectively and rapidly initiate H_2O_2 production in the chloroplast.

3.3 Results

3.3.A H_2O_2 accumulation in the high cyclic mutant *hcef1*

The Arabidopsis mutant, *hcef1* (69), which is deficient in chloroplastic fructose-1,6-bisphosphase (FBPase) activity, and displays constitutively high CEF rates, was checked for increased H_2O_2 accumulation. When H_2O_2 concentration is measured by resorufin fluorescence, the product of the reaction between Amplex Red and H_2O_2, *hcef1* has 3 times as much peroxide as the Col-0 (Figure 3.1, 2.99 ± 0.17 and 1.00 ± 0.13, respectively, $n = 3$, $p > 0.001$, student's t-test). Additionally, when stained with 3,3' diaminobenzidine (DAB), leaves of *hcef1* (Figure 3.1, inset *B*) showed qualitatively increased levels of H_2O_2 when compared to the wildtype strain, Columbia-0 (Col-0) (Figure 3.1, inset *A*). These results indicate that the loss of FBPase led to increased H_2O_2 accumulation, probably by a buildup of reducing intermediates of

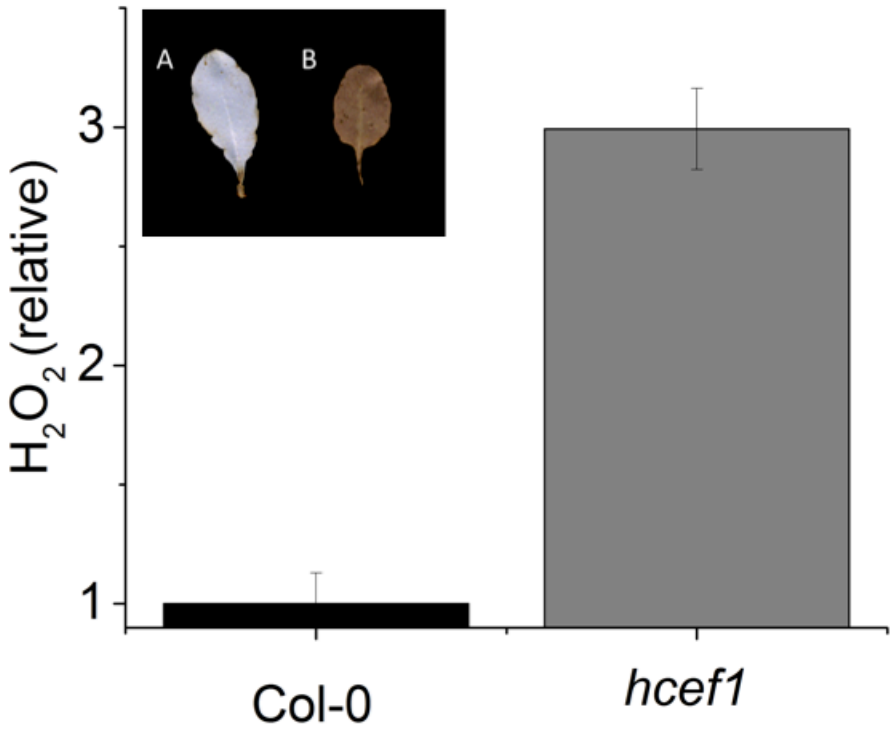

Figure 3.1 Relative H_2O_2 accumulation in *hcef1*. Quantitatively determined H_2O_2 content of leaves based on resorufin fluorescence against a standard curve and normalized to the average Col-0 H_2O_2 content. Data is based on a per area basis. Mean ± SD, n = 3[4]. Inset: Qualitative H_2O_2 accumulation measured by 3,3' diaminobenzidine (DAB) staining of representative leaves of Col-0 (A) and *hcef1* (B)[5]

[4] This data was kindly provided by Dr. Mio Satoh-Cruz.
[5] This data appears previously in (104) and has been generously provided by Dr. Aaron Livingston.

photosynthetic electron transfer, and are consistent with a correlation between H_2O_2 and CEF activation. We thus set out to determine if this relationship could be causal.

3.3.B Effects of H_2O_2 production by plants expressing glycolate oxidase in chloroplast

We next tested if CEF is activated in the presence of H_2O_2 by comparing photosynthetic properties of Col-0 and transgenic Arabidopsis plants that express glycolate oxidase (GO) targeted to the chloroplast (176). These "GO" plants produce H_2O_2 in the chloroplast by the oxidation of glycolate upon activation of photorespiration, and are thus useful tools for studying changes in photosynthetic activities induced by the metabolic generation of H_2O_2 in the chloroplast. We focus mainly on the GO5 line because of its relatively high and robust H_2O_2 production rates (176, 177) (Figure 3.2), but we obtained similar results with other lines (discussed below).

GO expression had measurable effects on several photosynthetic parameters (Figure 3.3). PS II photochemical efficiency (ϕ_{II}) (Figure 3.3*A*) and LEF (Figure 3.3*B*) saturated more rapidly with increasing light intensity in GO5 compared to Col-0, leading to a lower LEF, particularly at intensities above 200 μmol photons m^{-2} s^{-1}. GO5 showed stronger activation of q_E, response (Figure 3.3*C*), likely indicating an increase in light-induced *pmf* and lumen acidification. A substantial (about 2-fold) increase in *pmf* in GO5 was confirmed by the extent of the dark-interval electrochromic shift (ECS) absorbance changes, ECS_t (Figure 3.3*D*) (40–42, see Materials and Methods). This increased *pmf* occurred in GO5 despite lower LEF, suggesting that either proton influx was increased above that supported by LEF or that proton efflux was slowed.

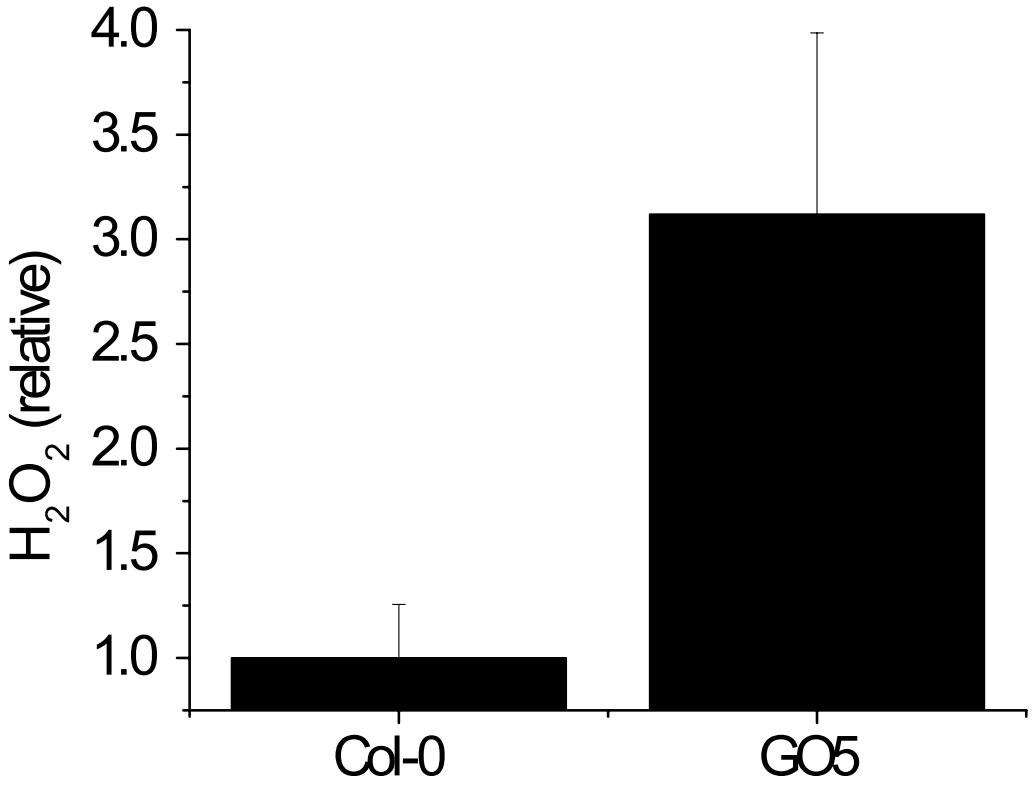

Figure 3.2 Relative H_2O_2 accumulation in GO5. Quantitatively determined H_2O_2 content of leaves based on resorufin fluorescence against a standard curve and normalized to the average Col-0 H_2O_2 content. Data is based on a per unit chlorophyll basis. Mean ± SD, n = 3. Assays were performed on leaves from fully mature rosettes just prior to bolting as described for spectroscopic assays.

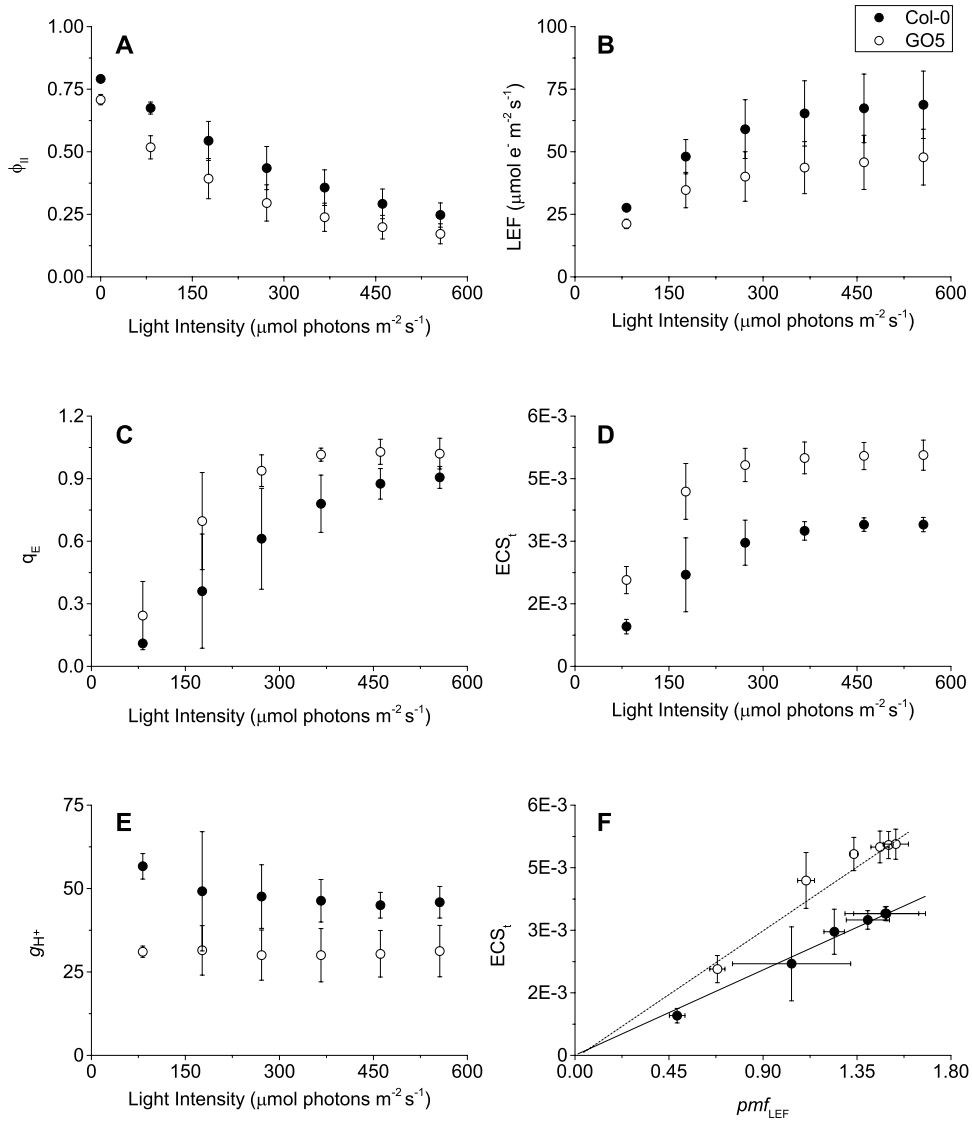

Figure 3.3 Effects of chloroplast targeted glycolate oxidase expression on photosynthesis.

Figure 3.3 (Cont'd) Comparison of photosynthetic parameters of Col-0 (black circles) and GO5 (open circles). Panels A-E show, as a function of light intensity; Photochemical efficiency of photosystem II (ϕ_{II} , Panel A); Linear electron flow (LEF, Panel B); rapidly reversible exciton quenching (q_E, Panel C); relative light-induced *pmf*, as measured by the total decay of the ECS (ECS_t, Panel D) ;and proton conductivity (g_H^+) of the ATP synthase, as estimated by the relaxation kinetics of the ECS signal (panel E). Panel F shows ECS_t as a function of the estimated *pmf* generated from LEF alone (pmf_{LEF}). Mean ± SD (n = 3).

The conductivity of the thylakoid to protons (g_H^+), which primarily reflects the activity of the ATP synthase, was estimated by the decay kinetics of the ECS signal (34, 178). In GO5, g_H^+ was approximately 30% lower than in Col-0 (Figure 3.3*E*), implying that, although the ATP synthase activity was somewhat decreased in the mutant, it could not by itself explain the large increase in light-induced *pmf*, suggesting an increase in CEF [see discussion in (33, 69)]. This conclusion was supported by a statistically significant (ANCOVA $p < 0.05$, $n = 3$) increase of about 36% in light-driven *pmf*, estimated by ECS_t as a function of pmf_{LEF} (Figure 3.3*F*), a parameter that estimates *pmf* generated by LEF alone (33, 179). These results indicate an increase in *pmf* above that attributable to LEF alone, suggesting that CEF was activated in GO5.

Increased CEF in GO5 was independently confirmed by comparing estimated light-driven proton flux (v_H^+) as a function of LEF (26, 33). As shown in Figure 3.4*A*, the slope of v_H^+ as a function of LEF was increased in GO5 in comparison to Col-0 by approximately 47.6% (Figure 3.4*A,* ANCOVA $p < 0.05$, $n = 3$). The increase in CEF was eliminated by infiltration of 100 μM methyl viologen, which blocks CEF by shunting electrons from PS I to O_2 (26) [see Figure 4.3*A* in (104)]. This increase in ratio of CEF/LEF ($\Delta v_H^+ / v_{H\ LEF}^+$, see Eq. 3.3, Materials and Methods) was not caused simply by decreasing LEF. Instead, assuming a similar ratio of proton translocation for electron flux, CEF increased in absolute terms from minimal activation in the control [as previously reported in (69)] to approximately 24 μmol electrons m^{-2} s^{-1} when LEF was 50 μmol electrons m^{-2} s^{-1}.

Analyzing the ECS and fluorescence data described in Eq. 3.3 (Materials and Methods), we estimated that v_H^+ was increased by about 50% in GO5 over Col-0. The difference in the

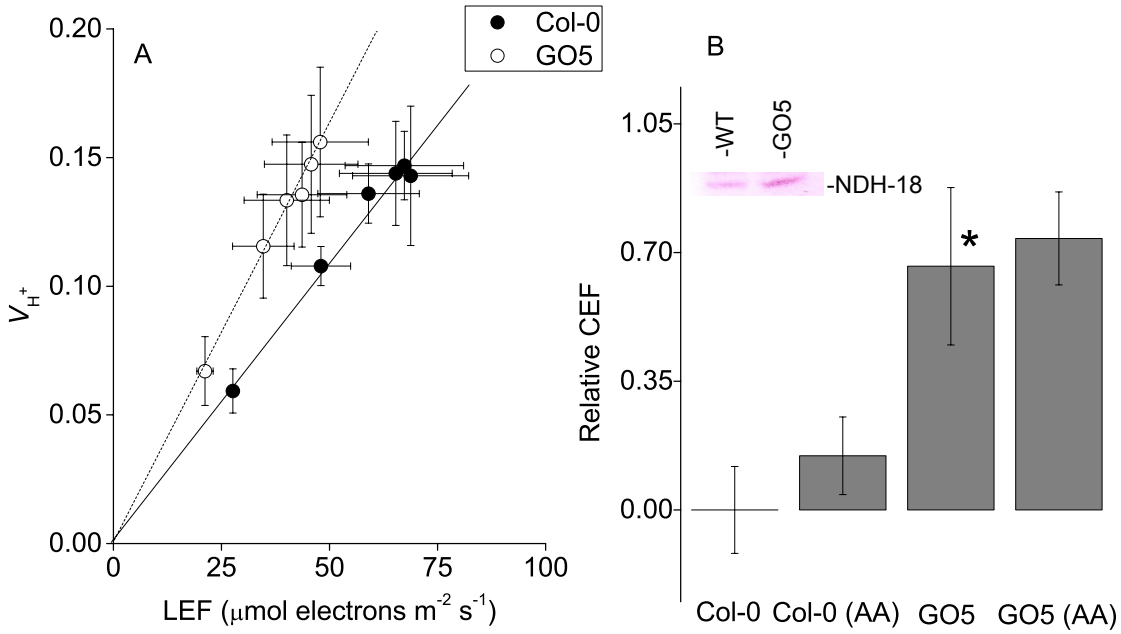

Figure 3.4. Increased CEF in GO5. A) light-driven proton flux (v_H^+) vs LEF in attached Col-0 (squares) and GO5 (circles) leaves B) Calculated relative CEF from intact leaves and leaves infiltrated with 20 μM antimycin A (AA). Mean ± (A) SD (n = 3) or (B) SEM (n ≥ 3). * Indicates statistical significance from Col-0, no significant differences were seen between water and AA within genotype. B, inset) NDH-18 levels in GO5 grown at ambient CO_2. Lanes were loaded with 10 μg total chlorophyll[6].

[6] Figure 3.4*B*, inset was kindly provided by Dr. John Froehlich.

apparent extents of CEF activation (about 36% versus about 50%) may be ascribed to differences in proton to electron stoichiometries for CEF versus LEF or to ambiguities in quantification of the proton and electron fluxes. Nevertheless, the multiple estimates of increased CEF were qualitatively consistent, and correlated well with the extent of H_2O_2 production in multiple GO lines with differing levels of GO activity (104, 176) [see Figure 4.3*A-C* in (104)]. In another independent assessment of CEF induction, we observed a strong increase in GO5 compared to Col-0 of the postillumination chlorophyll fluorescence rise (Figure 3.5), which is attributed to CEF-related reduction of the plastoquinone pool in the dark through the NDH complex (79, 84, 180).

Together, these results strongly imply that introduction of GO in chloroplasts induces increased CEF. However, in the GO plants, glyoxylate produced by the glycolate oxidase in the chloroplasts, also accumulates, and may induce CEF. To test this hypothesis we measured CEF in GO5 plants also coexpressing malate synthase targeted to the chloroplast (GOMS1 and GOMS14 lines), which can further convert glyoxylate to malate (176). We observed qualitatively similar photosynthetic effects of GO5 and GOMS14 (Figure 3.6), indicating that the production of H_2O_2 rather than glyoxylate is the likely inducer of CEF.

The observed increase in CEF was insensitive to infiltration with 20 μM antimycin A (Figure 3.4*B*, ANCOVA, $p > 0.05$, $n = 3$), well above the observed K_i for inhibition of the antimycin A sensitive pathway of CEF (115). There is also an increase in NDH content of GO5 when grown at ambient CO_2 levels (Figure 3.4*B*, inset). These results are consistent with the post-illumination rise (Figure 3.5) in suggesting the involvement of NDH in GO5 elevated CEF.

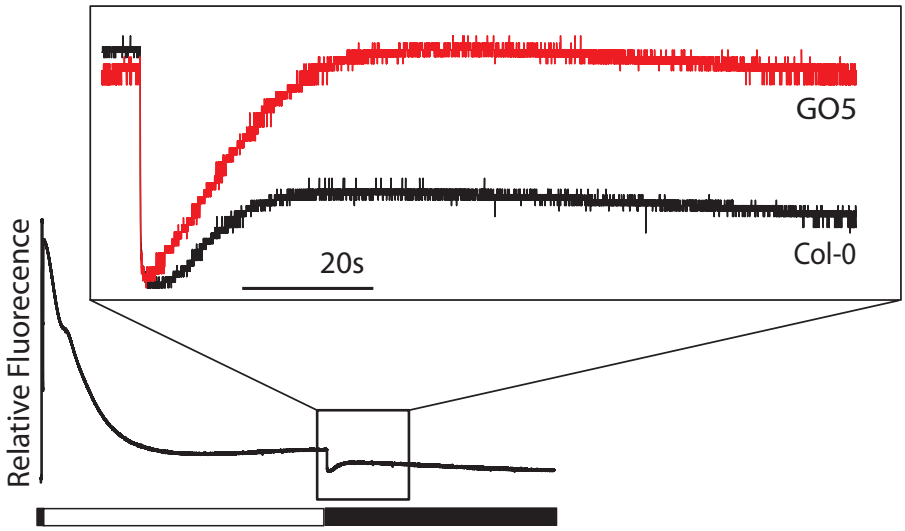

Figure 3.5 Increased dark reduction of the PQ/PQH$_2$ pool in GO5. Transient chlorophyll fluorescence rise in the dark after illumination with 150 μmol photons m^{-2} s^{-1} (635 nm). Col-0 (black) and GO5 (red) representative data of 3 independent experiments. The full data set is normalized to F_M, while the inset data is normalized to [0,1] for comparison.

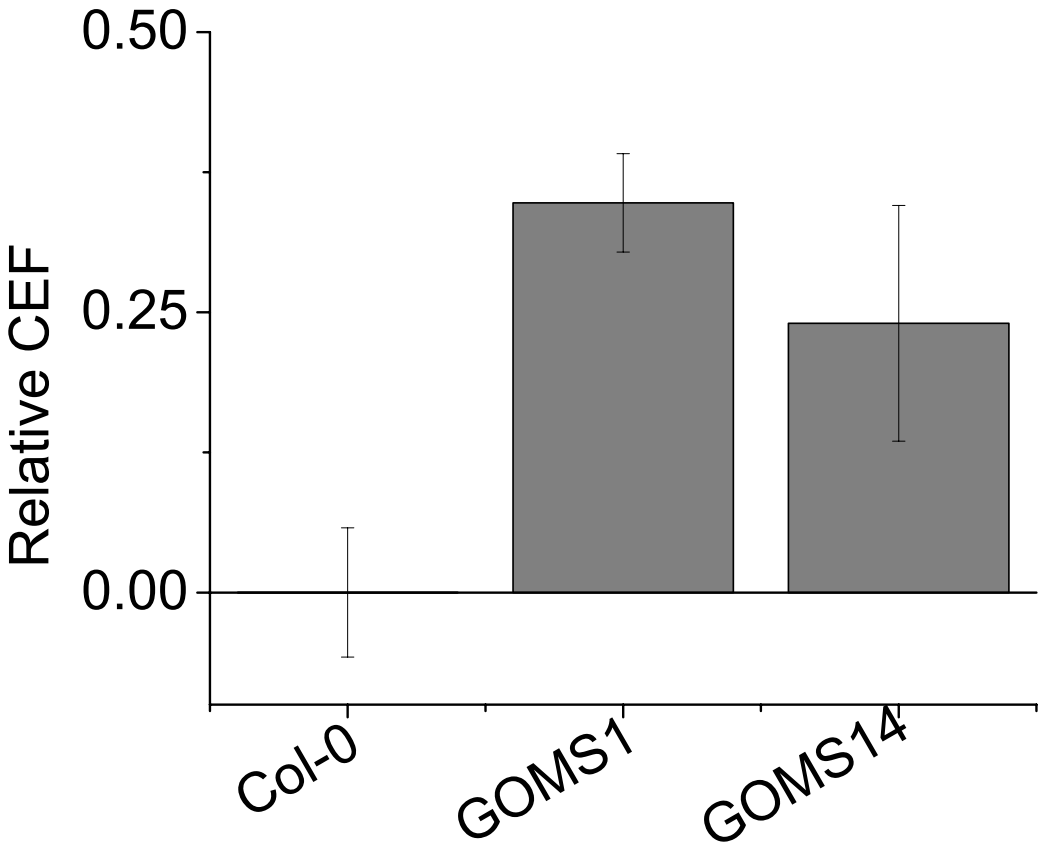

Figure 3.6 Increased CEF in mutants co-transformed with glycolate oxidase (GO) and malate synthase (MS) targeted to the chloroplast. Relative CEF calculated from v_H^+/LEF (Eq. 3.3) in Col-0, GOMS1 and GOMS14. Mean ± SD (n = 3).

3.3.C Kinetics of CEF induction upon activation of H_2O_2 production in GO5

Figure 3.7. shows the kinetics of induction of CEF in the GO5 plants upon rapid initiation of H_2O_2 production. GO5 plants were initially grown under high (3000 ppm) CO_2 conditions to minimize photorespiration (181, 182), therefore preventing the production of H_2O_2 by GO (176, 177). Photosynthetic parameters were measured in intact leaves under 2000 ppm CO_2 and then rapidly switched to ambient air (about 400 ppm CO_2) at time 0, activating H_2O_2 production. Steady state fluorescence and ECS measurements were made every 14 min and analyzed as in Figure 3.3*A* to estimate changes in CEF. Increased CEF appeared with a half time of about 21 min, reaching an apparent maximum relative CEF of 0.62, or a 62% increase in v_H^+/ LEF, in 42 min ($\Delta v_H^+ / v_H^+{}_{LEF}$, see Eq. 3.3, Materials and Methods). No increase in CEF was seen in similarly treated Col-0 leaves (Figure 3.7).

3.3.D Induction of CEF by infiltration of leaves with H_2O_2

In addition to using the GO plants to study CEF, preliminary studies showed a similar response with infiltration of Col-0 with exogenous H_2O_2 [Figure 3.2 in (104)]. Infiltration of leaves with as low as 300 μM (0.001%) H_2O_2 led to induction of significant CEF rates *in vivo* [Figure 3.2 in (104)]. The observed H_2O_2-induced increase in CEF depended on the concentration of H_2O_2 in the infiltrate, with an apparent half-saturation concentration of about 0.01%. Infiltration of Col-0 with 0.001%, 0.01% and 0.1% H_2O_2 increased relative CEF by 21%, 42% and 68% over water infiltrated leaves, respectively. In addition, infiltration of the mutant

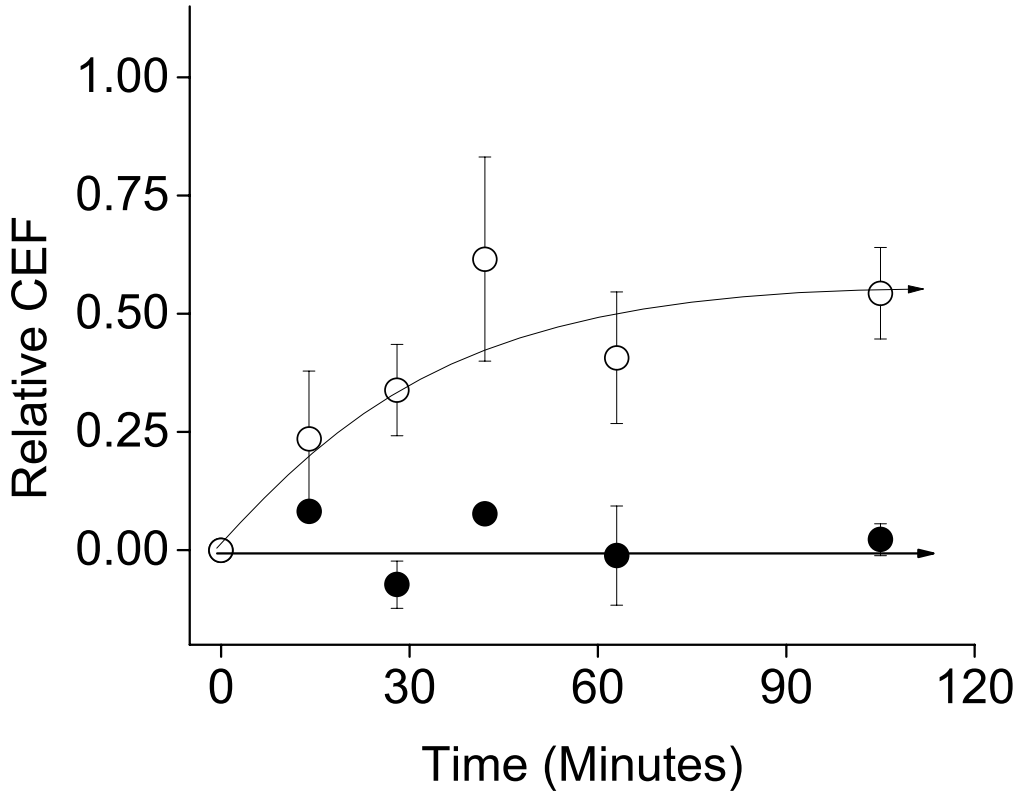

Figure 3.7 Induction kinetics of H_2O_2 activated CEF. CEF activation timecourse in Col-0 (closed circles) and GO5 (open circles). Relative CEF as a function time after switch from 2000 ppm CO_2 to 400 ppm CO_2. Reported values are the mean of 3 biological replicates ± SEM.

pgr5 (82), lacking the antimycin A sensitive-PGR5 dependent CEF pathway, resulted in activation of CEF at near Col-0 levels (65%), while the NDH deficient mutant, *crr2-2* (94, 183), accumulated very low levels of CEF (5%) [Figure 3.7 in (104)].

In addition, we assayed leaves incubated in 0.1% H_2O_2 for an increase in the postillumination chlorophyll fluorescence rise as seen in the GO5 mutant (Figure 3.6). Electrons in the stroma are used to detoxify H_2O_2, and it likely we are consuming these rapidly in the presence of H_2O_2. In the steady state there is a continuous supply of electrons being fed into the system via PS II to fuel CEF plastoquinone reductions, while in the dark our supply cannot be replenished. In order to get a reproducible response to H_2O_2 infiltration, we modified the experiment to include two far-red flashes during the dark interval and performed the measurements under nitrogen. This allows the system to be poised and supply substrate to our plastoquinone reductase. After infiltration with 0.1% H_2O_2 we noticed higher F_0 values, as well as higher F_S values than in the water control (Figure 3.8), which we interpret as an already more reduced quinone pool. When the light is shut off, the decay does not reach water levels. The initial decay was followed with a short far-red pulse to oxidize the quinone pool. After the far-red is turned off, we see a faster and overall larger increase in fluorescence, indicative of re-reduction of the quinone pool in the peroxide treated leaves (Figure 3.8, inset). These results suggest an increase in the rise via dark quinone reduction, and are consistent with steady state measurements of increased CEF activity in response to peroxide infiltration (104).

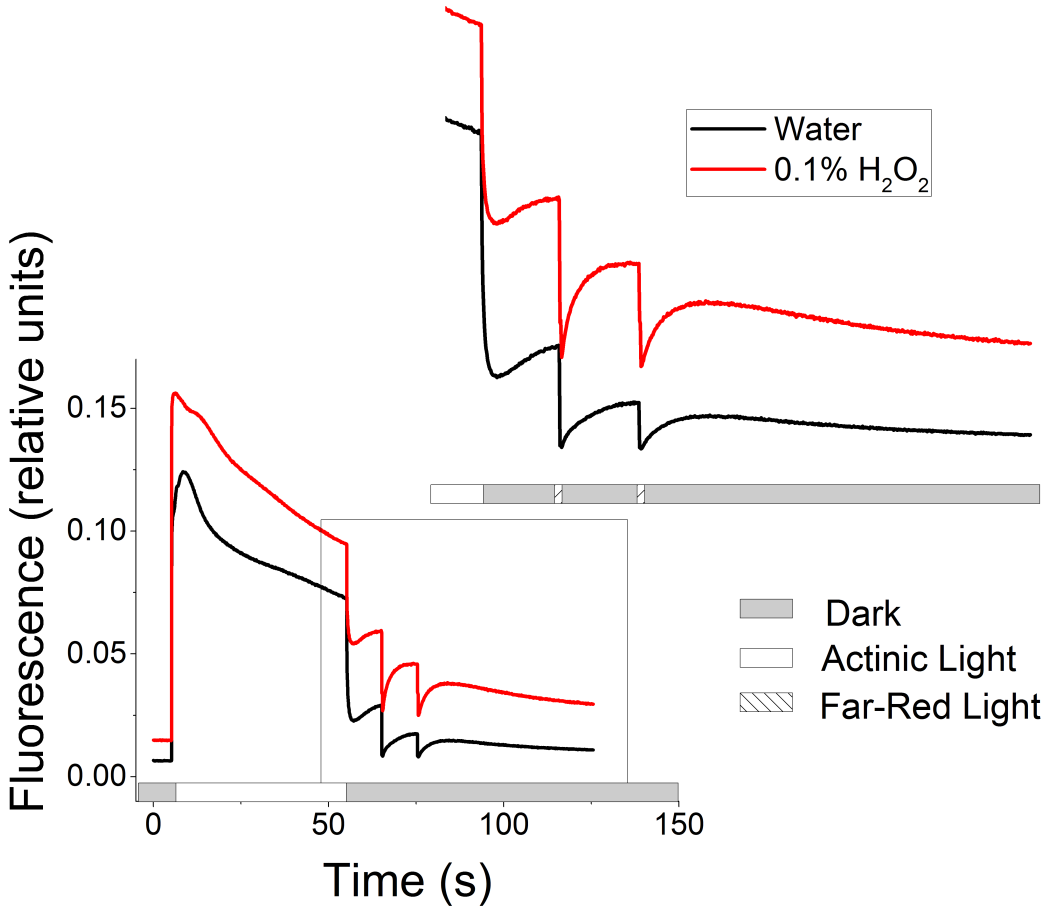

Figure 3.8 Increased dark reduction of the PQ/PQH$_2$ pool in leaves infiltrated with 0.1% H$_2$O$_2$ for 3 hours. Transient chlorophyll fluorescence rise in the dark after illumination with 150 μmol photons m^{-2} s^{-1} (635 nm) under 100% N_2 gas. Water (black) and 0.1% H_2O_2 (red) representative data of 2 independent experiments.

3.4 Discussion

3.4.A CEF correlates with, and is induced by, H_2O_2 production *in vivo*

Past work has shown that mutants in higher plants that accumulate highly reducing stromal redox components also induce elevated CEF, e.g. mutants deficient in FBPase (i.e. *hcef1*), aldolase, and glyceraldehyde-3-phosphate dehydrogenase (69, 70, 79). Similarly, certain environmental conditions, e.g. drought stress, lead to both increased H_2O_2 and elevated CEF (72, 184). In contrast, simply decreasing the rate of photosynthesis without increased of H_2O_2, does not appear to induce CEF (50, 70).

These observations suggest a regulatory link between H_2O_2 production and the activation of CEF. To test this possibility, we used transgenic GO plants, which express a chloroplast targeted glycolate oxidase, and conditionally produce H_2O_2 under photorespiratory conditions. Activation of H_2O_2 production in GO5 had strong effects on photosynthesis, decreasing LEF, increasing thylakoid *pmf* and activating q_E (Figure 3.2). Most strikingly, elevated H_2O_2 production led to strong activation of CEF (Figures 3.4 and 3.3*F*). CEF was similarly induced by infiltration of leaves with H_2O_2 [Figure 3.7, (104)], suggesting that the effects were primarily caused by H_2O_2 and not by GO-induced changes in metabolic intermediates. The activation of CEF was likely too rapid (halftime of about 20 min, Figure 3.7), to involve *de novo* protein synthesis, which is expected to be considerably slower (185, 186), suggesting that H_2O_2 can activate pre-existing CEF machinery. This doesn't exclude long term activation by accumulation of CEF enzymes as seen in previous studies (99) and Figure 3.4*B* (inset), but instead suggests an

additional mechanism of rapid induction of CEF to meet fluctuating ATP demands as proposed by Lascano et al. (102).

3.4.B H_2O_2 activates the antimycin A insensitive pathway

H_2O_2-induced CEF was insensitive to antimycin A (Figure 3.4*B*), implying that it does not involve the PGR5/PGRL1 pathway (82, 112, 113), suggesting instead the involvement of the chloroplast NDH complex, as previously shown in *hcef1* (69). In support of this possibility, an increase in NDH content was seen in GO5 (Figure 2*B*, inset) and the activation of CEF by infiltration with H_2O_2 was inhibited in the NDH-deficient *crr2-2* mutant (104), while the mutant deficient in PGR5 was activated to Col-0 levels. In addition, the NDH complex has been associated with increased activity in the presence of oxidative stress (99, 102), and its activation results in increased post-illumination fluorescence rise, which was increased in the GO5 mutant and after infiltration with H_2O_2 (Figures 3.5 and 3.8).

3.4.C A regulatory role for H_2O_2 in activation of CEF?

We emphasize that CEF is likely to be regulated at a number of processes in different species and under different conditions. Recent work by Takahashi et al. (155) and Lucker et al. (120) suggest that CEF in Chlamydomonas is regulated by stromal redox status, but it is not yet clear which redox components are involved. It is important to point out, though, that CEF in higher plants and Chlamydomonas likely involve distinct protein complexes, mechanisms and regulatory processes (86, 92).

Based on these results, we propose the hypothetical model (Figure 3.9) in which H_2O_2 production can regulate the activation of CEF. A deficit of ATP in the stroma should prevent the

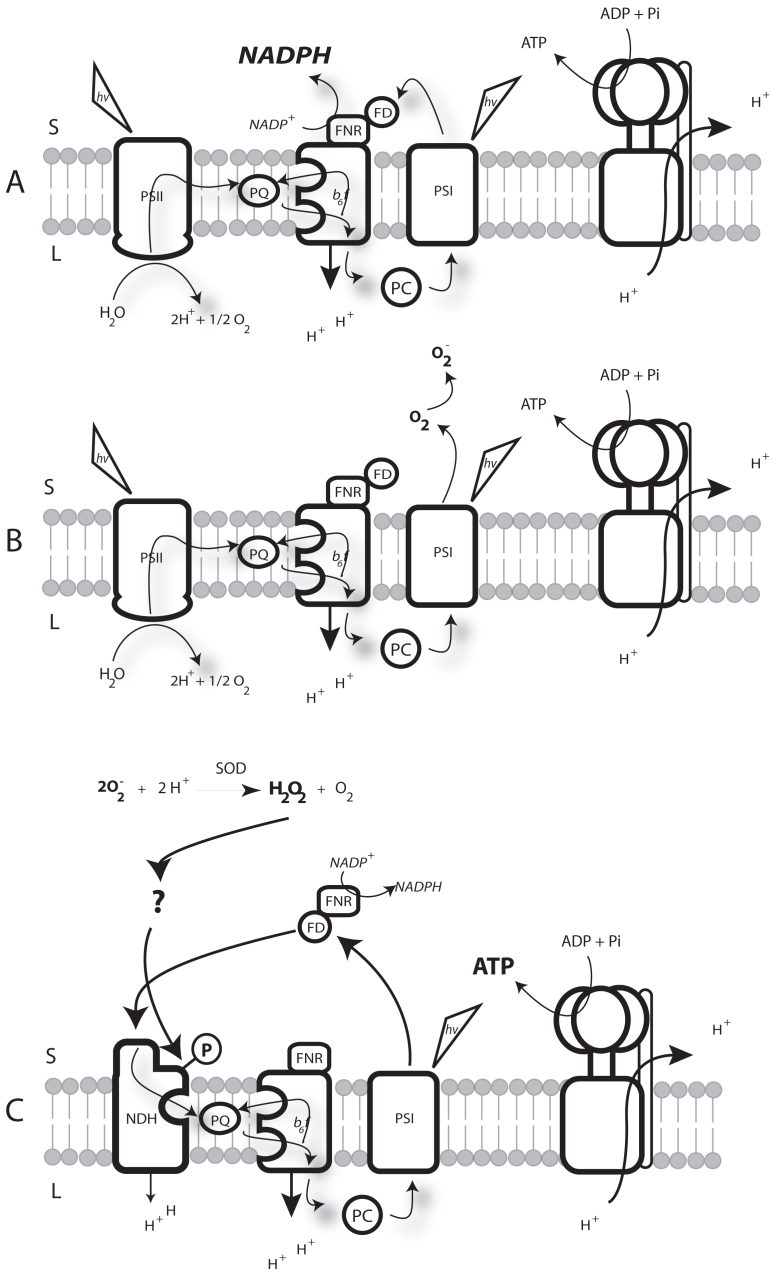

Figure 3.9 Model of CEF activation in response to H_2O_2. A) Imbalances in downstream metabolic processes lead to an excess of reductant in the stroma. B) This leads to increased oxygen reduction from photosystem I and generation of superoxide anion. C) Superoxide is dismutated to H_2O_2 and this signals the phosphorylation of NDH, activating CEF to supply ATP for metabolism, without net reduction of NADPH.

turnover of assimilatory reactions, and cause a buildup of reductants (NADPH, Fd and PS I acceptors) leading to generation of superoxide and H_2O_2. When the rate of H_2O_2 production exceeds that of its detoxification by the water-water cycle (45), it will accumulate and interact with one or more proteins regulating the activity of the antimycin A insensitive pathway of CEF, possibly via a signal cascade leading to the phosphorylation of NDH as suggested by Casano et al. and Lascano et al. (99, 102), or by inactivating CBB enzymes leading to secondary redox or metabolic signaling.

3.5 Methods

3.5A Plant material and growth conditions

All plants, Col-0, GO plants (expressing glycolate oxidase targeted to the chloroplast, 37), and *hcef1* (69) were grown in soil under growth chamber conditions with 16 h light of white light (~80 μmol photons m^{-2} s^{-1}), 8 h dark photoperiod, and a 22°C/18°C (day/night) cycle. Where noted, plants were grown under the same conditions but at high (3000 ppm) CO_2 to prevent the production of H_2O_2 and GO through the photorespiratory pathway.

3.5.B *In vivo* spectroscopic assays

Under ambient CO_2 conditions, the GO plants present with a slightly smaller, pale, and patchy leaf phenotype, however, the chlorotic phenotype disappears at maturity. Therefore, all spectroscopic measurements were made using intact fully expanded leaves in 25-30 day old plants just prior to bolting. To fully induce differential H_2O_2 production, GO5 and all controls were pre-illuminated for 1 hour at 350 μmol photon m^{-2} s^{-1}. Plants were then subsequently dark-adapted for 10 min prior to analysis. Actinic light intensities ranged between 50-600 μmol

photons m^{-2} s^{-1}. Chlorophyll *a* fluorescence yield changes and light induced absorbance changes were measured using on a spectrophotometer/fluorimeter (166) using the techniques described in (69). Saturation pulse chlorophyll *a* fluorescence yield parameters (F_0, F_M, F_S, $F_{M'}$, $F_{M''}$) were recorded as described in (7, 32, 33, 179), using 1 s saturation pulses of approximately 10,000 μmol photons m^{-2} s^{-1}. These measurements were used to estimated the yield of PS II (ϕ_{II}), LEF, and the rapidly reversible component of non-photochemical quenching, q_E (187, 188). LEF was calculated as:

Eq 3.1

$$\phi_{II} * i * 0.4$$

Where *i* is the actinic light intensity. Leaf absorptivity of the GO plants did not differ significantly from Col-0 ($p = 0.78$, n = 3).

The ECS measurements were normalized for variations in leaf thickness and pigmentation by the extent of the rapid rise single-turnover flash induced ECS (33, 69). The ECS_t and t_{ECS} parameters were taken from a first-order exponential decay fit as described in (179). The pmf_{LEF} parameter, estimating relative extents of *pmf* attributable to LEF, was calculated as:

Eq 3.2

$$pmf_{LEF} = LEF/g_{H^+}$$

Postillumination transient chlorophyll fluorescence transients were measured as described in (43).

3.5.C Infiltration of leaves with antimycin A and H_2O_2

Infiltrations of 20 μM antimycin A and 0.1% H_2O_2 were carried out soaking detached leaves between 2 saturated lab tissues in darkness for 3 hours. Successful infiltration with antimycin A was confirmed by loss of the transient fluorescence quenching during photosynthetic induction as previously described (189).

3.5.D Manipulation of gas concentrations

Humidified gas mixtures and ambient air were supplied to the underside of the leaf unless indicated otherwise. Fluctuating CO_2 concentrations were obtained using a gas mixer (LI-COR 6400) connected to a CO_2 gas cylinder. N_2 gas was supplied by a tank of 100% N_2 (Airgas).

3.5.E Measurement of H_2O_2 production in leaves

Hydrogen peroxide was detected by DAB staining as described in (104), and by resorufin fluorescence. Resorufin is the product of the peroxidase catalyzed reaction with Amplex Red and H_2O_2. H_2O_2 was extracted from leaf discs in 50 mM phosphate buffer (pH 7.6) and incubated with 2U horseradish peroxidase and 10 μM Amplex Red (Invitrogen) and resorufin fluorescence was normalized to the average Col-0 H_2O_2 content. For GO5 plants, leaf age was as describe above for spectroscopic assays. For *hcef1*, leaf age was as described for spectroscopic measurements in Livingston et al. (69).

3.5.F Protein extraction and western blot

Total leaf protein was extracted from fully mature rosettes (described above) as described in (69) and normalized to chlorophyll. Western blotting was performed as described in (69), using anti-NDH-18 (T. Shikanai, Kyoto University).

3.5.G Quantifications of CEF

To quantify relative CEF, which should be proportional to the increase in slope seen in Figure 3.3*A*, we used an approach modified from (104) and (120), in which relative CEF is expressed as a fractional increase over the v_H^+ due to LEF ($\Delta\, v_H^+ / v_{H^+LEF}$) and is calculated by:

Eq. 3.3

$$Relative\ CEF \propto \left(m_{(CEF+LEF)} - m_{(LEF)}\right)/m_{(LEF)}$$

where $m_{(CEF+LEF)}$ and $m_{(LEF)}$ are the linear slope of v_H^+ plotted against LEF in treated or mutant leaves and untreated or Col-0 leaves respectively. If the H^+/e^- of CEF was known, this could potentially be converted to electron flux, however, in higher plants possessing NDH, it is possible that CEF involves a proton pump that could significantly increase H^+/e^- (discussed in chapter 5). Therefore, we have chosen to omit this conversion and present relative CEF as the fraction increase of v_H^+ over LEF.

3.5.H Statistical analysis

Descriptive statistics and figures were generated using Origin 9.0 software (Microcal Software), and statistical analyses were performed using MATLAB R2012a (The Mathworks) or

Microsoft Excel. All p-values less than 0.05 were considered statistically significant and are noted within the text.

3.6 Author contributions

All data presented, except where noted, were obtained by Deserah D. Strand. However, significant intellectual contribution was also made by the co-authors. Specifically, Veronica G. Maurino suggested the experimental setup in Figure 3.7. and Aaron K. Livingston generated extensive preliminary data, which has been referenced within, as well as a preliminary draft of the manuscript.

3.7 Acknowledgements

The authors would like to thank Drs. Nicholas Fisher, Atsuko Kanazawa, and Jeffrey Cruz for helpful discussions. We would like to also thank Dr. Toshiharu Shikanai for his kind donation of *pgr5* and *crr2-2* seed. Work performed at MSU was funded by Grant DE-FG02-11ER16220 from the Photosynthetic Systems program from Division of Chemical Sciences, Geosciences, and Biosciences, Office of Basic Energy Sciences of the US Department of Energy (to David M. Kramer). The development of the GO mutants was funded by the Deutsche Forschungsgemeinschaft (DFG) through grant MA2379/11-1 (to Veronica G. Maurino).

Chapter 4

Uncoordinated expression of chloroplast proteins leads to H_2O_2 accumulation and activation of cyclic electron flow around photosystem I[7]

Deserah D. Strand, Aaron K. Livingston, Mio Satoh-Cruz, Tyson Koepke, Heather M. Enlow, Jeffrey A. Cruz, Deepika Minhas, Kim K. Hixson, Kaori Kohzuma, Amit Dhingra, Mary Lipton, and David M. Kramer

[7] Preliminary data for this manuscript has previously appeared in (104).

4.1 Abstract

In recent work, we identified a class of mutants in Arabidopsis that exhibit high rates of cyclic electron flow around photosystem I (CEF). Here we describe a new member of this class, high cyclic electron flow 2 (*hcef2*), possessing a nonsense mutation in the TADA1 (tRNA adenosine deaminase arginine) locus, coding for a plastid-targeted tRNA editing enzyme required for proper codon recognition. Both *hcef2* and *tada1* show increased thylakoid proton motive force, light-driven proton translocation relative to electron fluxes and increased dark reduction of plastoquinone, indicating increased CEF activity. Similar results were obtained for mutants defective in chloroplast translation, including *prsp3,* which is partially deficient in protein translation at the level of chloroplast ribosome. These mutants showed elevated H_2O_2, which we have previously shown to increase CEF. Inhibitor sensitivity and protein expression levels imply that increased CEF in *hcef2* occurs through the NADPH:plastoquinone oxidoreductate (NDH) pathway. Intriguingly, high-resolution proteomics showed that *hcef2* accumulated abnormal stoichiometries of proteins of multi-subunit complexes, including photosystems I and II, the cytochrome b_6f complex, and ATP synthase. These findings suggest that loss of coordination of plastid protein levels leads to accumulation of misassembled complexes, ROS production and subsequent activation of CEF through the NDH complex.

4.2 Introduction

In higher plants, light is harvested by two distinct photochemical reaction centers, photosystem II (PS II) and photosystem I (PS I) that stimulate electron transfer through series of redox carriers to store solar energy in forms to drive biochemical processes (3). When PS I and PS II are electronically connected in series, they drive linear electron flow (LEF), which results in the oxidation of water and the reduction of $NADP^+$ to NADPH. The electron transfer reactions

of LEF are coupled to the uptake of protons from the chloroplast stroma and their deposition into the lumen, establishing an electrochemical gradient of protons, or proton motive force (*pmf*). Protons are taken up during reduction of plastoquinone at the Q_B site of PS II and the Q_i site of the cytochrome b_6f complex (b_6f). Protons are released into the lumen during water oxidation at the oxygen evolving complex (OEC) of PS II and during plastoquinol oxidation at the Q_o site of the b_6f complex. The *pmf* generated in these electron and proton transfer reactions drives the synthesis of ATP at the chloroplast ATP synthase.

The *pmf* is also a central regulator of the light reactions through its effects on lumen pH dependent components of non-photochemical quenching (NPQ) (1), and electron flow through the b_6f complex (26, 190). The *pmf*, in turn, is modulated in response to environmental and metabolic conditions (32, 34, 72, 78) (Chapter 1), coordination of photosynthetic electron transport and carbon metabolism. The major points of *pmf* regulation lie at the ATP synthase and with cyclic electron flow (2, 25, 78). Both of these processes have different effects on the stoichiometry of the photosynthetic products ATP and NADPH produced from the light reactions. While modulation of the ATP synthase results in unaltered ATP:NADPH output of the light reactions, CEF increases the ATP:NADPH output.

Cyclic electron flow around PS I (CEF) involves PS I but not PS II (112). Electrons from PS I are transferred to plastoquinone (PQ) forming plastoquinol (PQH_2), which is subsequently oxidized by the b_6f complex and shuttled back to PS I by plastocyanin. The uptake of protons in the Q-cycle, catalyzed by the b_6f complex, results in translocation of protons from the chloroplast stroma to the lumen and thus contributes to the formation of *pmf* and ATP synthesis without net

reduction of NADPH (115). In this way, CEF can act to augment an ATP deficit, and has thus been implicated in balancing the chloroplast energy budget, and is thus thought to be physiologically important under conditions of elevated ATP demands. For example, CEF is induced under environmental stresses including drought (72, 191), high light (157), and chilling (192) where ATP may be needed to repair cellular machinery, maintain ion homeostasis, transport proteins, etc. CEF is also thought to supply ATP for CO_2 concentrating mechanisms, including the C_4 cycle in plants (91) and the carbon concentrating mechanism (CCM) in green algae (120), and appears to be critical under anoxia (153) or when CO_2 is limiting (120), in the green alga *Chlamydomonas reinhardtii*.

It is also possible that CEF plays a regulatory role in photosynthesis by acidifying the thylakoid lumen and thus activating the photoprotective q_E response and slowing electron flow at the b_6f complex (82, 157). It is important to recognize that uncontrolled activation of CEF will also result in a change to the ATP/NADPH output stoichiometry, a situation that can lead to deleterious secondary effects. Thus, chloroplasts also have alternate mechanisms of regulating lumen acidification that do not result in alteration of ATP/NADPH, including modulation of ATP synthase rates, and these appear to play primary roles in regulating photoprotection (reviewed in Chapter 1).

Several alternative CEF pathways have been proposed, that involve different PQ reductases, including the PGR5/PGRL1 dependent, antimycin A sensitive pathway (82, 87, 112, 153), the Q_i site of the b_6f complex (110), and the NAD(P)H dehydrogenase complex (NDH) (84, 85). It is possible that different CEF pathways are activated in different species, and/or

under different conditions. To make matters more complex, a range of regulatory signals have been proposed for CEF, including sensing of ATP/ADP ratios (64, 109), chloroplast redox status (111, 119, 152, 153), metabolic intermediates (68), state transitions (92, 106), calcium (154), and reactive oxygen species (99, 102, 104) (see Chapter 3).

Previously, we initiated an effort to discover new CEF structural and regulatory components by isolating mutants of Arabidopsis (*Arabidopsis thaliana*) with constitutively elevated CEF, which we named high cyclic electron flow (*hcef*) mutants (69, 70). The first of these mutants to be reported, *hcef1*, was mapped to a missense mutation in the chloroplast-targeted fructose 1,6 bisphosphatase (FBPase), and appears to *indirectly* activate CEF by disrupting redox balance (70) (see Chapter 3), possibly by activating a futile metabolic cycle that consumes ATP (69). Results from a series of double mutants and inhibitors indicate that CEF activated in *hcef1* involves the chloroplast NDH complex and not the proposed PGR5/PGRL1 pathway.

In this work, we report on the isolation and characterization of *hcef2*, which was mapped to an unexpected locus involving tRNA editing. Despite a very different mutation, and proteomic consequences, *hcef2* is found to have similar levels of CEF activation and photoprotection as *hcef1*. This has strong implications for the role of CEF, including the possible involvement of reactive oxygen species in its regulation, and the critical importance of strict regulation of plastid proteome stoichiometries.

4.3 Results

4.3.A Genetic selection of *hcef* mutants

As described in Livingston et al. (69),we selected *hcef* mutants using a multi-stage selection process from a pool of ethyl methanesulfonate (EMS) mutagenized seeds (Columbia

ecotype [Col-0], Lehle seeds [M2E-02-05]). We first screened for plants that displayed high photoprotective 'exciton quenching' (q_E) phenotypes using chlorophyll *a* fluorescence imaging. We then subjected this population to secondary screening using direct measurements of light-driven electron transfer, based on analysis of chlorophyll *a* fluorescence and proton fluxes based on analysis of the electrochromic shift (ECS) signal (7, 69, 178, 179) to identify mutants with elevated CEF.

4.3.B Growth of *hcef2*

The *hcef2* mutant grew photoautotrophically in soil, at a decreased rate as described in (104) and shown in Figure 4.1. The *hcef2* mutant displayed a slightly pale appearance owing to lower accumulation of chlorophyll compared to Col-0 levels per leaf area (157.8 mg/m^2 ± 5.7 and 271.6 mg/m^2 ± 5.1 respectively, p = 0.00001, student's t-test, n = 3).

4.3.C Photosynthetic electron transfer properties of *hcef2* compared to Col-0: responses of the photosynthetic electron transport to the *hcef2* mutation

Chlorophyll *a* fluorescence was used to estimate linear electron flow (LEF) and q_E responses, accounting for differences in leaf absorptivity using the approach described in (69, 193). The *hcef2* mutant showed suppressed LEF rates across all light intensities used, about 4-fold lower than Col-0 at saturating light (21.2 ± 1.7 and 82.6 ± 2.8 μmol e^- m^{-2} s^{-1}, respectively, ~480 μmol photons m^{-2} s^{-1}) (Figure 4.2*A*). The half saturation irradiance for LEF in *hcef2* (~90 μmol photons m^{-2} s^{-1}) was ~65% that of Col-0 (~140 μmol photons m^{-2} s^{-1}). In addition to differences in PS II electron transfer rates, Col-0 and *hcef2* have distinct 77K fluorescence emission spectra (Figure 4.2*B*), reflecting large changes in the composition and state distribution

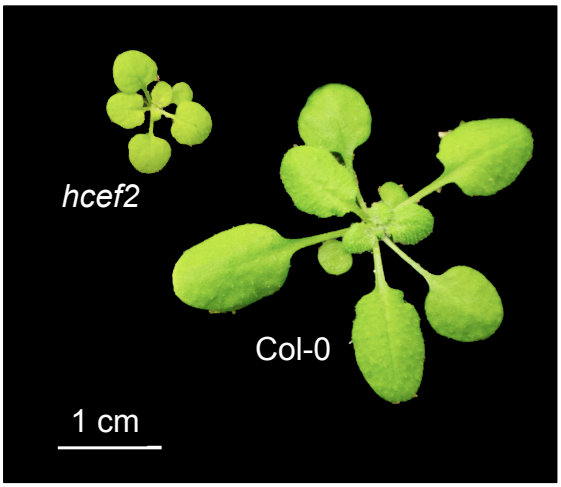

Figure 4.1 Growth phenotype of *hcef2* at 24 days. Plants were grown photoautotrophically on soil with a 16:8 light/dark photoperiod at ~100 μmols photons m^{-2} s^{-1}, white light. For interpretation of the references to color in this and all other figures, the reader is referred to the electronic version of this dissertation.

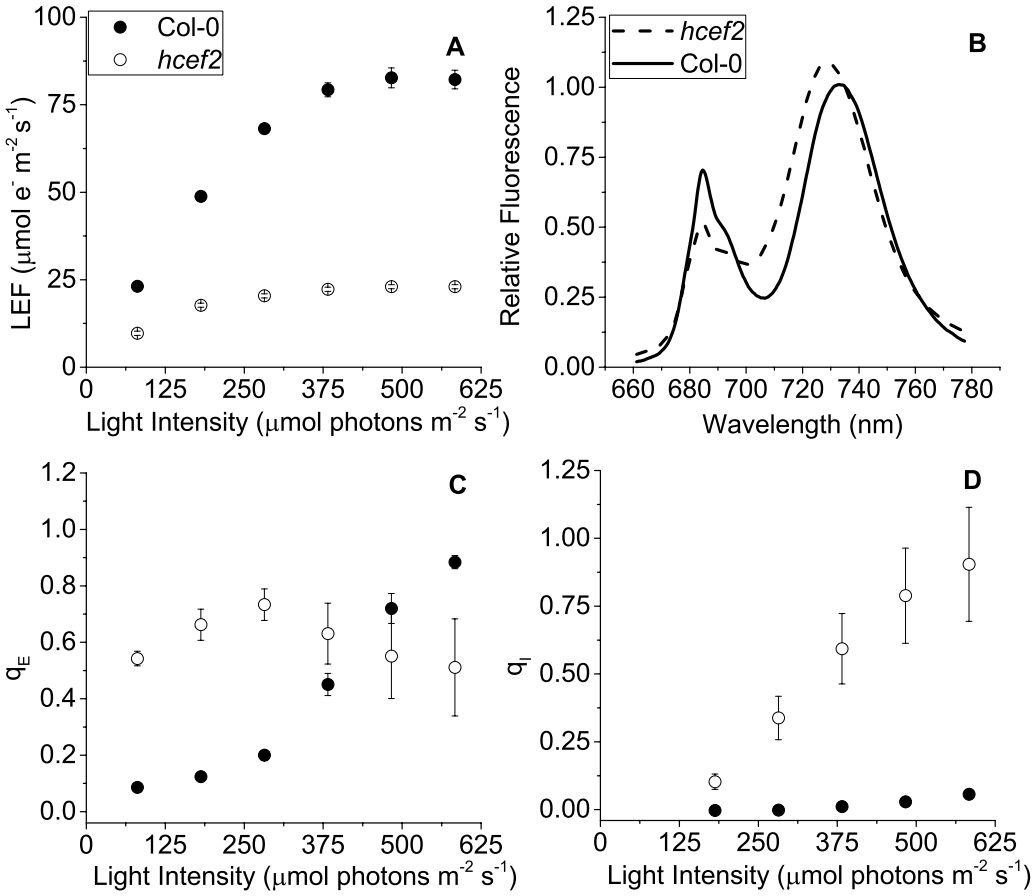

Figure 4.2 Effects of *hcef2* on photosynthetic properties. A) Photosynthetic linear electron flow (LEF) as a function of light intensity. Col-0 (closed circles) and *hcef2* (open circles). Mean ± SD, n = 3. B) 77k emission spectra. Col-0 (solid line) and *hcef2* (dashed line). Emission spectra are representative of 3 independent experiments. C) Energy dependent exciton quenching (q_E) as a function of light intensity. Col-0 (closed circles) and *hcef2* (open circles). Mean ± SD, n = 3. D) Photoinhibition (q_I) as a function of light intensity. Col-0 (closed circles) and *hcef2* (open circles). Mean ± SD, n = 3.

of photosynthetic antenna complexes. The *hcef2* mutant shows a large increase in the relative emission of long-wavelength (~735 nm) emission associated with PS I antenna complexes, compared to shorter wavelength (685 nm) emission reflecting antenna complexes associated with PS II [for review see (194)]. In addition, the PS I associated peak showed a strong blue shift, likely reflecting dissociation or loss of LCHI complexes from the PS I core (see below).

Col-0 showed typical sigmoidal responses of q_E to light intensity (Figure 4.2*C*), with an apparent half-saturation point at 375 μmol photons m^{-2} s^{-1} reaching approximately 0.9 at the highest light intensity tested, similar to previous results on plants grown under similar conditions (69). The photoprotective responses of *hcef2* were distinct from those of Col-0, exhibiting high levels of q_E even at low light intensities. For example, at 80 μmol photons m^{-2} s^{-1}, q_E in *hcef2* was ~4-fold higher than in Col-0 (0.54 ± 0.026, 0.09 ± 0.12, respectively) (Figure 4.2*C*). In *hcef2*, q_E reached a maximum at about 280 μmol photons m^{-2} s^{-1} with a value of 0.73 (± 0.055, n = 3), and decreased slightly at higher intensities. This decrease in q_E likely reflects the accumulation of photodamage at higher light in *hcef2*, which is seen as an increase in photoinhibition, or q_I (Figure 4.2*D*). Estimates of q_I in *hcef2* are likely even lower than reported due to an already low maximal photochemical efficiency of PS II in dark-adapted leaves of *hcef2* (0.59 ± 0.066) compared to Col-0 (0.80 ± 0.003).

4.3.D Responses of the photosynthetic proton circuit of *hcef2*

We analyzed the dark interval relaxation kinetics of the electrochromic shift (ECS) to analyze the proton circuit of photosynthesis. The extent of light-driven *pmf* was estimated from the total amplitude of the decay signal (ECS_t); the relative rate of light-driven proton flux (v_H^+)

was estimated from the initial slope of the ECS decay; and the conductivity of the thylakoid membrane to protons (g_H^+), which reflects the activity of the chloroplast ATP synthase, was estimated from the lifetime of the ECS decay (78, 178, 179). From these values we calculated relative electron and proton fluxes through thylakoid components, and inferred the activation state of CEF (69, 70).

The *hcef2* mutant showed strongly decreased LEF compared to Col-0 (Figure 4.2*A*), yet produced substantially *higher* light-driven *pmf*, as indicated by increased ECS_t values as a function of LEF (Figure 4.3*A*). At an LEF value of 20 μmol electrons m^{-2} s^{-1}, *hcef2* had a 4-fold higher ECS_t than Col-0 (2 ± 0.1 and 4.2 ± 0.075 miliabsorbance units, respectively, n = 3). The increased *pmf* is associated with qualitatively elevated q_E in *hcef2* (Figure 4.3*B*), as would be expected based on the lumen pH-dependence of the q_E response (1). While Col-0 showed a sigmoidal dependence of q_E on ECS_t, as previously reported (26), *hcef2* showed high activation of q_E at even low ECS_t values, but saturated at relatively low LEF or ECS_t extents (Figures 4.3*B* and 4.3*C*). The higher sensitivity of q_E responses in *hcef2* was more sensitive to estimated *pmf* changes (ECS_t) in *hcef2* compared to Col-0, indicating additional factors beyond the *pmf* play a role in modulating the q_E response in *hcef2* (discussed below).

As discussed earlier (32, 78), thylakoid *pmf* can be increased with respect to LEF by either accelerating proton influx through CEF or retarding proton efflux from the lumen by inactivating the chloroplast ATP synthase. To distinguish between these possibilities, we assessed the relative proton conductivity of the thylakoid membrane (g_H^+) using the ECS decay

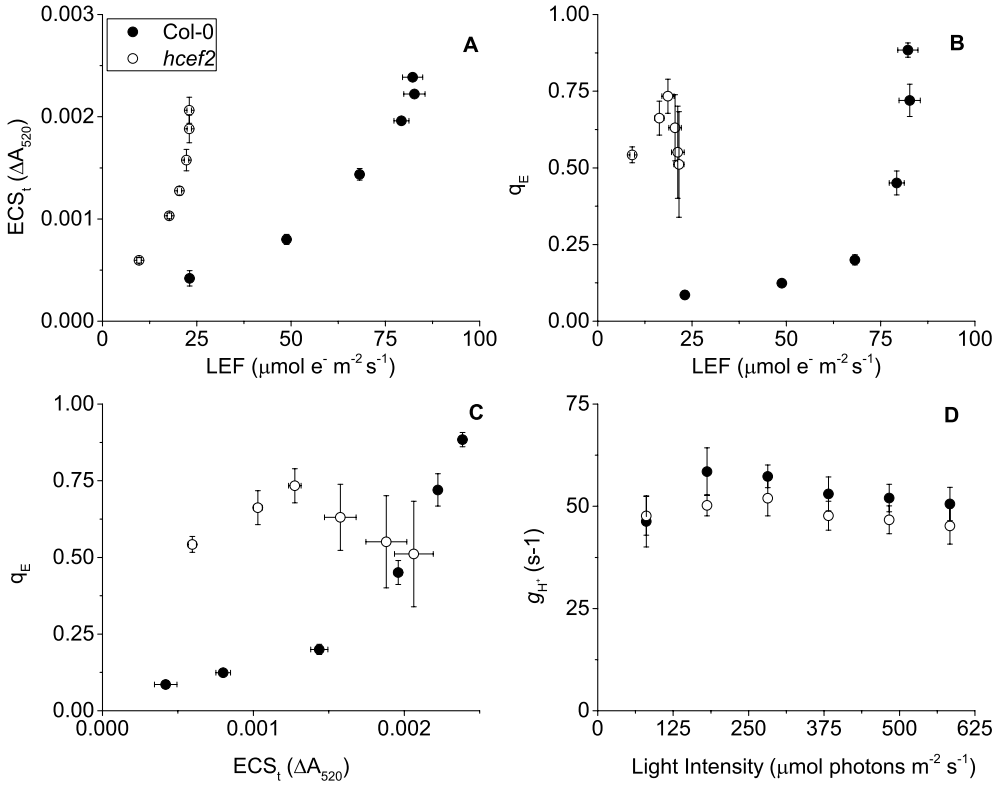

Figure 4.3 Effects of *hcef2* on the photosynthetic proton circuit. A) Light driven transthylakoid *pmf* as measured by ECS_t as a function of LEF. Col-0 (closed circles) and *hcef2* (open circles). Mean ± SD, n = 3. B) q_E as a function of LEF. Col-0 (closed circles) and *hcef2* (open circles). Mean ± SD, n = 3. C) q_E as a function of ECS_t. Col-0 (closed circles) and *hcef2* (open circles). Mean ± SD, n = 3. D) Thylakoid proton conductivity (g_H^+) as a function of light intensity. Col-0 (closed circles) and *hcef2* (open circles). Mean ± SD, n = 3.

lifetime measurements. As shown in Figure 4.3*D*, g_H^+ values for Col-0 and *hcef2* were nearly identical, varying by less than 10%, indicating that the observed increases in *pmf* and q_E responses in *hcef2* could not be explained by down-regulation of the chloroplast ATP synthase.

4.3.E Estimates of CEF in *hcef2*

We next used three different approaches to directly assess the activation of CEF in *hcef2*. In the first approach, we compared proton flux estimated from initial decay rates of the ECS signal (v_H^+) with LEF estimated from chlorophyll *a* fluorescence parameters. When v_H^+ was plotted as a function of LEF (Figure 4.4*A*), *hcef2* showed a ~3-fold increase in slope over Col-0 (0.0039 ± 0.0011 and 0.0013 ± 0.0003, respectively, p = 0.0103 ANCOVA, n = 3), indicating an increase in the light-driven fluxes of protons over LEF. Because LEF produces a fixed H^+/e^- stoichiometry, the additional protons would need to be supplied independently of PS II, i.e. by activation of CEF.

In the second approach (Figure 4.4*B*), we compared relative light-driven *pmf*, estimated by the ECS_t parameter with calculations of the *pmf* from LEF alone (pmf_{LEF}) (35). This approach is based on different assumptions and largely independent of extrinsic factors, such as the leaf content of ECS-responding carotenoids, etc. (33, 179). The dependence of ECS_t on pmf_{LEF} was approximately 3-fold higher in *hcef2* compared to Col-0 (0.0037 ± 0.0005 and 0.0012 ± 0.0003, respectively, $p < 0.0001$ ANCOVA n = 3), indicating that *hcef2* accumulates larger extents of *pmf* than can be attributed to changes in LEF, supporting the conclusion that CEF is strongly activated in *hcef2*. It should be noted that estimates of LEF by analysis of chlorophyll fluorescence depend on the fraction of light energy absorbed by PS II. The 77K fluorescence

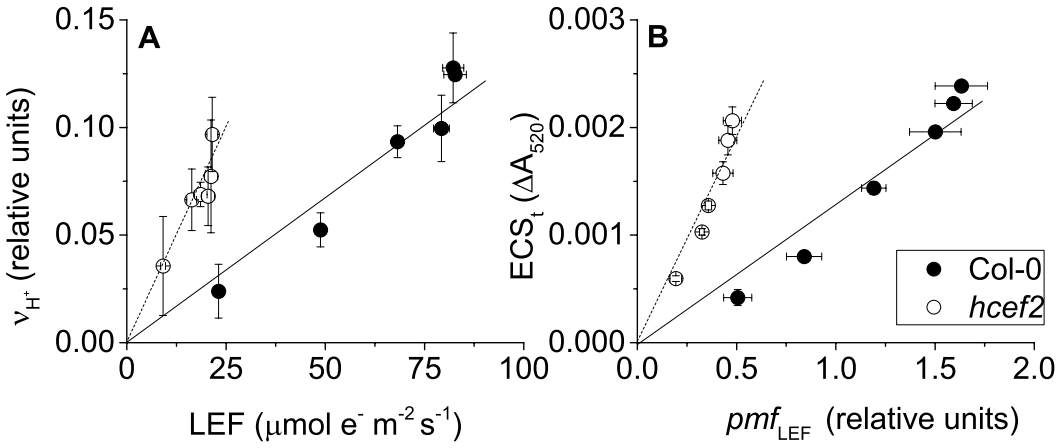

Figure 4.4 Activation state of CEF in Col-0 and *hcef2*.

A) Light driven transthylakoid proton flux (v_H^+) as a function of LEF. Col-0 (closed circles) and *hcef2* (open circles). Mean ± SD, n = 3. B) ECS_t as a function of *pmf* generated by LEF (pmf_{LEF}). Col-0 (closed circles) and *hcef2* (open circles). Mean ± SD, n = 3.

emission spectra (Figure 4.2*B*) show a decrease in the relative fluorescence of PS II at 685 nm relative to that attributable to PS I at about 735 nm, possibly indicating a decrease in PS II relative to PS I excitation. In any case, the possible error introduced by this antenna change would lead to an overestimate of LEF, and therefore an underestimation increased CEF for the data in Figures 4.4*A* and 4.4*B*.

In the third approach we measured postillumination changes in chlorophyll *a* fluorescence that indicate the non-photochemical reduction of the PQ pool associated with activation of the NDH-pathway for CEF (79, 84, 85, 180). Typically, such fluorescence rise experiments are conducted by exposing leaves to continuous illumination for a few minutes and the fluorescence yield is followed after switching off the light. An initial decrease of fluorescence is caused by rapid oxidation (on tens to hundreds of milliseconds time scale) of Q_A by PQ. When NDH is active, this initial phase is followed by a slower fluorescence rise as PQ becomes progressively reduced by NDH. During initial trials, we found that the decay and rise phases were more clearly resolved when leaves from growth conditions were partially dark-adapted (for 10 min) and exposed to short (10 ms duration) pulses of intense actinic light. As shown in Figure 4.5, each pulse resulted in increased fluorescence yield reflecting light-induced reduction of Q_A. The fluorescence yield then deceased in multiple phases after each flash. A rapid phase, with a half time of less than a few ms, reflected the equilibration of Q_A and PQ redox states in the dark. In Col-0 (Figure 4.5*A*, black line), each pulse resulted in progressively more reduced PQ pool as indicated by the increases in dark fluorescence levels. This interpretation was confirmed by the decreased in fluorescence yield induced by far-red (730 nm) illumination (Figure 4.5*A*, gray line), which preferentially excites PS I photochemistry resulting

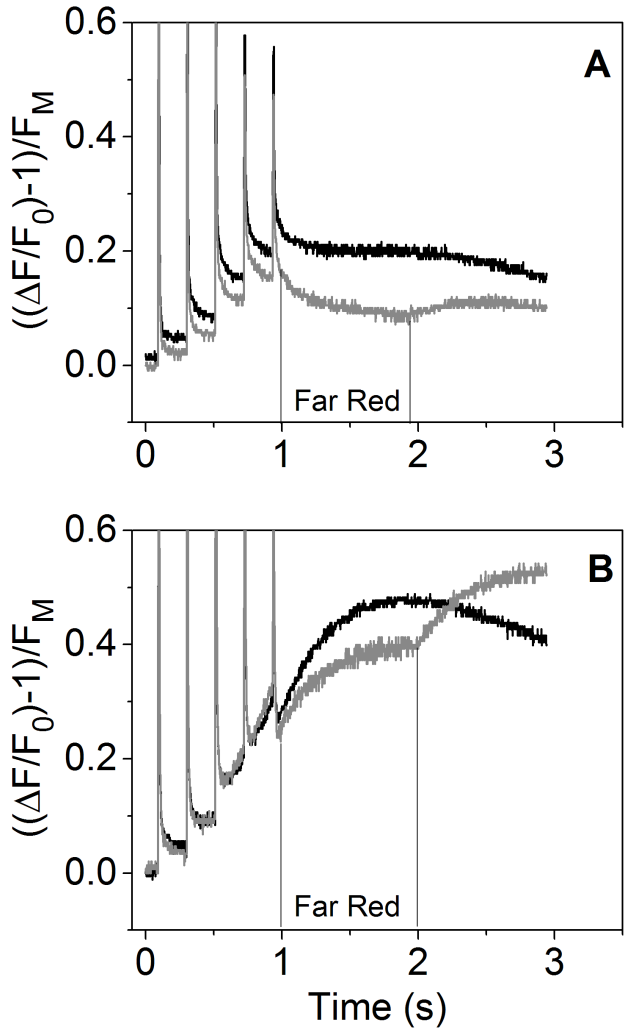

Figure 4.5 Kinetics of postillumination fluorescence rises in Col-0 and *hcef2*[8].

Relative fluorescence yield changes in Col-0 **(A)** and *hcef2* **(B)** in the dark after a series of actinic flashes (black) and changes with far-red illumination after the actinic flashes (gray). Data is representative of 3 independent experiments.

[8] Data for Figure 4.5 was kindly provided by Dr. Jeffrey Cruz.

in net oxidation of the PQ pool and Q_A. Cessation of far-red illumination resulted in a slow return to higher fluorescence yields indicating the activity of a PQ reductase. These phenomena were also observed in *hcef2* (Figure 4.5*B*, black line), but were stronger and more rapid. In fact, a distinct fluorescence rise phase was seen after the third flash in *hcef2* that we interpret as indicating strong activation of PQ reductase activity. The interpretation was confirmed by application of far-red illumination (Figure 4.5*B*, gray line), which resulted in substantial quenching of the signal. Rise occurred after each additional flash and continued during the following dark period. We conclude that *hcef2* has a substantially higher activity of PQ reductase than Col-0.

4.3.F Antimycin A infiltration of *hcef2*

In Col-0 we observed no significant differences in the ratio of v_H^+/LEF between leaves infiltrated with water or 20 μM antimycin A (Figure 4.6, 0.0015 ± 0.0025 and 0.00158 ± 0.00026, respectively $p > 0.05$ $n = 3$). The elevated ratio of v_H^+/LEF in *hcef2* was also unaffected by 20μM antimycin A (Figure 4.6, 0.00551 ± 0.0014 and 0.00461 ± 0.00095, respectively $p > 0.05$ $n = 3$), indicating *hcef2* CEF is antimycin A insensitive.

4.3.G Identification of the genetic locus of *hcef2* as TADA1

Map based cloning and deep sequencing was used to identify the probable genetic locus for the *hcef2* mutation to a point mutation in TADA1 (At1G68720). This C>T mutation introduces a stop codon at R643 (Figure 4.7), eliminating the C-terminus of the protein containing the active site required for function (195, 196).

The T-DNA insert line GK-119G08 contains an insertion in the first exon in At1G68720 (196). Similar to *hcef2*, *tada1* showed strongly increased CEF as indicated by a 5-fold increase

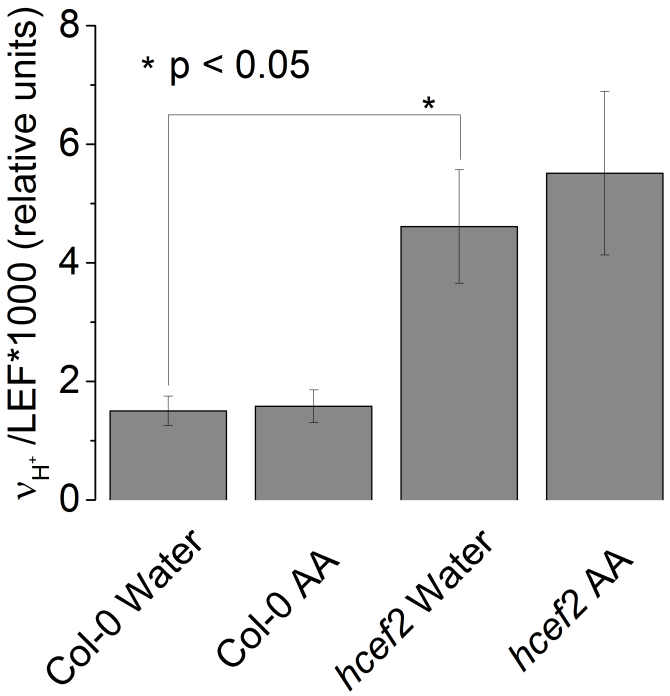

Figure 4.6 Antimycin A insensitivity of CEF in *hcef2*. Slope of v_H^+/LEF in leaves infiltrated with either water or antimycin A (AA). Mean ± SD, n = 3.

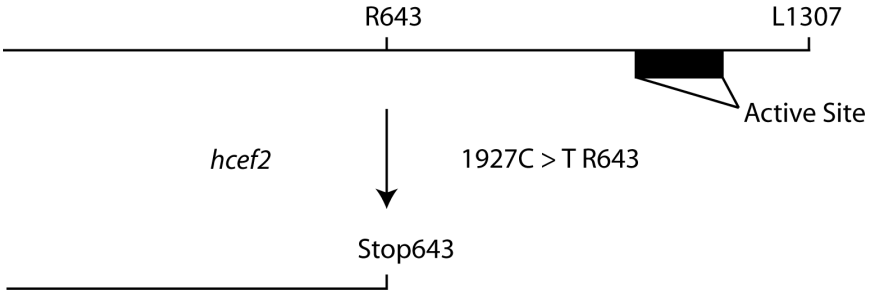

Figure 4.7 Introduction of a stop codon into the TADA1 locus in *hcef2*. Translation is terminated before the active site of TADA1, leading to the loss of function[9].

[9] The genetic mapping leading to the creation of *hcef2* leading to the creation of Figure 4.7 was performed by Dr. Mio Satoh-Cruz.

relative to Col-0 of v_H^+/LEF (0.0063 ± 0.003 and 0.0011 ± 0.0004, respectively, $p < 0.05$ n = 3) (Figure 4.8*A*) as well as in ECS_t/pmf_{LEF} (0.0057 ± 0.001 and 0.0011 ± 0.0003, respectively, $p < 0.001$, n = 3) (Figure 4.8*B*) relationships. These results indicate increased CEF equal to or greater than *hcef2* and support the identification of *hcef2* mutation within TADA1. Likewise, GK-119G08 showed no statistical difference from *hcef2* in leaf chlorophyll content or absorptivity (data not shown).

Delannoy et al. (196) showed that the *tada1* phenotype was reversed by expressing the C-terminus of TADA1 behind a 35S promoter. We transferred this construct by crossing the complimented *tada1* mutant with *hcef2* followed by segregation and genotyping for homozygocity of the *hcef2* mutation, lack of the *tada1* insertion, and possession of the P35S:ΔNTADA1 construct. Verified lines were analyzed spectroscopically for suppression of the *hcef2* phenotype. The increased v_H^+ as a function of LEF seen in *hcef2* (Figure 4.4*A*) was completely suppressed in the *hcef2* P35S:ΔNTADA1 line (Figure 4.9), i.e the slope returned to Col-0 values (0.0013 ± .00029 and 0.0013 ± 0.00031, respectively, $p > 0.05$, ANCOVA n = 3). These results confirm TADA1 as the site of the mutation causing elevated CEF in *hcef2*.

4.3.H Translational defects in the chloroplast lead to increases in CEF.

The TADA1 gene codes for a tRNA editing enzyme, suggesting that a defect in translation machinery somehow leads to increased CEF. To test if this effect is a general consequence of decreased chloroplast translation efficiency, we assayed for increased CEF in mutants defective in nuclear encoded peripheral ribosomal proteins. The *prsp3* mutant contains a T-DNA insert in the At1g68590 locus with a complete loss of PRSP3 (197). The *rps17* mutant contains a T-DNA insert in the At1g79850 locus, resulting in decreased expression of RPS17 by

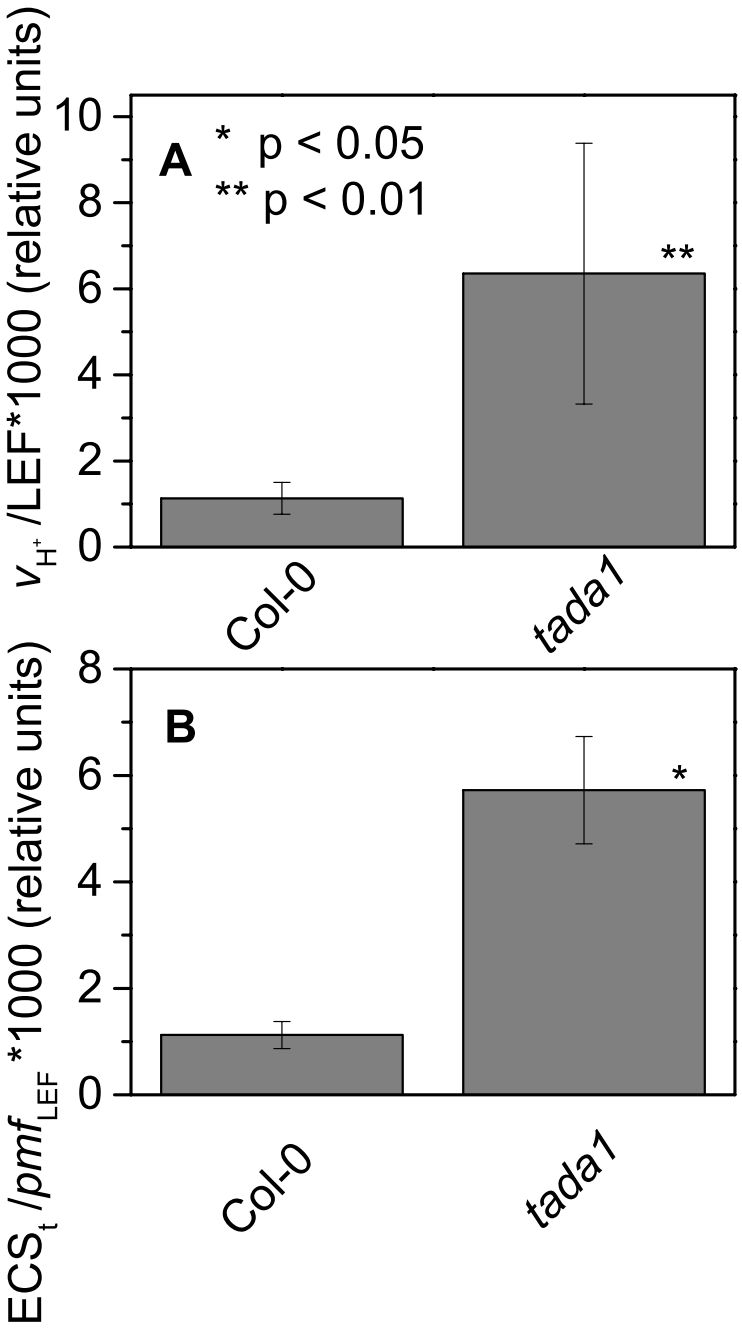

Figure 4.8 Elevated CEF in *tada1*. The ratios of A) v_H^+/LEF and B) ECS_t/pmf_{LEF} of intact leaves were measured and estimated as described in Material and Methods and Figure 4.4. Date represent the mean ± SD with n = 3. Asterisks indicate statistical difference from Col-0.

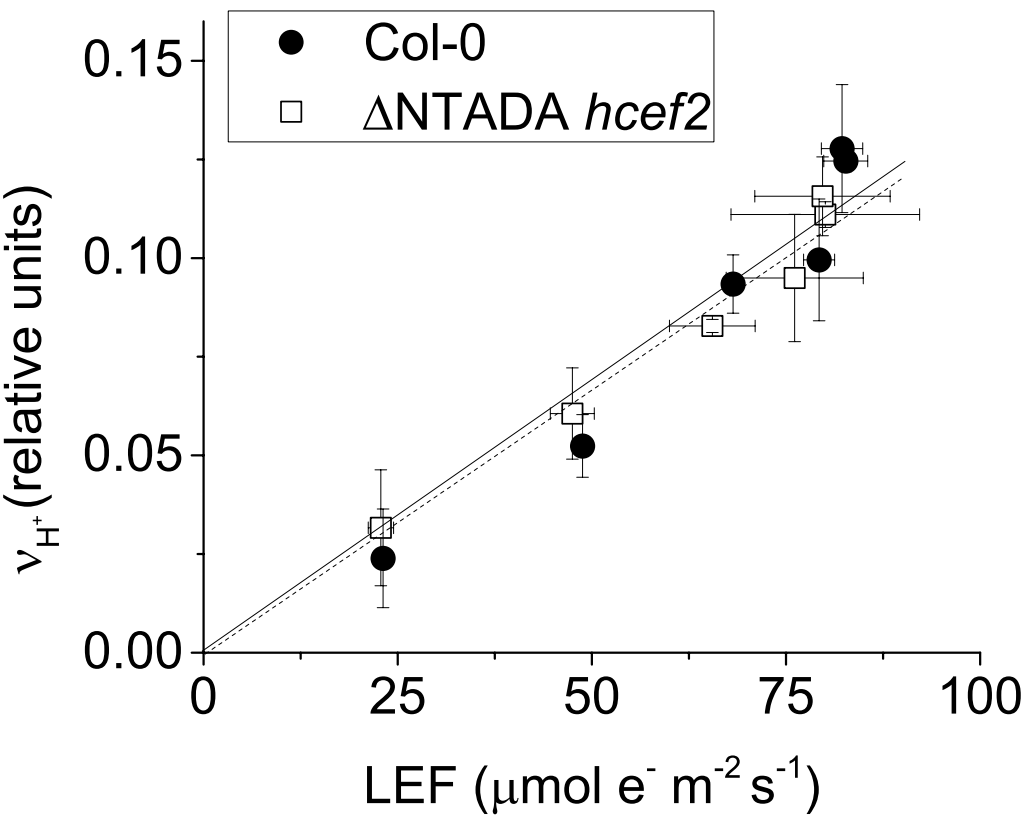

Figure 4.9 TADA1 complementation of *hcef2*. v_H^+/LEF of intact leaves of Col-0 (filled circles) and *hcef2* P35S:ΔNTADA1 (open squares). Mean ± SD, n = 3.

85% (197). Both of these mutations result in partial loss of ribosomal proteins and impaired chloroplast translation (197). The extents of CEF as measured by v_H^+/LEF were increased by about 2-fold compared to Col-0 in both *prsp3* (0.0033 ± 0.0005 and 0.0017 ± 0.0001, respectively, $p < 0.001$, $n = 3$) (Figure 4.10), and *rps17* (0.0017 ± 0.0001 and 0.0055 ± 0.0004, respectively, $p < 0.001$, $n = 3$). These results suggest that elevated CEF may be a general response to disruption of chloroplast translation.

4.3.I Mass spectrometry proteomics

We used high-resolution proteomics (see Materials and Methods) to assess the effects of *hcef2* on the accumulation of both nuclear and plastid-encoded chloroplast proteins (Figure 4.11). Figure 4.11 shows statistically significant fold changes from Col-0 (log2, $p < 0.05$) of thylakoid proteins in *hcef2* grouped by complex. Each component of the electron transport chain had significant changes for two or more subunits.

Strikingly, the relative changes of several thylakoid complexes were non-stoichiometric, i.e. the changes in individual components of a complex differed from one another (Figure 4.11). This effect is highly interesting because it should result in the accumulation of partially assembled, and in many cases non-functional or dysfunctional, complexes. In photosystem II, the PSBO2 (an isoform of the 33 kD protein of the oxygen evolving complex) (198) and PSBR (involved in stabilizing the oxygen evolving complex) (199), proteins were diminished while PSBF (the cytochrome b_{559} protein) was strongly increased ($p < 0.01$, $n = 3$).The PETB subunit of the cytochrome b_6f complex showed much higher accumulation than two other subunits of this complex, PETA and PETC ($p < 0.01$, $n = 3$). Non-stoichiometric changes were also observed in the accumulation of PS I antenna components, with non-stoichiometric decreases in PS I antenna

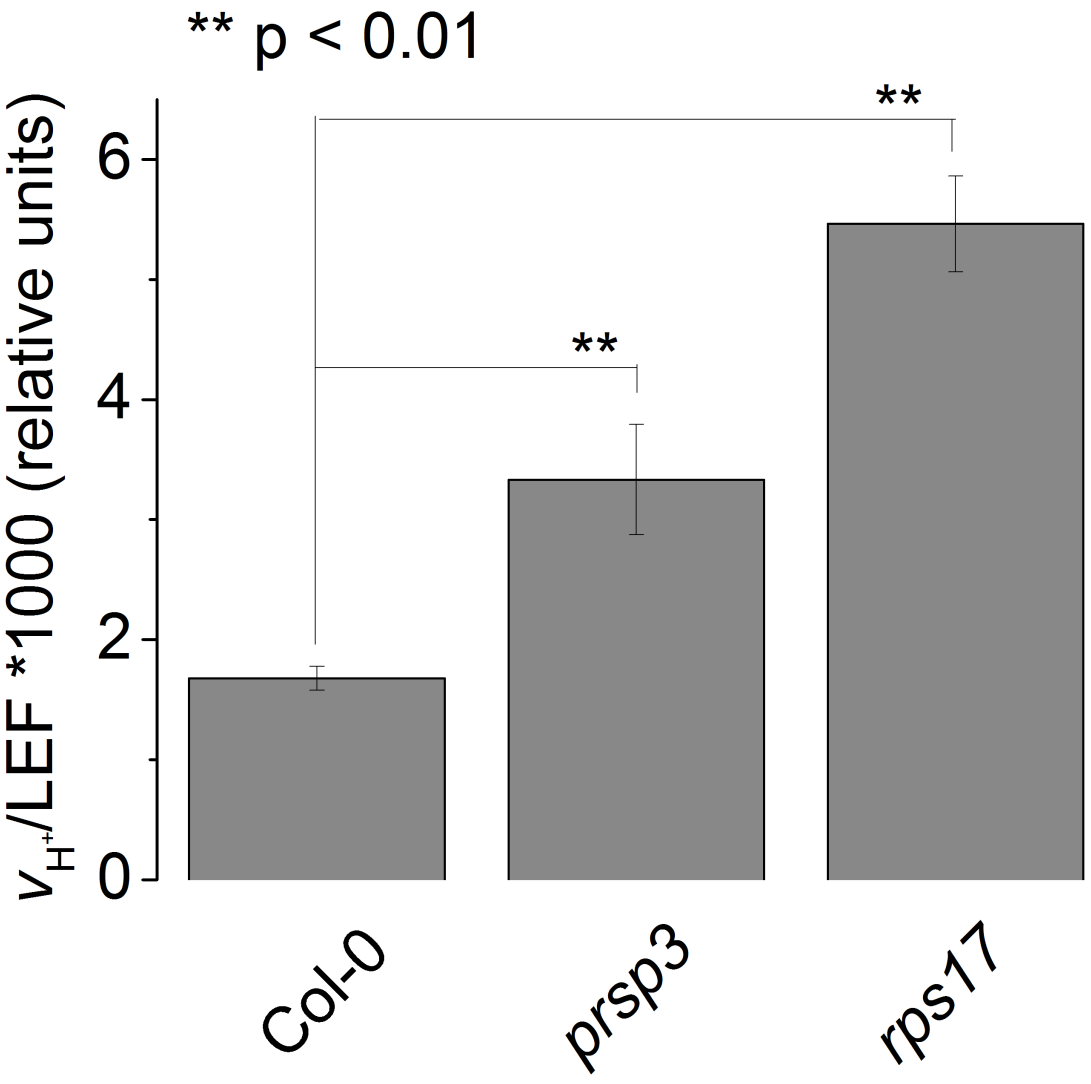

Figure 4.10 Elevated CEF in the ribosomal mutants *prsp3* and *rps17*. v_H^+/LEF of intact leaves. Mean ± SD, n = 3.

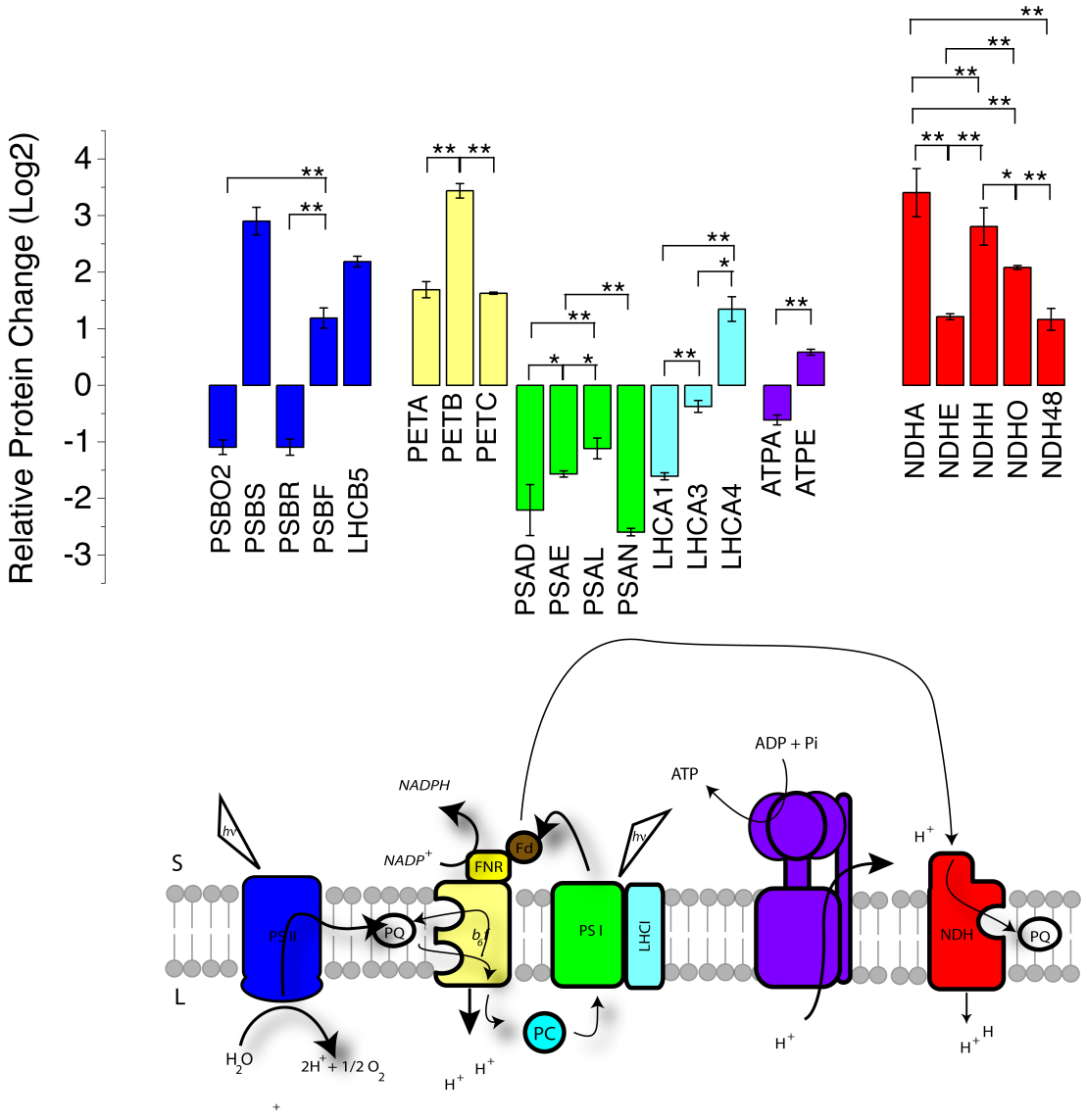

Figure 4.11 Changes in the thylakoid proteome of *hcef2*. A) Fold changes from mean Col-0 values (log2) in the thylakoid proteome of *hcef2*. Mean ± SD, n = 3. B) Model of the thylakoid membrane. Column colors of (A) correspond to the complex they are associated with in (B)[10]. * $p < 0.05$, ** $p < 0.01$

[10] The data used to generate Figure 4.11*A* were obtained by Kim K. Hixson and Mary Lipton at the Environmental Molecular Sciences Laboratory, Pacific Northwest National Laboratory, Richland, Washington 99354, USA

components LHCA1 and LHCA3 ($p < 0.01$, $n = 3$), while LHCA4 increases ($p < 0.05$, $n = 3$). Likewise, the ATP synthase subunit ATPA decreased, while ATPE increased ($p < 0.01$, $n = 3$). Finally, we also observed increases in relative abundance of all measured NDH subunits (NDHA, NDHE, NDHO and NDH48, Figure 4.11), but the extent of accumulation varied substantially ($p < 0.05$, $n = 3$).

4.3.J Flash induced relaxation kinetics in dark-adapted leaves of *hcef2*

The decay of the flash-induced ECS signal has been used to monitor the generation of electric field across the thylakoid and its dissipation by the activity of the ATP synthase and counterions (129). In dark-adapted leaves, or leaves infiltrated with methyl viologen (Figure 4.12), the ATP synthase becomes inactivated by oxidation of regulatory thiols, slowing the decay of the ECS signal. The residual decay, measured at low flash intensity to prevent re-activation of ATP synthase, reflects leakage of protons and counterions across the thylakoid membrane. In Col-0, this residual decay was slow, with a lifetime of about 0.8 s, similar to previously described results (129). A substantially increased ECS decay rate was about two-fold faster in *hcef2* (lifetime = ~0.4 s, Figure 4.12), indicating an increased rate of proton or ion leakage from the lumen.

4.3.K *hcef2* and related mutants show elevated H_2O_2 production

Figure 4.13 shows relative leaf H_2O_2 content in Col-0, *hcef2*, *tada1*, *hcef2* P35S:ΔNTADA1, *prsp3*, and *hcef1*. Both *hcef2* and *tada1* had significantly higher H_2O_2 accumulation than Col-0 (2.67 ± 0.57, 1.67 ± 0.29, and 1.00 ± 0.06, respectively, $p < 0.01$ and $p < 0.02$ respectively, $n = 3$) while the complimented line, *hcef2* P35S:ΔNTADA1, had H_2O_2 levels similar to Col-0 (1.13 ± 0.16 $p = 0.25$, $n = 3$). The plastid ribosomal mutant *prsp3* also had

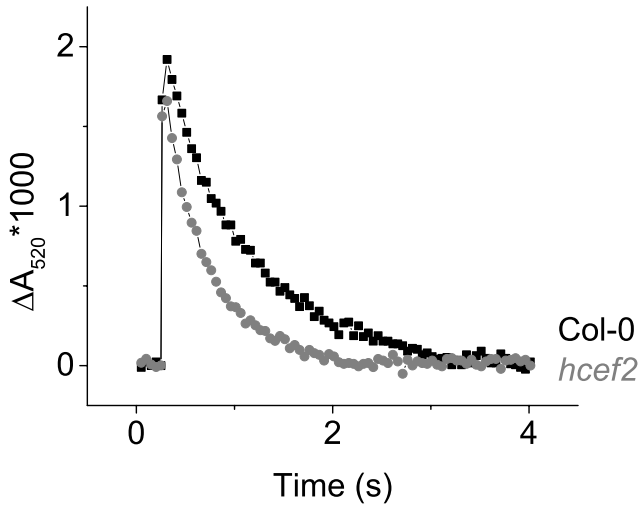

Figure 4.12 Flash induced relaxation kinetics of the electrochromic shift in Col-0 (black) and *hcef2* (gray) leaves infiltrated with 100 μM methyl viologen. Data is representative of 3 independent experiments.

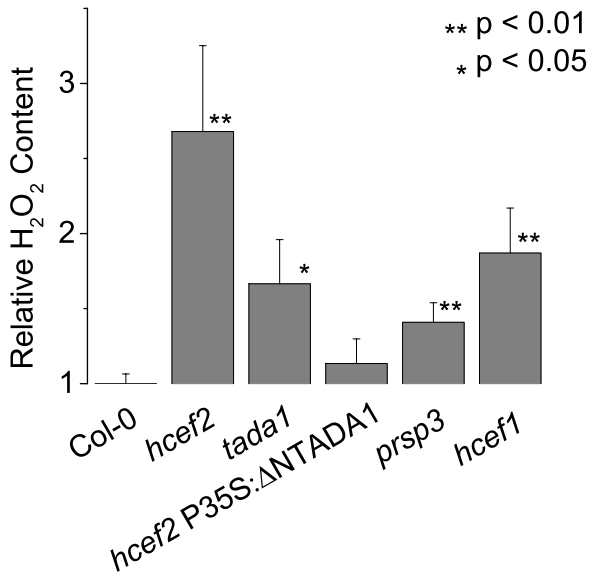

Figure 4.13 Relative accumulation of H_2O_2 in Col-0 and mutant lines. H_2O_2 levels were assayed by resorufin fluorescence and normalized to chlorophyll content of the sample and then normalized to average Col-0 fluorescence. Mean ± SD, n = 3. Asterisks indicate statistical difference from Col-0.

a significantly higher level of H_2O_2 (1.41 ± 0.13, $p < 0.01$, n = 3). In addition, the *hcef1* mutant also was shown to accumulate increased levels of H_2O_2 than Col-0 (1.87 ± 0.30 $p < 0.01$, n = 3).

4.4 Discussion

4.4.A Disruption of protein translation in *hcef2* leads to accumulation of H_2O_2 and activation of CEF involving the chloroplast NDH complex

The *hcef2* mutant was identified using a progressive screening approach as having constitutively activated CEF. Several independent approaches demonstrated that *hcef2* exhibits strong activation of CEF, including comparison of proton and electron fluxes (Figure 4.4*A*), *pmf* related parameters (Figure 4.4*B*), and postilumination fluorescence yield changes (Figure 4.5). The elevated CEF in *hcef2* was found to be insensitive to antimycin A, which inhibits the PGR5/PGRL1 associated ferredoxin:plastoquinone reductase pathway (FQR) (87, 115) (Figure 4.6) arguing against the participation of the FQR pathway. Instead, the strong increase in postillumination fluorescence rise and increased expression of the NDH complex (Figure 4.11) suggests activation of the NDH pathway in *hcef2*.

4.4.B The *hcef2* mutation disrupts chloroplast translation and leads to mis-assembly of chloroplast protein complexes

The *hcef2* gene was mapped to the TADA1 locus (At1G68720), coding for tRNA Adenosine Deaminase Arginine, which is important for efficient chloroplast translation (195, 196). This assignment is supported both by observation of a similar phenotype in the knockout mutant, *tada1* (Figure 4.8), and by the loss of phenotype when *hcef2* was complimented with the C-terminus of the protein, containing the active site [Figure 4.9, see also (196)]. The C>T transition in *hcef2* introduced a nonsense mutation at R643, and effectively deleted the active site of the enzyme (Figure 4.7), thus decreasing the ability of the chloroplast translation machinery to

recognize Arg codons CGC and CGA via the wobble mechanism of tRNA pairing (196).The mutant must instead rely on the less efficient 'two-out-of-three CGN' codon recognition (196). It was previously shown that disabling TADA1 affects the efficiency (or rate) of translation, but does not impact its fidelity, i.e. proteins are made more slowly in *tada1*, but the amino acids are inserted correctly (195, 196). This slowing of translation is likely the primary cause of decreased growth in both *hcef2* and *tada1*.

Strikingly, our proteomics results show that partially inhibiting plastid translation by limiting availability of specific tRNA leads to alterations not only in the levels of photosynthetic complexes, but in the stoichiometries of their component proteins. Of particular interest are non-stoichiometric changes in in subunits of PS II, the b_6f complex, NDH and the chloroplast ATP synthase (Figure 4.11). Because these complexes require a full complement of subunits for function, *hcef2* likely accumulates inactive or partially active complexes.

We also observed large changes in the stoichiometries of antenna complexes that appear to alter photosynthetic responses. For example, an increase in the accumulation of PSBS, as seen in *hcef2* (Figure 4.11), is expected to increase the sensitivity of q_E to *pmf* (24), as observed in our results (Figure 4.3*C*). Likewise, a there was a alteration in the relative accumulation levels of PS I antenna and core complex in *hcef2* (Figure 4.11), which may explain the appearance of a 77K fluorescence emission peak at 735 nm, and suggests loss of attachment of LHCI to PS I (200), supporting our hypothesis that complex formation is impaired in this mutant.

By extrapolation, we propose that partially assembled redox enzymes, e.g. the cytochrome b_6f complex, would very likely result in production of reactive oxygen species. We also observed altered ATP synthase subunit stoichiometric with ATPA decreasing and ATPE

increasing (Figure 4.11). Altered stoichiometry of this complex could result in an uncoupled thylakoid membrane, as also suggested by the more rapid decay of the flash induced ECS signal of dark-adapted leaves (Figure 4.12). Loss of protons through leakage or slip would disrupt the output balance of ATP/NADPH resulting in inhibition of downstream metabolic reactions and require the activation of additional ATP production processes, including CEF (2).

In chloroplasts of wildtype cells, disrupting one integral protein of a complex typically leads to loss of all subunits, i.e. the expression and stability of the subunits are high regulated to prevent the buildup of partially assembled complexes (100, 201, 202). In *hcef2* this regulation appears to be violated, leading to severe consequences for the function of photosynthesis. The effect on subunit stoichiometry may be caused by the overall slowing of translation in *hcef2* of the CGC and CGA codons for arginine. The distribution of these codons within the chloroplast genome is not even, and the efficiency of translation of a transcript is likely a function of CGC and CGA codon content within the transcript. In effect, translation in *hcef2* may not be slowed evenly across the entire proteome, which may lead to a lag time during assembly and accumulation of long-lived intermediates in complex assembly.

This hypothesis is supported by the hyper-accumulation of PETB protein in *hcef2* (Figure 4.11). PETB attachment to subunit IV is the first step in assembly of the b_6f complex (203) followed by attachment of the Rieske protein (PETC). This may also explain stoichiometric amounts of PETA and PETC in *hcef2*. Cytochrome b_{559} (PSBF) is thought to be part of an early subcomplex in PS II assembly (204), and this protein accumulates at a higher level in *hcef2*, while other PS II subunits decrease (Figure 4.11).

4.4.C Modifying chloroplast translation leads to accumulation of H_2O_2, a likely activator of CEF

While the effect of the *hcef2* mutation is certainly pleiotropic, likely affecting many processes related directly and indirectly to photosynthesis, it could lend some insight into regulation of CEF. For example, is was previously shown that simply suppressing overall photosynthesis does not, by itself, trigger high rates of CEF (70, 78). Instead, CEF appears to be dependent on the redox state of the chloroplast (69, 109, 119, 120), leading us to propose that activation of CEF in *hcef2*, *tada1* and related mutants may involve altered redox regulation.

Several lines of evidence suggest that this redox regulation may act through, or be modulated by, the reactive oxygen species H_2O_2 (70, 99, 102, 119) (see Chapter 3). Several mutants of the CBB cycle have found to have high CEF (69, 70, 79), all of which show elevated H_2O_2 levels, and production of H_2O_2 within the chloroplast leads to a rapid increase of CEF *in vivo* (Chapter 3).

The NDH complex has previously been shown to increase both accumulation and activity in response to H_2O_2 (99, 102), suggesting a role for the observed increases in H_2O_2 in *hcef1* (Figure 4.13) in the increased NDH activity in *hcef2*, as previously proposed (69, 104).

Because the codons affected in *hcef2* (and *tada1*) are present in >80% of the protein coding genes within the chloroplast genome (205), the overall effect on plastid translation is expected to similar to that of *prsp3*, and *rps17*, but through a different mechanism. In other words, the fact that *hcef2*, *tada1*, *prsp3*, and *hcef1* all showed both increased levels of H_2O_2 (Figure 4.13) and elevated CEF (Figures 4.4, 4.8, and 4.10), suggests a model in which defects in chloroplast translation lead to discoordination of protein homeostasis, leading to elevated H_2O_2

thus activating CEF. Finally, our results have immediate implications for any attempt to screen for high CEF mutants as they may also identify lesions in the translational (and related) machinery (as seen in the ribosomal mutants *prsp3* and *rps17*, (Figure 4.10) in addition to defects that directly involve photosynthetic processes.

4.5 Methods

4.5.A Plant materials and growth

All plants were grown photoautotrophically on soil in a controlled growth chamber with a 16:8 light/dark photoperiod (~100 μmols photons m^{-2} s^{-1}, white light). Seed for *tada1* (GK-119G08) and the *tada1* line complimented with P35S:ΔNTADA1 was graciously provided by Dr. Jośe Gualberto. Seed for *prsp3* (Salk_010806) and *rps17* (Salk_066943) were provided by the ABRC. The *tada1* insertion was verified as described in (196). The *hcef2* mutation in the *tada1* locus was verified by sequencing. The presence of the P35S: ΔNTADA1 construct was verified using primers for the 35S promoter (5'-CCACTGACGTAAGGGATGACG-3') and the C-terminus end of TADA1 (5'-TGCTTTAGAACCCTCTCGAAT-3'). Verification of homozygous *prsp3* and *rps17* was performed using primers generated from the SIGnAL T-DNA primer design tool (http://signal.salk.edu/tdnaprimers.2.html).

4.5.B Isolation of *hcef* mutants

hcef2 was initially identified and isolated as a high NPQ mutant as described in (69). Identification of backcrossed lines and F2 mapping populations with high NPQ was performed in a high-throughput fluorescence-imaging chamber as described in (J. Cruz, L. Savage, R. Zegarac, W. Kovac, C. Hall, J. Chen, R. Last, D. Kramer, submitted).

4.5.C 77K fluorescence spectroscopy

Fresh light adapted leaf material was flash frozen in liquid nitrogen, ground to a fine powder and diluted to <5 μg/ml in ice as described in (206). Emission spectra were detected using a spectrofluorimeter (Ocean Optics, HR200+ES) by a blue (440 nm) diode laser, controlled by SpectraSuite software (Ocean Optics). The spectra were normalized to the 735 nm peak.

4.5.D *In vivo* spectroscopy

All *in vivo* spectroscopic measurements were performed on fully expanded leaves in mature plants just prior to bolting. Comparisons were made between mature leaves, despite age, due to the inhibited growth in the mutant lines. Steady-state chlorophyll *a* fluorescence yield and light-induced absorption changes were made as extensively described elsewhere (7, 32, 35, 69, 70, 179, 187) on a spectrophotometer/fluorimeter described in (166). To account for changes in pigmentation of the mutants, LEF was calculated using the approach of (69, 193) using the following equation:

Eq. 4.1

$$LEF = \phi_{II} * i * A * 0.5$$

where *i* is the actinic light intensity and *A* is the absorptivity of the leaf quantified using an integrating sphere described in Idle and Proctor (207).

Electrochromic shift measurements were corrected for changes in leaf properties by normalizing to leaf chlorophyll content. This correction gives similar results as corrections described in (35, 69, 70).

For chlorophyll *a* fluorescence yield in response to short actinic pulses, plants were dark-adapted for 10 minutes prior to the experiment. For each trace the excitation light was pulsed at a frequency of 500 Hz, contributing minimally to the kinetics of chlorophyll *a* fluorescence induction in the absence of actinic illumination. 5 actinic flashes (10 msec at ~12,000 μmol photons m^{-2} sec^{-1}) were given 0.2 s apart. A second experiment was performed in which an interval of far red illumination was inserted after the last actinic flash. Data was normalized to F_0 and F_M, and the baseline was set to 0.

4.5.E Map-based cloning of *hcef2*

The *hcef2* mutant was mapped on chromosome 1 between At1G68560 (25,733,701bp) and At1G69020 (25,947,401), a 213.7 kb region, using molecular markers based on Simple sequence length polymorphisms (SSLPs) and cleaved amplified polymorphic sequences (CAPS) (208). Polymorphism sequence information between Col-0 and Landsberg erecta, from the ABRC TAIR website (http://www.arabidopsis.org/browse/Cereon/index.jsp), was used to design SSLPs and/or CAPS marker for mapping. F2 plants were derived from breeding homozygous *hcef2* (Col-0 background) and wildtype (Landsberg *erecta* background). The *hcef2* mutation was found to be recessive, and genomic DNA was isolated from homozygous F2 plants (*hcef2 hcef2)* with high NPQ by chlorophyll a fluorescence imaging (described above). To determine the *hcef2* mutation, we performed whole genome sequencing on homozygous *hcef2* plants. Genomic DNA from the mutant line was used to create a sequencing library using the Illumina TruSeq DNA Library Kit following manufacturers recommendations. The library was then sequenced on an Illumina GAIIx using single end with 50 base reads. All next generation sequencing was conducted by the Genomics Core of the Research Technology Support Facility at Michigan State

University. Illumina reads were assembled using SeqMan NGen software (DNASTAR). SNPs were compared across multiple samples of the same Col-0 background and SNPs unique to *hcef2* were confirmed by Sanger sequencing.

4.5.F CAPS marker for *hcef2* genotype

To genotype *hcef2* without sequencing we designed a CAPS marker for the *hcef2* mutation. A PCR fragment spanning the mutation site was amplified (5'-GAGGCTGATTGGTCAAGGA-3', forward; 5'-GGATGTTCAAAGGCTGTGGT-3', reverse) and then digested with NruI (R0192, New ENGLAND BioLabs). The Col-0 sequence is cut with NruI, and homozygocity/heterozygocity was determined by comparing banding patterns on a 2% agarose gel.

4.5.G Infiltrations

Freshly detached leaves were infiltrated with 20 μM antimycin A in distilled water in the dark by soaking between 2 saturated lab tissues for 3 hours. Successful infiltration of antimycin A was confirmed by secondary effects of this chemical on NPQ responses probed by chlorophyll fluorescence (189). Leaves were infiltrated with 100 μM methyl viologen in a similar manner for 1 hour prior to measurement.

4.5.H H_2O_2 quantification

To quantify relative H_2O_2 accumulation, leaves were flash frozen in the light and H_2O_2 was extracted in 50 mM potassium phosphate (pH 7.4). Total H_2O_2 of the extract was quantified using resorufin fluorescence, a byproduct of the reaction between Amplex Red (Invitrogen) and H_2O_2, as described in Chapter 3.

4.5.I Determination of protein changes in *hcef2*

Total protein was extracted from whole leaf tissue as described in (69) and quantified using a combination of SCX, LC, ESI, and MS/MS and analyzed using the peptide identification software SEQUEST (209) in conjunction with the annotated protein translations from the genome sequence of *Arabidopsis thaliana* TAIR 10 annotation (http://www.arabidopsis.org/). Detailed methods are described in Appendix 1.

4.6 Author contributions

All data presented, except where noted, were obtained by Deserah D. Strand. Mapping of the *hcef2* mutation was started at WSU by Aaron K. Livingston, Heather M. Enlow, and Deepika Minhas under the direction of Amit Dhingra. Mapping was finished by Mio Satoh-Cruz and Tyson Koepke. Extensive preliminary data, and a preliminary version of the manuscript was generated by Aaron K. Livingston (104). For the proteomics experiment, Kaori Kohzuma designed the biological samples and replicates, and Kim K. Hixson performed the experiments under the direction of Mary Lipton at PNNL. Kim K. Hixson and Mary Lipton analyzed the raw data and transformation of the proteomics experiment, and assisted with the analysis and interpretation of the final data sets.

4.7 Acknowledgements

The authors would like to thank Drs. Ralph Bock, Nicholas Fisher, and Jeff Landgraf for helpful discussions. Experiments performed at MSU and WSU were funded by Grant DE-FG02-11ER16220 from the Photosynthetic Systems program from Division of Chemical Sciences, Geosciences, and Biosciences, Office of Basic Energy Sciences of the US Department of Energy (to DMK). The Department of Energy Office of Biological and Environmental Research

Genome Sciences Program supported the high throughput proteomics component of this research under the Pan-omics project. Work was performed in the Environmental Molecular Science Laboratory, a U.S. Department of Energy national scientific user facility at Pacific Northwest National Laboratory (PNNL) in Richland, WA. We would also like to thank our outstanding technicians, Amelia Barhanovich, Brendan Johnson, Ryan Vink, and Ben Wolf for their maintenance of plants and general assistance within the lab.

Chapter 5

Evidence for a proton pumping plastidic NAD(P)H dehydrogenase complex involved in cyclic electron flow around photosystem I

Deserah D. Strand, Nicholas Fisher, and David M. Kramer

5.1 Abstract

Photosynthetic cyclic electron flow around photosystem I is thought to help balance the ATP/NADPH energy budget of the chloroplast. In order to do this, it reroutes electrons from the accepter side of photosystem I to reduce the plastoquinone pool. The proposed mechanisms of plastoquinone reduction allow for, not only additional ATP production, but an alteration in the H^+/e^- stoichiometry of the process itself. In this paper we show evidence that CEF *in vivo* through the thylakoid NADPH dehydrogenase complex (NDH), homologous to respiratory Complex I, has proton pumping function. This may allow for increased efficiency of ATP production via CEF by increasing the H^+/e^- of CEF from the 2/1 expected of a non-proton pumping route, to above 3/1, and may explain the low concentration of the NDH complex within the thylakoid. In addition, a proton pumping NDH may allow a reversible process in which *pmf* is consumed to oxidize plastoquinol and reduce NADPH, further adjusting the output of the light reactions to meet downstream metabolic demands.

5.2 Introduction

The proton and electron circuits of photosynthesis are tightly coupled to each other. The textbook 'z-scheme' model of linear electron flow, perhaps the best understood electron transfer pathway in the thylakoid, provides a fixed number of protons transferred into the lumen, generating proton motive force (*pmf*) for ATP synthesis, as electrons are passed through the photosynthetic machinery. This ratio of electrons to protons is only altered if there is a slip or leak in the reactions or alternative electron pathways are activated. Slip or leak is detrimental to the organism because it has the potential to create reactive oxygen species (in the case of electrons) or decrease the efficiency of photosynthesis (in the case of protons). Alternative electron pathways in the chloroplast seem to be a more preferred option to the thylakoid, and

there are many that have evolved in plants, such as the plastid terminal oxidase, the water-water cycle, the malate shunt, chlororespiration, and cyclic electron flow around photosystem I (CEF) (41, 50, 59, 151) (discussed in Chapter 1). CEF as a process is interesting in that it seems to involve multiple redundant pathways, and knocking out any one of them does not result in much of a growth phenotype except under stress conditions (87, 100, 114). The best understood pathway, at least structurally, is the thylakoid NADPH dehydrogenase complex (NDH), which is analogous to respiratory Complex I. Another pathway is the antimycin A sensitive, PGR5/PGRL1 associated pathway, in which it has been proposed these proteins form a complex which is able to directly reduce plastoquinone to plastoquinol (PQ/PQH_2) from electrons donated from ferredoxin (Fd) (82, 83, 112, 113).

It is interesting that plants have conserved both of these routes of alternative electron transfer, as they both are able to reduce PQ, and seem to have the same donor, Fd (82, 113, 167). However, structurally we may have a clue to why these two are maintained. A complex of PGR5 and PGRL1 would likely only pass electrons to PQ, and any *pmf* generated from this process would come from plastoquinol oxidation at the Q_o site of the cytochrome b_6f complex (b_6f), therefore the H^+/e^- stoichiometry of this route of electron transfer would be 2/1. On the other hand, if the NDH is functionally similar to Complex I, it has the potential to increase the H^+/e^- stoichiometry of CEF by pumping protons. The actual number of protons pumped per electron in Complex I is still debated, but the consensus is 2/1 [reviewed in (210)]. If NDH maintains this ratio, then NDH catalyzed PQ reduction, coupled with PQH_2 oxidation by the b_6f complex, the H^+/e^- stoichiometry of this route of CEF could be as high as 4/1 (14, 15).

Based on several lines of evidence, including a high-resolution crystal structure, a consensus model of Complex I proton pumping has emerged in which the reduction of the N2 iron-sulfur cluster leads to a conformational change of the membrane subunit NUOL, a transmembrane proton channel which contains 2 C-terminal transmembrane alpha helices that cross three additional transmembrane proton channels. This is thought to move polar residues buried within each of the proton channels, releasing up to 4 protons (1 proton per channel) into the intermembrane space (98, 210). It should be addressed that this proton number is still debated, however the consensus from experimentation is that the H^+/e^- of Complex I is two protons pumped for each electron passed to the quinone acceptor [reviewed in (210)].

In this work we show data supporting the hypothesis that NDH also acts as a proton pump. We propose that the apparent redundancy in the routes of CEF exist in order to further fine-tune the light reactions of photosynthesis to balance the chloroplast energy budget.

5.3 Results

A sequence alignment (Clustal Omega, Jalview) of *Arabidopsis thaliana*, *Spinacia oleracea*, and *Nicotiana tabacum* single subunit membrane fraction NDH subunits with the membrane fraction subunits of Complex I from *Escherichia coli*, *Thermus thermophilus*, *Yarrowia lipolytica*, and *Bos taurus*, shows conservation of the indispensible polar residues E144 and K234 (NUOM numbering, Figure 5.1) in all analogous proton channels of NDH.

To test proton pumping capacity of NDH, we used the *hcef1* mutant, which shows an increase in relative CEF through the NDH complex (69). Using changes in absorbance of 820 nm during a dark interval, we can calculate relative electron transfer rates through PS I (v_{P700}). Comparisons of transthylakoid proton flux (v_{H^+}) and electron transport rates through PS I and PS

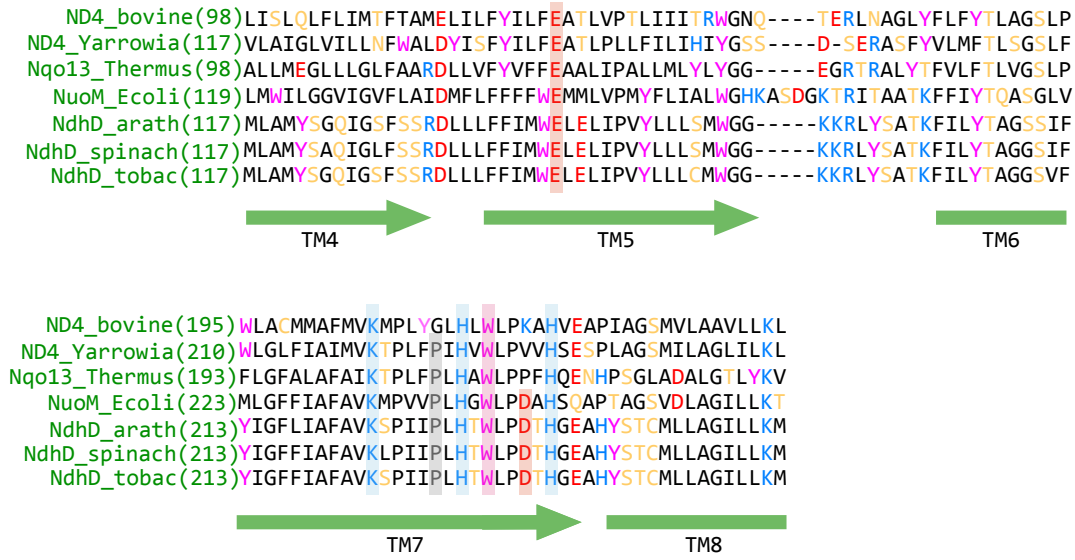

Figure 5.1 Residues essential for proton pumping are conserved in the NDH membrane fraction. Representative proton channel alignment of plant NDH subunits with Complex I. NdhD is analogous to ND4, Nqo13, and NuoM in respiratory Complex I[11]. Sequences are from the UniProt database for *Bos taurus* (bovine), *Yarrowia lipolytica* (Yarrowia), *Thermus thermophilus* (Thermus), *Escherichia coli* (Ecoli), *Arabidopsis thaliana* (arath), *Spinicia oleracea* (spinach), and *Nicotiana tabacum* (tobac).

[11] Figure 5.1 was kindly generated by Dr. Nicholas Fisher.

II, we can calculate the H^+/e^- stoichiometry for CEF in this mutant. In Figure 5.2*A* we see an increase in v_{P700} of ~50% in *hcef1* when compared to Col-0, (m = 0.19 +/- 0.04 and 0.135 +/- 0.011, respectively, p = 0.0002, n = 3), while in Figure 5.2*B* we see a nearly 4-fold increase in v_H^+ as a function of LEF in *hcef1* when compared to Col-0 (m = 1.28 +/- 0.24 and 0.26 +/- 0.037, respectively, p < 0.0001, n = 3). This suggests H^+/e^- stoichiometry in excess of the 3/1 expected of LEF. Additionally, Figure 5.2*C* shows an increase in the amount of v_H^+ to electron transfer through photosystem I, indicating proton pumping CEF in *hcef1*. If the H^+/e^- of CEF in *hcef1* were 2/1 as expected for a non-proton pumping route, we would expect a decrease in the slope of this relationship.

To qualitatively test for proton pumping, we monitored ATP synthesis, using luciferase phosphorescence, in the dark after addition of electron donors to the cuvette. There was a slow, but reproducible, increase in slope, indicating ATP synthesis (Figure 5.2*D*), and therefore *pmf* generation in the dark, which, since there is no electron sink to drive the b_6f complex, could only be explained by a proton pumping plastoquinone reductase. In addition, ATP synthesis was insensitive to tridecyl stigmatellin, a potent inhibitor of the b_6f complex, and oligomycin, a mitochondrial specific ATP synthase inhibitor (data not shown), eliminating *pmf* contribution due plastoquinol oxidation at the b_6f complex or by mitochondrial contamination.

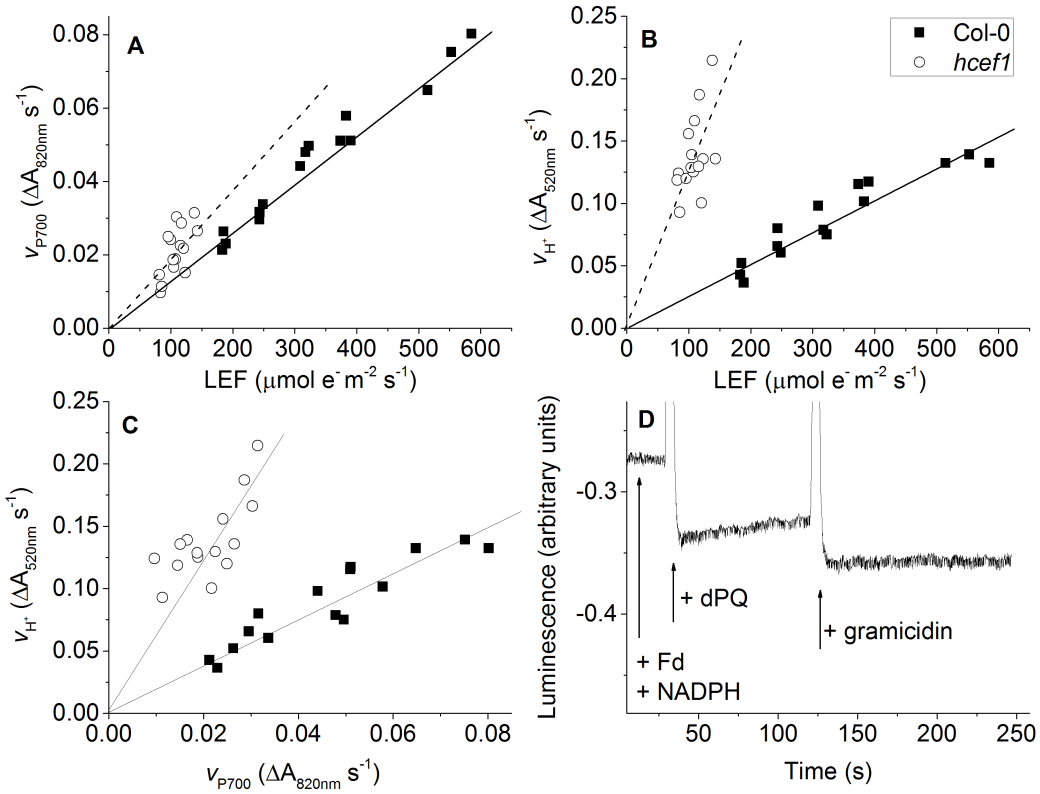

Figure 5.2 Evidence for involvement of a proton pump in CEF. A) Electron flux through PS I (v_{P700}) as a function of electron flux through PS II (linear electron flow, LEF). B) Transthylakoid proton flux, v_H^+, as a function of LEF. C) v_H^+ as a function of v_{P700}. D) ATP synthesis, monitored by luciferase luminescence, in DCMU treated spinach thylakoids in the dark after addition of decylplastoquinone (dPQ)[12].

[12] Figure 5.2*D* was graciously supplied by Dr. Nicholas Fisher.

5.4 Discussion

5.4.A CEF involves a proton pump

Using the Arabidopsis mutant *hcef1*, which is proposed to have high rates of CEF primarily through the NDH complex, we have shown the first evidence of a proton pumping CEF *in vivo*. The *hcef1* mutant accumulates high levels of NDH dependent CEF. There have been multiple mechanisms of CEF proposed in higher plants and algae. Of these known pathways, the only protein complex that may be structurally capable of proton pumping would be the NDH complex. Despite its usually low expression levels, the proton pumping activity would allow for higher ATP generation via CEF than the other proposed pathways.

The NDH complex is homologous to Complex I, and evolution has conserved many of the residues proposed to be involved in the mechanism of proton pumping. The apparent H^+/e^- stoichiometry for CEF in these conditions is above 3/1, which is in agreement with a >1/1 stoichiometry of a Complex I like NDH assuming a b_6f ratio of $2H^+/1e^-$ is maintained (14).

It should be mentioned that the proton pumping capability of NDH must satisfy thermodynamic constraints. At equilibrium, the relationship between protons pumped (H^+/e^-) into the lumen against the *pmf* (Δp) per electron, with a redox span of ΔE_h mV is given by:

Eq. 5.1

$$\Delta E_h \geq n\Delta p$$

where *n* represents the H^+/e^- ratio. With Fd as electron donor to NDH, ΔE_h equals 518 mV assuming 90% reduction of the PQ and Fd pools respectively. Assuming a Δp of -180 mV across

the thylakoid membrane in the light, NDH would be capable of acting as a $4H^+/2e^-$ pump. This assertion also holds for a predominantly oxidised (90%) Fd pool. If NADPH is the electron donor to NDH the energetics are more constrained, with a ΔE_h of 380 mV under conditions of 90% reduction of the NADPH and PQ pools. $4H^+/2e^-$ pumping is possible only up to a Δp of -190 mV in this instance. *In vivo* it has been estimated that under light saturating conditions maximum *pmf* is ~175 mV (26), a value that still allows for the forward reaction of a $4H^+/2e^-$ proton pumping NDH complex. Mitochondrial Complex I is confronted by this problem during respiratory state 4 (ADP exhausted) when the *pmf* force may approach -220 mV, and there is insufficient redox energy for the enzyme to operate as a $4H^+/2e^-$ pump (211). Under these types of conditions we would not expect a need for NDH to operates as this would likely represent an ATP surplus, and may lead to the reverse reaction of the enzyme (discussed below).

This observation may explain why there are multiple routes of differentially regulated cyclic electron flow in chloroplasts (reviewed in Chapters 1-5). We propose a model in which the two most studied routes of CEF, in higher plants, are activated step-wise when the downstream metabolism decreases ATP/NADPH. First, a reducing environment is generated as NADPH accumulates, and CEF activated through the presumably non-proton pumping, rapidly reversible antimycin A sensitive pathway (see Chapter 2, Figure 2.5*A*). Under conditions in which this route of CEF is not able to augment the ATP deficit, and restore redox homeostasis to the chloroplast, ROS is generated and activates a proton pumping NDH complex [see chapter 3, Figure 3.9 and (99, 102)]. This would increase ATP formation per e^- transfer, increasing the efficiency of ATP production via CEF. This route of CEF is not as rapidly activated as the FQR

(see chapters 2 and 3), and long term ROS generation leads to not only activation of already assembled complexes, but an increase in total NDH content (99, 102), likely indicating slower reversibility of this response.

5.4.B A proton pumping NDH would be reversible

The discovery of a proton pumping NDH has further implications for energy balance within the chloroplast in that a proton pumping NDH should also be reversible, consuming *pmf* to oxidize PQH_2 and reduce $NADP^+$ to NADPH. Using several assumptions in relation to the mechanism of a reversible NDH, including a reaction of $4H^+/2e^-$ and $NADP^+$ as an acceptor, we can calculate the free energy of the reverse reaction (ΔG_{rev}) of NDH under a variety of conditions. Figure 5.3 shows ΔG_{rev} (25°C, pH 7.5) as a function of *pmf* at different redox states of the donor (PQH_2) and acceptor (assumed to be $NADP^+$). The reaction is favored with increasing *pmf* and with increasing reduction of the PQ pool and oxidation of the NADPH pool.

We might expect reversibility of this process to be physiologically important during conditions where NADPH is limiting, but *pmf* and plastoquinol are high. This situation may occur during induction of photosynthesis where reducing equivalents (Fd, NADPH) are being consumed by the thioredoxin-dependent activation of sink metabolism and ATP synthase, leading to a NADPH deficit. Inactive ATP synthase could potentially lead to a high *pmf* and slowed quinol oxidation at Q_o, leading to an increase in PQH_2/PQ. These conditions would favor the reverse reaction of NDH, which may have a dual role in chloroplast energy balance as it would consume *pmf*, and the potential for ATP production, to produce NADPH, altering the ATP/NADPH of the light reactions (Figure 5.4).

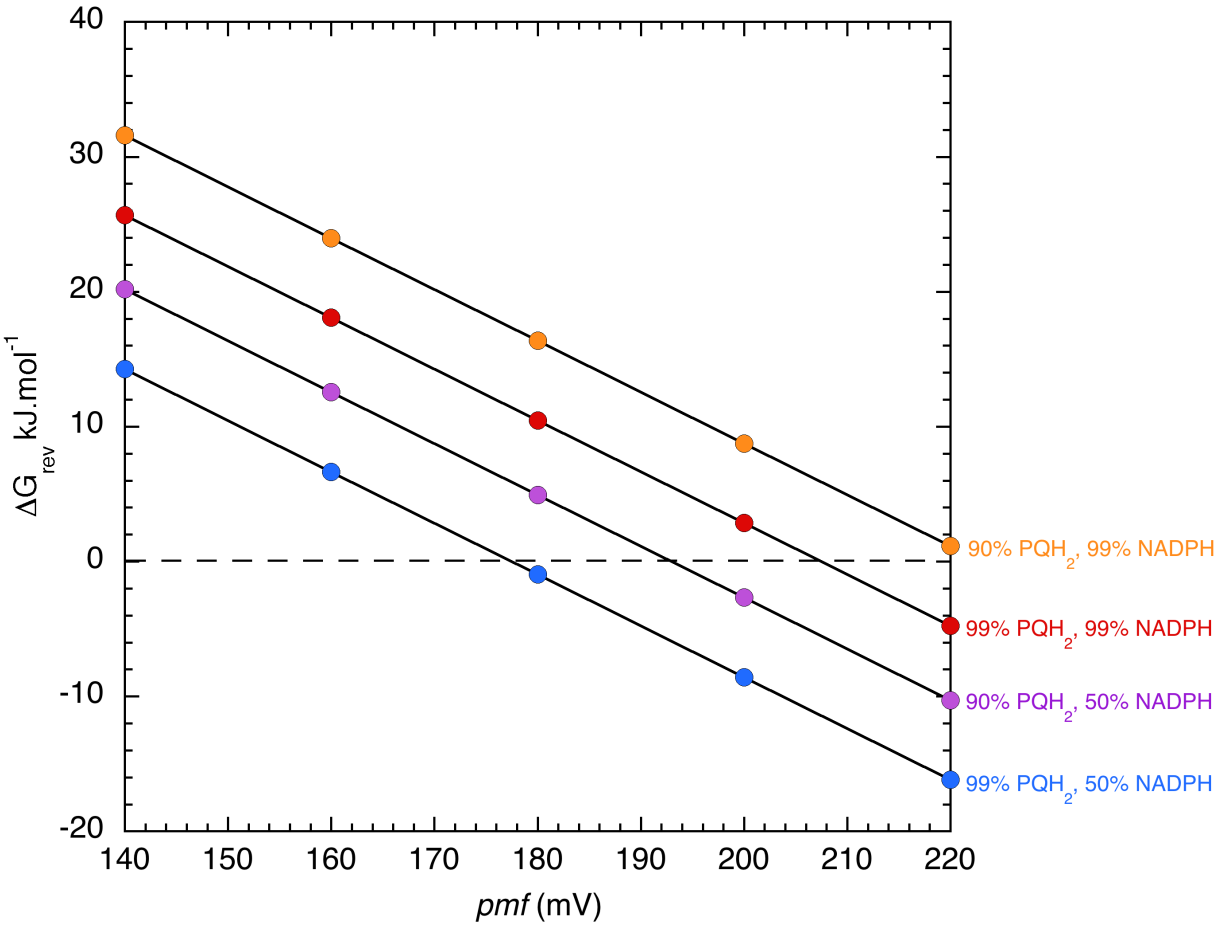

Figure 5.3 Directionality of NDH. Conditions in which the forward reaction of NDH is favorable (above dashed line), or the reverse reaction of NDH is thermodynamically favorable (below dashed line)[13]. Calculations were performed assuming a $2H^+/e^-$ NDH.

[13] Figure 5.3 was graciously supplied by Dr. Nicholas Fisher.

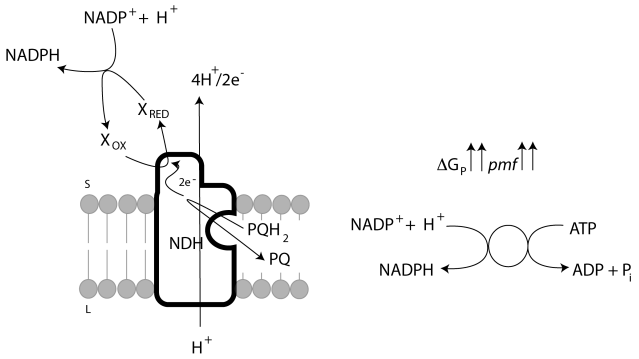

Figure 5.4 Hypothetical model of the reversible reactions of NDH. When ΔG_{ATP} is large, *pmf* is correspondingly large, in such an instance, protons are consumed from the lumen to drive oxidation of PQH_2 and ultimately, reduction of $NADP^+$ to NADPH.

It should be clarified that these calculations are made with many broad assumptions, many of which, if violated, may lead to the complex being irreversible. First, it has been proposed that Fd is the electron donor to NDH in the forward reaction (167), but if Fd is the acceptor in the reverse reaction, *pmf* required to drive the reaction is calculated to be too high to be physiologically relevant, and under these conditions the complex would be essentially irreversible. Secondly, the pH of the quinol binding pocket of NDH is an unknown, and in Figure 5.3, assumed to be 7.5. Within the calculation of ΔG_{rev}, as pH decreases, the amount of *pmf* required to drive the reverse reaction increases, and could conceivably reach a point where the reaction is irreversible.

5.5 Methods

5.5.A Plant materials and growth conditions

Arabidopsis thaliana plants were grown in a 12:12 light:dark photoperiod. Col-0 was measured at 3-4 weeks of age. Slow-growing *hcef1* was measured at the same developmental stage as Col-0, which was around 6-7 weeks of age.

5.5.B *In vivo* spectroscopy

Variable chlorophyll *a* fluorescence was used to calculate the quantum yield of PS II (ϕ_{II}) as described in (7, 187). In order to determine LEF rates, we took a more complex approach expanded on in Appendix 2.

Redox state of PS I was monitored using absorbance changes at 820 nm in a protocol modified from (68). Plants were poised by illuminating with 700 nm actinic light, and the initial rate of $P700^+$ re-reduction kinetics were used as the relative rate of electron transfer through PS I (v_{P700}, $\Delta A_{820\ nm}\ m^{-2}\ s^{-1}$).

Transthylakoid proton flux (v_H^+, $\Delta_{A520\ nm}\ m^{-2}\ s^{-1}$) was calculated using the electrochromic shift of the carotenoids at 520 nm as described in (69) and Chapters 3 and 4. To correct for variability in leaf pigmentation between Col-0 and *hcef1* total extent of ECS was normalized to the amplitude of the PS I contribution to ECS in the presence of DCMU (see Appendix 2, Figure A2.4). This gave similar results to other methods of normalization described in (69) and Chapters 3 and 4.

5.5.C Quantification of *in vitro* ATP production

Proton pumping *in vitro* was measured in the dark as ATP production using the Promega (ENLITEN) luciferase/luciferin reagent kit with a laboratory-constructed PMT phosphoroscope. Osmotically ruptured spinach chloroplasts (prepared in the presence of 10 mM DTT) were present at a chlorophyll concentration of 40 μg/ml. DCMU was present at 10 mM. Fd and NADH were present at 5 μM and 1 mM respectively. The assay buffer (pH 7.6) consisted of 10 mM HEPES, 10 mM potassium phosphate, 5 mM $MgCl_2$, 10 mM potassium phosphate with 2 mM DTT and was supplemented with 10 mM ADP and 100 μM diadenosinepentaphosphate (an adenosine kinase inhibitor). Proton pumping was initiated by the addition of 50 μM decylplastoquinone (dPQ), and the proton gradient was collapsed by the addition of 10 μM gramicidin. The plastid ATP synthase was activated by actinic illumination (625 nm) for two minutes immediately prior to the start of data collection.

5.6 Author contributions

All data presented, except where noted, were obtained by Deserah D. Strand. Dr. Nicholas Fisher optimized and performed the *in vitro* assay for ATP synthesis in the dark.

5.7 Acknowledgements

I would like to thank Dr. Nicolas Fisher and Dr. Jeff Cruz for helpful discussions. This work was supported by Grant DE-FG02-11ER16220 from the Photosynthetic Systems program from Division of Chemical Sciences, Geosciences, and Biosciences, Office of Basic Energy Sciences of the US Department of Energy (to David M. Kramer).

Chapter 6

Conclusions and future directions

Deserah D. Strand

6.1 Abstract

This chapter summarizes current consensus in the field in light of the data presented in this dissertation, and discusses questions that remain open, or have emerged from the findings in the previous chapters.

6.2 Conclusions

Throughout human history crop yields have been improved through trial and error with traditional breeding and selection. As the world increases its demand for food and renewable fuel sources, the need to understand plant and algal physiology and biochemistry increases in parallel. We have entered an age of technology and human understanding of complex biochemical processes, yet we have made very little progress in improving the photosynthetic reactions of plants and algae, despite these reactions being some of the best characterized in all of biology. Clearly we still have unanswered questions.

Many of these unanswered questions lie in the alternative electron pathways within the chloroplast, which are present in much more abundance than in the mitochondria alternative electron transport chain. As discussed in Chapter 1, some of these do not seem to contribute significantly towards energy balance, but instead are important during development (plastid terminal oxidase) (212), under prolonged environmental stress (malate dehydrogenase, NDA2) (41, 43, 44, 117), or for redox poising of the PQ pool (NDA2) (86, 116). In light of the work presently being carried out in the Kramer lab on mutants in chloroplast targeted genes with unknown functions, it is likely the full extent of the roles of these alternative electron transport proteins is yet to be discovered (J. Cruz, L. Savage, R. Zegarac, W. Kovac, C. Hall, J. Chen, R. Last, D. Kramer, submitted). In line with this, CEF pathways could also be considered among some of the last uncharacterized complex(es) in photosynthesis.

In light of recent work it may seem as if the FQR has been identified as a PGRL1-PGR5 complex that acts as a quinone reductase. However, this is not yet the case. As discussed in chapter 1, there are major flaws in the enzymatic assays that are used to support this conclusion, and therefore the identity of the antimycin A sensitive FQR is still yet undetermined. It is clear that PGRL1 and PGR5 have a role in the antimycin A sensitive pathway of CEF in plants, but they may be part of an even larger complex as is seen in algae, or may be regulatory as proposed by Aro and coworkers (114). Chapter 2 discusses the rapid modulation of the FQR by redox state, and suggests the involvement of a regulatory thiol. The E_m of FQR activity is in agreement with the E_m of a thiol present on PGRL1, and supports a regulatory role of this complex as part of, or in association with the FQR. A broader regulatory role for PGR5 is suggested by the large defect in ATP synthase modulation in its absence, a defect that is more likely to explain the dramatic loss of NPQ in this mutant than the loss of CEF. These distinctions are important, because increased emphasis on the role of CEF could lead to an inaccurate model of the light reactions and their regulation.

Despite extensive work on the characterization of NDH (84, 94–96, 167, 183, 213), there are still many unknowns about this complex. There is difficulty in studying NDH, and this may lie in the scarcity of the complex in unstressed Arabidopsis leaves (69, 95). With the recent crystal structure of Complex I a complete structural set of the respiratory electron transport chain has been obtained, and increasing mechanistic studies are possible (97, 98, 210, 214). In the future we can expect similar discoveries with NDH, unlocking one of the last unknowns of the photosynthetic electron transport chain. In the absence of a structure for NDH, we still have discovered many things about this complex. Several groups have done extensive work on identifying the subunits of NDH, and we now have identified >22 nuclear and plastid encoded

genes, as well as several that are plant specific (94). Ongoing research by a number of groups continues to lend insight into assembly, association, and expression of NDH (95, 183, 215).

Functional understanding of NDH is complicated by the difficulty of assessing the activity of the complex. Activity has been measured indirectly by ferricyanide reduction, in gel reduction of NBT in the presence of NADH, and chlorophyll *a* fluorescence changes (84, 85, 99, 213). Quinone reduction assays have also been attempted with soluble quinones, but are likely not physiologically relevant (85). These methods together have yielded new insights but have also led to some key discrepancies (i.e. rates of electron flow) (84, 87, 163) and contradictions (i.e. identity of electron donor) (85, 99, 167). It is clear there is a lot of work to still be done in order to understand even the basic function of this complex.

While *in vitro* work seems to be the standard for NDH activity, the Kramer lab has an increasing body of research on CEF activity *in vivo*. In this dissertation I have presented some key data that begins to fill in the gaps of our understanding of CEF regulation. In addition to the *in vitro* observations of FQR activity in response to redox state described in Chapter 2, Chapter 3 is the first description of CEF (via NDH) activation in response to ROS *in vivo*. These findings are complimentary in that we see differential activation of the two independent pathways of CEF, allowing a response to an ATP deficiency that could have the consequences of both a more reduced stroma, or the buildup of reactive intermediates and subsequently ROS. We additionally see differences in the rate of activation of the two patways, with the FQR rapid (seconds to minute timescale, Chapter 2, Figure 2.4) and the NDH slower (minutes timescale, Chapter 3, Figure 3.6). Additionally, Chapter 5 supports the NDH as a proton pumping quinone reductase, indicating that the two pathways operate at different ATP generating efficiencies. This supports the model proposed in Chapter 2 that the FQR is a 'first response' to ATP/NADPH imbalance,

and allows a more inclusive model of both CEF pathways as a way to fine tune alternative electron transport in the chloroplast.

Chapter 5 also postulates the function of a reversible proton pumping NDH in the thylakoid (Figures 5.3 and 5.4) in which an imbalance in the ATP/NADPH production with and excess of ATP could be corrected by NDH consuming *pmf* to drive oxidation of PQH_2 and reduction of $NADP^+$. This would allow for the increased flexibility of bulk H^+/e^- transfer by the electron transport chain.

6.3 Future directions

Obviously there are still many unanswered questions involving chloroplast energy budget and specifically CEF. The models proposed within this dissertation are far from complete, and require additional rigorous testing. Despite a clear role for ROS signaling in CEF (99, 102) (Chapter 3), we still do not know much about the processes that lead from the signal to activation. The inducible system introduced in Chapter 3 and (176) may serve as a valuable tool in the elucidation of this pathway, and the next step from this work could be a suppressor screen of the GO5 mutant. Previous work points to the potential role of Ca^{2+} signaling and phosphorylation in activation of CEF (102), and it may be that we find proteins involved in either of these that when absent lead to the insensitivity of NDH to peroxide. With the observations presented in (102) and Chapter 3, the field is very open for experimentation.

Likewise, determining the proteins involved in FQR-mediated CEF is the next step in the study of this pathway. Evidence for PGRL1 acting as a direct quinone reductase is ambiguous (discussed above), however, PGRL1 is a good target to look for a complex formation or interaction with a protein that would serve as an appropriate quinone reductase. This has been proposed to be the Q_i site of the cytochrome b_6f complex (b_6f), as the b_6f complex possesses an

additional heme C_i not seen in other *bc* complexes, and closely associates with FNR (110, 168). It is possible that PGRL1 and PGR5 associate further with the b_6f complex to facilitate or activate electron transfer through the heme C_i, and similar associations have been proposed previously (92, 109, 113). This is a difficult hypothesis to test, as we currently lack the ability of inhibit the Q_i site of the b_6f complex, and quinone reduction would likely still occur with the Q_o site inhibited. The reverse genetics approach, despite the difficulties presented in chapter 4, has proven to be quite useful in CEF research, as it has allowed the identification of several mutants with relatively high rates of CEF. While a good proportion of mutants we have identified as *hcef* accumulated high levels of H_2O_2, and as such are likely activated in the NDH pathway of CEF, we have found a few that do not, and these may have increased rates through the FQR. If this is the case, these mutants may provide valuable tools in which to study the antimycin A sensitive pathway. While results are still very preliminary, I am very optimistic and excited to see what comes of these studies.

Finally, as discussed in Chapter 5, the confirmation of a proton pumping NDH is a major discovery in the field of chloroplast bioenergetics. This finding not only substantially increases our structural and evolutionary understanding of NDH, it also increases our regulatory understanding of photosynthesis. It allows for an integrated model of the multiple proposed routes of CEF, and gives insight for why these seemingly redundant pathways have been conserved in plants. The calculations presented in Chapter 5 also show a large gap in our knowledge of NDH (discussed in Chapter 5). We know nothing about the quinone binding site of NDH, we have contradictory evidence as to the identity of the donor (84, 99, 167), and we don't yet know the H^+/e^- of the proton pumping process. These unknowns lead to an incomplete model

as to contribution of *pmf* by the NDH and the conditions in which we would expect NDH to be reversible, and it is very likely this model is not sufficiently descriptive. Therefore, the next steps in this line of research are to characterize the NDH structurally and functionally. This is much easier said than done, but with time and effort we may make the same extraordinary progress as has been seen recently with respiratory Complex I.

Together, the findings within this dissertation are another step towards our complete understanding of CEF and chloroplast energy balance. I look forward to what the scientific community will learn in the next decade and beyond.

APPENDICES

Appendix I

Supplemental methods for chapter 4[14]

[14] These methods were supplied by Kim K. Hixson and Mary Lipton at Pacific Northwest National lab, and will appear in the supplemental material of the published form of chapter 4.

A1.1 Analysis of protein abundance

The following chemicals used, unless otherwise noted, were obtained from the Sigma-Aldrich Company (St. Louis, MO) and were of analytical grade. After extraction, protein was separated into the soluble and membrane fractions and each sample was dried down using evaporative centrifugation and was suspended in 200 mL of 7M urea, 2M thiourea, 4% CHAPS, 2 mL of TCEP in 50 mM ammonium bicarbonate, pH 7.8. Vortexing and sonication were used to aid in solubilizing the pellet. Total protein concentration was determined by Bradford (Pierce, Rockford, IL).

A1.2 Trypsin digestion and cysteine alkylation

Proteins were denatured and digested with trypsin as described elsewhere (216). 20mM iodoacetamide was added and samples were then incubated at room temperature in the dark. Samples were dried using evaporative centrifugation and resuspended in 1 mL of 25% acetonitrile and 10 mM ammonium formate, pH 3.0 with vortexing brief sonication. Samples were centrifuged at 13,500 x *g* for 5 min and the supernatant was used in subsequent steps.

A1.3 Peptide concentration and cleanup

The digests were desalted using Supelco (St. Louis, MO) Discovery 1mL 50 mg SCX SPE tubes. Columns were washed with 1 mL of methanol followed by 2 mL of 25% acetonitrile in 10 mM ammonium formate, pH 3.0. Samples were then loaded and washed with 6 mL of 25% acetonitrile in 10 mM ammonium formate, pH 3.0. Samples were eluted with 5% NH_4OH, 15% water, and 80% methanol, dried via evaporative centrifugation, and resuspended in 60 mL of nanopure water with vortexing and sonication. Samples were then centrifuged at 13,500 x *g* for 5 min the supernatant was taken. Total protein concentration was determined by Bradford, and diluted to a concentration of 1 mg/mL. A peptide sequence library, containing peptide sequences,

elution time, and parent peptide mass, was constructed by MS/MS data acquisition using peptide pools with equal mass from each sample.

A1.4 Strong cation exchange (SCX) fractionation of peptides for potential mass and time (PMT) tag acquisition and capillary LC separations

300 mg of each peptide pool were separated with a SCX fractionation as described elsewhere (217). All SCX fractions and 2.1 mg of each sample were individually separated by an automated in-house designed HPLC system as described next. The HPLC system consisted of a custom configuration of 100 mL Isco Model 100DM syringe pumps (Isco, Inc., Lincoln, NE), 2-position Valco valves (Valco Instruments Co., Houston, TX), and a PAL autosampler (Leap Technologies, Carrboro, NC), allowing for fully automated sample analysis across four separate HPLC columns (218). Reversed-phase capillary HPLC columns were manufactured in-house by slurry packing 3 mm Jupiter C_{18} stationary phase (Phenomenex, Torrence, CA) into a 60 cm length of 360 μm o.d. x 75 μm i.d. fused silica capillary tubing (Polymicro Technologies Inc., Phoenix, AZ) that incorporated a 0.5 mm retaining screen in a 1/16" custom laser-bored 75 mm i.d. union (screen and union - Valco Instruments Co., Houston, TX; laser bore - Lenox Laser, Glen Arm, MD). Mobile phase consisted of 0.2% acetic acid and 0.05% TFA in water (A) and 0.1% TFA in 90% acetonitrile/10% water (B). The mobile phase was degassed by using an in-line Degassex Model DG4400 vacuum degasser (Phenomenex, Torrence, CA). The HPLC system was equilibrated at 10 kpsi with 100% mobile phase A, and then a mobile phase selection valve was switched 50 min after injection, which created a near-exponential gradient as mobile phase B displaced A in a 2.5 mL active mixer. A 30-cm length of 360 mm o.d. x 15 mm i.d. fused silica tubing was used to split ~20 mL/min of flow before it reached the injection valve (5 mL sample loop). The split flow controlled the gradient speed under conditions of constant

pressure operation (10 kpsi). Flow through the capillary HPLC column when equilibrated to 100% mobile phase A was ~500 nL/min.

A1.5 Peptide mass and time tag (PMT) acquisition

The elute from the HPLC was directly electrosprayed into an ion trap MS (LTQ, ThermoFinnigan, San Jose, CA) using electrospray ionization (ESI). The mass spectrometer operated in a data-dependent MS/MS mode and the peptides were analyzed with one full *m*/*z* range (400-2000) each. The details for PMT generation are described elsewhere (219). A total of 152 peptide fraction and complex peptide sample runs produced MS/MS spectra which were analyzed using the peptide identification software SEQUEST (209) in conjunction with the annotated protein translations from the genome sequence of *Arabidopsis thaliana* TAIR 10 annotation (http://www.arabidopsis.org/). A dynamic modification search (i.e., the presence and absence of the modification was searched) for methionine and proline oxidation and a static search (i.e., presence of the modification was searched only) for alkylation of the cysteines by iodoacetamide. Non-enzyme cleavage constraints were applied. Qualitative/cursory identifications in the putative mass and elution time (PMT tag) peptide library were based on a minimum cross correlation (Xcorr) score of 2 for all peptides identified at least twice in all MS/MS experiments.

A1.6 Accurate mass and time (AMT) tag identification and alignment

Using 2.1 μg of total peptide from each individual time point sample, intact peptide mass (MS) data were obtained using the same HPLC system but using a ThermoScientific Exactive Orbitrap mass spectrometer (Thermo Scientific, San Jose, CA) outfitted with a custom built electrospray ionization (ESI) interface. The electrospray emitter was custom made using 150 mm o.d. x 20 mm i.d. chemically etched fused silica column (220). The heated capillary

temperature and spray voltage were 200°C and 2.2 kV, respectively. Data were acquired for 100 min., beginning 65 min. after sample injection (15 min. into gradient). The mass spectrometer was set to record spectra from *m/z* 400 to 2000 at a resolution of 100,000 and AGC setting of $3x10^6$. Each sample was run in duplicate. The run order for each run set of duplicates was randomized in a Latin Squares design. A mass calibration mixture was infused at the end of each analysis, and the masses of the compounds in the mixture were used to calibrate all of the spectra within the analysis.

The MS data obtained from the Exactive MS were subsequently processed using the PRISM Data Analysis System, a series of software tools developed in-house. The data were initially de-isotoped to give a monoisotopic mass, charge, and intensity of the major peaks in each spectrum. The data were then analyzed in a two-dimensional fashion to determine the groups of peaks that were observed in sequential spectra.

Each group identified as a unique mass class (UMC) feature, was characterized as having a distinctive median mass, central normalized elution time (NET) (221), and its abundance was estimated by the maximum of the intensity for its MS peaks. Each UMC was determined by comparing the mass and NET to those in the PMT tag database that passed the p-value cutoff of 0.01 using the in-house developed software Viper (http://omics.pnl.gov/software) (222). Filter tolerances were set to ± 2 ppm for the mass and ± 2.5% for the elution time. Those UMCs (MS only data from the Exactive) that most closely matched the PMT tags (MS/MS peptide data from the LTQ iontraps) and whose predicted parent mass was verified by the high mass measurement accuracy provided by the Exactive Orbitrap MS were validated as Accurate Mass and Time (AMT) tags resulting in a list of peptides observed and an abundance value for each which was

calculated by Viper as the sum of the peak intensity of each eluting peptide over the time it was observed for the most abundant charge state.

A1.7 Normalization of replicate analyses

Peptide data that resulted after peak matching and STAC_UP score filtering (> 0.5), were then transformed into log2 values and were normalized using the mean center normalization function in the publically available software Inferno (https://code.google.com/p/inferno4proteomics/). Proteins with peptides shared among many proteins were grouped together. Next all the peptides unique to one protein and the peptides that are shared among multiple proteins, were "rolled up' into a single protein or protein group value by using the Rrollup function in Inferno. Rrollup works by first identifying the most abundant and prevalent (seen in most LC-MS runs) peptide for each protein or protein group. Using the abundance value profile of this peptide all other abundance profiles for all other peptides belonging to that protein are scaled (normalized) to it. The protein value is then calculated by taking the median value of all normalized peptides in that run. For proteins seen 5% of the time in all datasets with 1 or more unique peptides identified, an additional Grubbs' test (p-value cutoff 0.1) was performed to eliminate outlier profiles from the rollup calculation. Proteins with only 1 peptide identified were included for consideration and so the number of peptides identified for each protein is included in all data tables so that those proteins can still be considered but given less weight.

A1.8 Log fold change determination

Log2 values of the Rrollup protein/protein groups were transformed back to a non-log transformed value by calculating 2^(log2 changes in protein abundance). Missing values were imputed with 160 which was a value less than the minimum abundance value in the entire

dataset. Protein abundances determined to be significantly represented within the data set were isolated for each protein complex of interest and positive and negative fold changes were then determined for each *hcef2* sample versus the average Col-0 abundance for either the insoluble or soluble samples.

Appendix 2

Towards a more precise measure of electron transfer rates through photosystem II

Deserah D. Strand and David M. Kramer

A2.1 Abstract

The use of chlorophyll *a* fluorescence in photosynthetic measurements is considered the gold standard in labs all over the world. However, the calculations for photosynthetic electron transport often make many assumptions about the system being measured. This manuscript discusses these assumptions and proposes conditions in which these assumptions are likely violated. Specifically, the method for calculating PS II electron transfer rates, or linear electron flow, is discussed, and a method for the careful correction of these rates is presented.

A2.2 Introduction

Chlorophyll *a* fluorescence yield is frequently used to calculate photosynthetic parameters in a relatively simple and non-invasive manner. It has been used extensively in basic research to identify and characterize structural and regulatory components of the photosynthetic electron transport chain (7, 82, 84, 223). In addition to this, chlorophyll fluorescence imaging has been used in a wide range of crop specific research, such as breeding efforts to identifying plants with increased stress or disease resistance and in the mapping of beneficial QTLs (224–226) [reviewed in (227)]. The current trend of research towards high-throughput screening methods using this technique, in conjunction with fluctuating light or stress conditions, has allowed the identification of conditions in which mutants in chloroplast targeted proteins show a fluorescence phenotype when none was previously described, and has the potential to make a large impact on our understanding of photosynthesis and how it relates to downstream metabolism and stress response (J. Cruz, L. Savage, R. Zegarac, W. Kovac, C. Hall, J. Chen, R. Last, D. Kramer, submitted).

One particularly vital parameter is electron transfer rates through photosystem II, or linear electron flow (LEF). This has traditionally been done by using chlorophyll *a* fluorescence

to calculate the quantum yield of PS II (ϕ_{II}) (187, 228), which is then multiplied by light intensity and leaf absorbance to yield a rate of electron transfer on an area basis (μmoles e^- m^{-2} s^{-1}). This method, and the variations of this method, correlate well with O_2 evolution and CO_2 assimilation, and have become a cornerstone measurement in photosynthesis research. However, this calculation of LEF makes many assumptions, which may not be valid when applied to the mutant or ecotype populations that are currently the subject of large-scale imaging experiments.

During large screening programs it may be beneficial to isolate subpopulations or phenotypes of interest by these more simplistic and rapid methods; however, after isolation of the desired phenotype, a careful consideration of the elements that determine electron transfer rates, and appropriate corrections for these may yield even more vital information as to the nature of any perceived changes. In this work we discuss the variables applied in the traditional calculation of LEF, the assumptions that are made in the application of these variables, and conditions in which violation of these assumptions may make a large difference in perceived electron transfer rates.

A2.2.A What do we need to know to calculate LEF rates?

To measure electron transfer rates through PS II, we need to know several parameters: The incident light intensity, i, the fraction of the light that is absorbed by PS II bound chlorophylls, f_{II}, and the quantum yield of PS II, i.e. the fraction of open PS II centers, ϕ_{II} (7, 187). These parameters combine to give electron transfer rates on a per leaf area basis (μmoles e^- m^{-2} s^{-1}).

Eq. A2.1

$$LEF \propto i * f_{II} * \phi_{II}$$

This equation is similar to past methods (7, 69, 227, 229), with one key difference; the f_{II} parameter is difficult to directly measure where:

Eq. A2.2

$$f_{II} \propto \frac{Chl_{II}}{Chl_{II} + Chl_{I}}$$

or, f_{II} is fraction of total chlorophyll bound to PS II. Assuming that all chlorophylls absorb evenly and all chlorophylls are bound, or chlorophyll that is not attached to a photosystem are constant or negligible. In the absence of a simple way to determine the fraction of total chlorophyll bound to PS II, previous corrections for quantifying LEF included measuring total leaf absorptivity using an integrating sphere, and assuming that all light absorbed was directed toward photosystems (69).

In the absence of a state transition, or differences in antenna size, it has been generally accepted to assume total absorbance (per area unit) is attributed to equal absorbance of PS II and PS I bound chlorophylls and that these are equally distributed between the photosystems. However, accounting for LEF differences when there is a state transition (even a small one) is not easily done. There may also be changes in antennae size that do not appear as a state transition, i.e. if there is not a change in the excitation ratio of the photosystems a state transition is not perceived. This problem is compounded if there is a combination of these differences when

comparing mutants within a species, or plants between species. In these cases, it may be vital to quantify f_{II}. To assign a value to f_{II}, we can begin by looking at the rate of fluorescence rise with low illumination, in the presence of DCMU (230).

Under these conditions the rate constant of the rise is dependent on the size of the antenna, B_{II} , and the quantum efficiency of PS II, ϕ_{II}

Eq. A2.3

$$\phi_{II} * B_{II} \propto k_{rise}$$

and which rearranges to:

Eq. A2.4

$$B_{II} \propto \frac{k_{rise}}{\phi_{II}} \propto \frac{Chl_{II}}{[PSII]}$$

in which B_{II} is proportional to the number of chlorophylls bound to each PS II. Then by substitution:

Eq. A2.5

$$B_{II} \propto \frac{\frac{1}{\tau_{rise}}}{\frac{f_v}{f_m}}$$

Where τ_{rise} is the halftime of the fluorescence rise, and f_v/f_m is the maximal quantum yield of PS II (7).The incident light intensity would also be factor, however, if the intensity is held as a constant, it can be ignored.

This tells us the relative amount of chlorophyll attached to each individual PS II, but does not yet give us the fraction of total chlorophyll that is bound to a PS II. To get at this, we need to know the concentration of PS II. It is much simpler (and accessible) to measure relative PS I content by total absorbance changes at 820 nm in DCMU treated leaves where:

Eq. A2.6

$$[PSI] \propto \Delta\Delta A_{820nm}$$

Where:

Eq. A2.7

$$\Delta\Delta A_{820nm} = \Delta A_{820nm-light} - \Delta A_{820nm-dark}$$

in which the concentration of PS I is proportional to the difference in absorbance of 820 nm light of the reduced (dark adapted) and completely oxidized (during the second saturation flash) forms of P700 (121) (Figure A2.1).

By giving two successive saturating flashes in the presence of DCMU it should be possible to completely oxidize PS I, as the PC pool is oxidized by PS I following the first flash. Partially oxidized PS I remains as indicated by the sustained increase of 820 nm absorbance

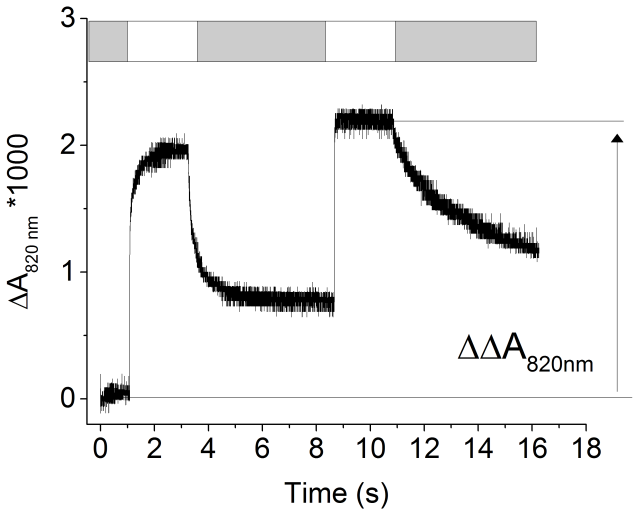

Figure A2.1 Representative experimental data for the calculation of [PSI]. $\Delta A_{820\ nm}$ increases with concentration of $P700^+$. First, a 2 second saturation flash is applied to a dark-adapted, DCMU infiltrated leaf. The following dark interval does not decay to dark-adapted leaves, as DCMU blocks electrons from PS II from reducing $P700^+$. A second 2 second saturating flash is able to then further (and fully) oxidize the remaining P700. The difference between the $\Delta A_{820\ nm}$ of the second saturating flash and the $\Delta A_{820\ nm}$ of the dark-adapted state is proportional to [PSI].

during the dark interval. A second flash should completely oxidize PS I, allowing a total absorbance change to be measured which is relative to total PS I content on a per leaf area basis.

Then, to calculate PS I/PS II, we use the electrochromic shift of the carotenoids at 520 nm in response to an electric field across the thylakoid membrane (Figure A2.2). A short multiple-turnover saturating flash (10 μs) will excite the photosystems and induce charge separation and electric field. In the presence of DCMU there is no contribution to electric field by protons, therefore, the initial amplitude of the ECS is proportional to the charge separation of both PS I and PS II. PC reduces PS I after oxidation by the first flash, leading to a long-lived maintenance of electric field. A second flash drives charge separation only through PS I, allowing the calculation of ECS attributed to PS I alone [discussed in Kramer and Crofts (129)].

This allows us to calculate the fraction or ratio of PS II to PS I, or *E*:

Eq. A2.8

$$E \propto \frac{ECS_{ft} - ECS_{fI}}{ECS_{fI}} \propto \frac{[PSII]}{[PSI]}$$

And if we take the product of these 3 parameters:

Eq. A2.9

$$B_{II} * E * \Delta\Delta A_{820nm} \propto \frac{Chl_{II}}{[PSII]} * \frac{[PSII]}{[PSI]} * [PSI]$$

which simplifies to Chl_{II}, or relative number of chlorophylls bound to PS II. To determine the fraction of chlorophylls bound to PS II, we need to know the total chlorophyll content per leaf

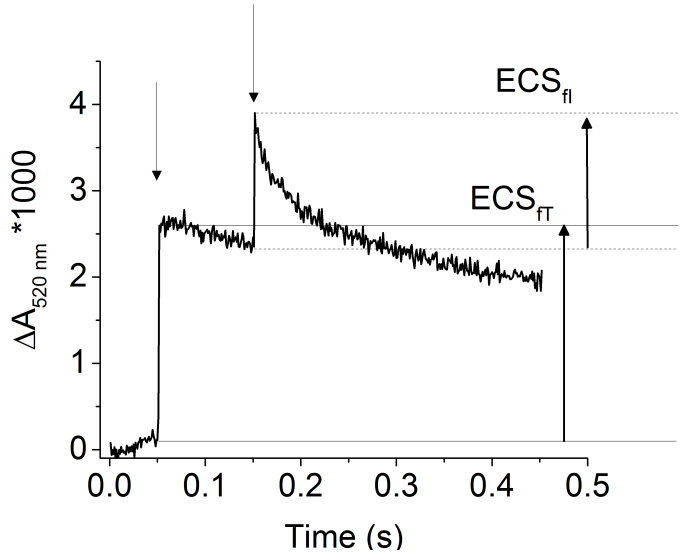

Figure A2.2 Representative experimental data for the calculation of *E*. Under an electric field, there is a shift in the absorbance spectrum of the carotenoids towards 520 nm, the so-called electrochromic shift. A short saturating flash (downward arrows) is applied to a dark-adapted, DCMU infiltrated leaf and there is a sharp rise in $\Delta_{A520\ nm}$ due to charge separation at PS I and PS II. A second saturation flash generates further ECS due to charge separation at PS I alone, and *E* is calculated as described in Eq. A2.8.

area. This may be determined as described in Chapter 4, or in the absence of a change in the composition of the carotenoids to chlorophyll ratios, the ECS_{ft}. However, without this information, if we use the relative number of chlorophylls bound to PS II for the f_{II} parameter, in place of the fractional amount of total chlorophyll:

Eq. A2.10

$$f_{II} \propto B_{II} * E * \Delta\Delta A_{820nm}$$

Under normal growth chamber conditions, or in mutants that do not display large differences in either state transitions or chlorophyll *a*/*b*, this extensive correction of LEF may not be necessary. However, under conditions where there is a large state transition, less pigmentation, or skewed chlorophyll *a*/*b*, we have outright violated the assumptions generally made while calculating LEF, and a very careful correction is required.

This thesis presents several mutants in which it is likely that the standard assumptions within the LEF calculation are likely violated (Chapters 3 and 4) despite careful corrections described within those manuscripts. There are also likely multiple instances in the literature that would likely benefit from a more complete characterization of LEF rates. One such mutant that is currently being studied in multiple labs is an Arabidopsis mutant with increased rates of cyclic electron flow around photosystem I (69) (E-M Aro, E. Tyystjärvi, personal communication). It has been proposed that *hcef1* has increased rates of CEF through the NDH complex (69). This interpretation of the data is dependent on a precise measurement of LEF in this mutant. Traditional methods suggested a greater increase in the slope of v_H^+/LEF than in the slope of

ϕ_I/ϕ_{II} (69), which could be interpreted as an increase in the H^+/e^- stoichiometry of CEF over the so-called LEF, and would require the involvement of a proton-pumping plastoquinone reductase. To truly attempt a calculation of the H^+/e^- ratio of CEF *in vivo*, it is vital that we develop a more careful approach to LEF quantification. Therefore, we developed a combined set of methods that allow us to do this. In the process we have discovered thylakoid architecture changes in *hcef1* that have direct implications for CEF levels described in Livingston et al. (69), and functional properties of NDH.

A2.3 Results and Discussion

A2.3.A PS II antenna size

When leaves infiltrated with DCMU are iluminated at low (>100 μmol photons m^{-2} s^{-1}) light, it allows a slow fluorescence increase, of which the halftime and quantum yield can be easily calculated. The inverse of the τ_{rise} is proportional to the product of the antenna size (B_{II}) and quantum yield of PS II (ϕ_{II}) (see Eq. A2.3) and simple rearrangement of parameters allows us to calculate B_{II} (see Eq. A2.4). In Col-0 and *hcef1* these values were calculated as 0.76 and 1.26 (from Eq. A2.5) when using 700 nm illumination as necessitated by Chapter 5 conditions, this indicates an effective increase in *hcef1* PS II antennae size of 66% over Col-0.

A2.3.B Relative PS I content

Figure A2.3 shows the absorbance changes of P700 at 820 nm from dark to light in DCMU treated leaves of Col-0 (Figure A2.3*A*) and *hcef1* (Figure A2.3*B*). As we show in Eq. A2.6, the total amplitude of $\Delta A_{820\ nm}$ is proportional to PS I content (per area unit). Therefore,

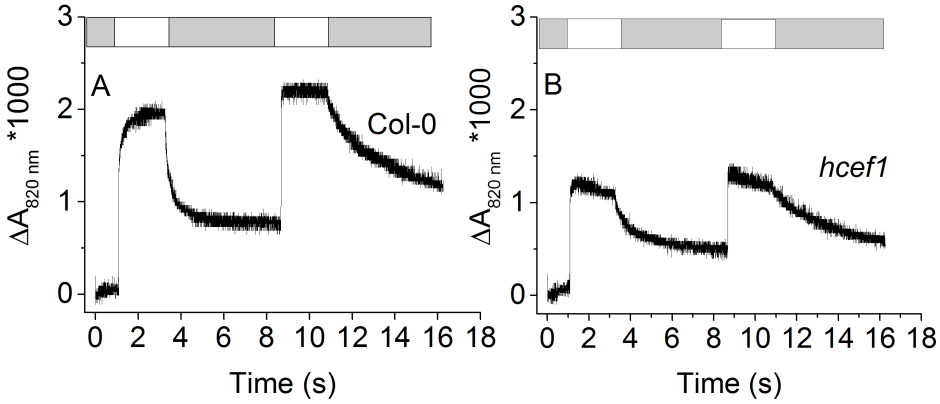

Figure A2.3 Decreased [PSI] in *hcef1*. $\Delta A_{820\ nm}$ in dark-adapted, DCMU infiltrated leaves of Col-0 (A) and *hcef1* (B) after two 2 second saturating flashes as described in Figure A2.1.

we use this value as [PSI]. We see 58% less [PSI] in *hcef1* than in Col-0 (1.4 and 2.4 milliabsorbance units, respectively).

A2.3.C PS II/PS I content

Using Eq. A2.8 and the amplitude of the ECS induced by two multiple turnover flashes 100 ms apart (Figure A2.4), we are able to calculate *E* in Col-0 and *hcef1* (0.67 and 0.4 respectively). This measurement reveals changes in the makeup of the thylakoid membrane of *hcef1*. Specifically, *hcef1* has less PS II/PS I content. Coupled with the relative PS II antenna size increase in *hcef1*, this data may explain the perceived state I condition of *hcef1* (D. Strand and D. Kramer, unpublished), however to fully determine this PS I antenna size must be addressed.

This method allows careful determination of relative LEF values, and may be of vital importance when comparing LEF rates in not only mutants, but under conditions where changes in light absorbance may occur, such as different quality of light. In Chapter 5 we use 700 nm light as an actinic source to poise the system with a more oxidized PS I pool, in which case the fraction of total photons absorbed by PS II are certainly lower than the fraction absorbed from 625 nm LEDs used in previous studies (33, 69, 72) (Chapters 3 and 4). However, when B_{II} is calculated from a 625 nm LED and a 700 nm LED, both *hcef1* and Col-0 lose the same fraction of total photons absorbed, suggesting that despite the change in antennae size, there is no difference in the makeup of the antennae structure of *hcef1* (Data not shown). This method of calculating LEF may also be of value when comparing the effects of different wavelengths on photosynthesis or photoinhibition, where less absorbance of a specific wavelength may lead to more open PS II centers, and therefore higher perceived rates of LEF.

While there have been no newly described methods in this manuscript, the combination of methods allow for a new way to calibrate LEF across a variety of conditions. This does not

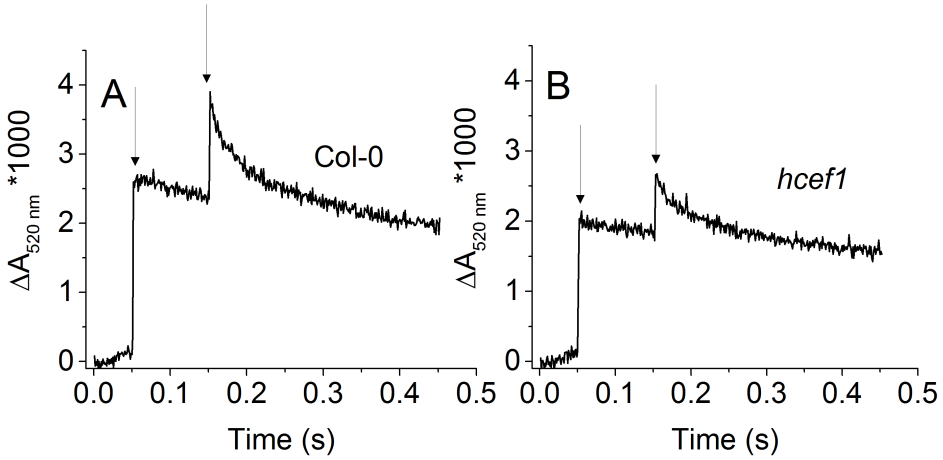

Figure A2.4 Altered [PSII]/[PSI] in *hcef1*. $\Delta A_{520\ nm}$ in dark-adapted, DCMU infiltrated leaves of Col-0 (A) and *hcef1* (B) after two 10 μs saturating flashes as described in Figure A2.2.

correct any assumptions that may be violated within the ϕ_{II} measurement, and any attempt to do so has been described extensively elsewhere (179, 187, 228, 231, 232).

A2.4 Materials and Methods

A2.4.A Plant materials and growth conditions

Plants and growth conditions are as described in Chapter 5.

A2.4.B *In vivo* spectroscopy

Chlorophyll a fluorescence and absorbance spectroscopy was performed on a spectrophotometer described in detail previously (166). In all assays leaves were infiltrated with 50 μM DCMU by incubating detached leaves in the dark for 3 hours between 2 saturated lab tissues.

A2.5 Acknowledgements

I would like to thank Dr. Nicolas Fisher, Dr. Atsuko Kanazawa, and Dr. Jeff Cruz for helpful discussions. This work was supported by Grant DE-FG02-11ER16220 from the Photosynthetic Systems program from Division of Chemical Sciences, Geosciences, and Biosciences, Office of Basic Energy Sciences of the US Department of Energy (to David M. Kramer).

REFERENCES

REFERENCES

1. Müller P, Li XP, Niyogi KK (2001) Non-photochemical quenching. A response to excess light energy. *Plant Physiol* 125:1558–66.

2. Kramer DM, Evans JR (2011) The importance of energy balance in improving photosynthetic productivity. *Plant Physiol* 155:70–8.

3. Eberhard S, Finazzi G, Wollman F-A (2008) The dynamics of photosynthesis. *Annu Rev Genet* 42:463–515.

4. Zhu X-G, de Sturler E, Long SP (2007) Optimizing the distribution of resources between enzymes of carbon metabolism can dramatically increase photosynthetic rate: a numerical simulation using an evolutionary algorithm. *Plant Physiol* 145:513–26.

5. Long SP, Zhu X-G, Naidu SL, Ort DR (2006) Can improvement in photosynthesis increase crop yields? *Plant Cell Environ* 29:315–30.

6. Hambourger M et al. (2009) Biology and technology for photochemical fuel production. *Chem Soc Rev* 38:25–35.

7. Baker NR (2008) Chlorophyll fluorescence: a probe of photosynthesis in vivo. *Annu Rev Plant Biol* 59:89–113.

8. Pfannschmidt T (2003) Chloroplast redox signals: how photosynthesis controls its own genes. *Trends Plant Sci* 8:33–41.

9. Cruz JA et al. (2005) Plasticity in light reactions of photosynthesis for energy production and photoprotection. *J Exp Bot* 56:395–406.

10. Li X-P et al. (2004) Regulation of photosynthetic light harvesting involves intrathylakoid lumen pH sensing by the PsbS protein. *J Biol Chem* 279:22866–74.

11. Van Amerongen H, Croce R (2013) Light harvesting in photosystem II. *Photosynth Res* 116:251–63.

12. Croce R, van Amerongen H (2011) Light-harvesting and structural organization of Photosystem II: from individual complexes to thylakoid membrane. *J Photochem Photobiol B* 104:142–53.

13. Croce R, van Amerongen H (2013) Light-harvesting in photosystem I. *Photosynth Res* 116:153–166.

14. Cape JL, Bowman MK, Kramer DM (2006) Understanding the cytochrome *bc* complexes by what they don't do. The Q-cycle at 30. *Trends Plant Sci* 11:46–55.

15. Cramer WA, Hasan SS, Yamashita E (2011) The Q cycle of cytochrome *bc* complexes: a structure perspective. *Biochim Biophys Acta* 1807:788–802.

16. Osmond B, Förster B (2006) *In* Advances in Photosynthesis and Respiration, Vol. 21. eds Demmig-Adams B, Adams III W, Mattoo, AK (Springer Netherlands) pp 11–22.

17. Baginsky S, Link G (2006) *In* Advances in Photosynthesis and Respiration, Vol. 21. eds Demmig-Adams B, Adams III W, Mattoo, AK (Springer Netherlands) pp 269–287.

18. Demmig-Adams B et al. (2006) *In* Advances in Photosynthesis and Respiration, Vol. 21. eds Demmig-Adams B, Adams III W, Mattoo, AK (Springer Netherlands) pp 39–48.

19. Allahverdiyeva Y, Aro E (2012) *In* Advances in Photosynthesis and Respiration, Vol. 34. eds Eaton-Rye JJ, Tripathy BC, Sharkey TD (Springer Netherlands, Dordrecht), pp 275–297.

20. Kirilovsky D (2007) Photoprotection in cyanobacteria: the orange carotenoid protein (OCP)-related non-photochemical-quenching mechanism. *Photosynth Res* 93:7–16.

21. Bailey S, Grossman A (2008) Photoprotection in cyanobacteria: regulation of light harvesting. *Photochem Photobiol* 84:1410–20.

22. Holt NE, Fleming GR, Niyogi KK (2004) Toward an understanding of the mechanism of nonphotochemical quenching in green plants. *Biochemistry* 43:8281–9.

23. Holt NE et al. (2005) Carotenoid cation formation and the regulation of photosynthetic light harvesting. *Science* 307:433–6.

24. Li X-P, Muller-Moule P, Gilmore AM, Niyogi KK (2002) PsbS-dependent enhancement of feedback de-excitation protects photosystem II from photoinhibition. *Proc Natl Acad Sci USA* 99:15222–7.

25. Kramer DM, Avenson TJ, Edwards GE (2004) Dynamic flexibility in the light reactions of photosynthesis governed by both electron and proton transfer reactions. *Trends Plant Sci* 9:349–57.

26. Takizawa K, Cruz JA, Kanazawa A, Kramer DM (2007) The thylakoid proton motive force *in vivo*. Quantitative, non-invasive probes, energetics, and regulatory consequences of light-induced *pmf*. *Biochim Biophys Acta* 1767:1233–44.

27. Kramer DM, Sacksteder CA, Cruz JA (1999) How acidic is the lumen ? *Photosynth Res* 60:151–163.

28. Krieger A, Weis E (1993) The role of calcium in the pH-dependent control of Photosystem II. *Photosynth Res* 37:117–30.

29. Tyystjärvi E, Aro EM (1996) The rate constant of photoinhibition, measured in lincomycin-treated leaves, is directly proportional to light intensity. *Proc Natl Acad Sci USA* 93:2213–8.

30. Nishiyama Y, Allakhverdiev SI, Murata N (2006) A new paradigm for the action of reactive oxygen species in the photoinhibition of photosystem II. *Biochim Biophys Acta* 1757:742–9.

31. Sarvikas P, Hakala M, Pätsikkä E, Tyystjärvi T, Tyystjärvi E (2006) Action spectrum of photoinhibition in leaves of wild type and npq1-2 and npq4-1 mutants of Arabidopsis thaliana. *Plant Cell Physiol* 47:391–400.

32. Kanazawa A, Kramer DM (2002) *In vivo* modulation of nonphotochemical exciton quenching (NPQ) by regulation of the chloroplast ATP synthase. *Proc Natl Acad Sci USA* 99:12789–94.

33. Avenson TJ, Cruz JA, Kramer DM (2004) Modulation of energy-dependent quenching of excitons in antennae of higher plants. *Proc Natl Acad Sci USA* 101:5530–5.

34. Avenson TJ et al. (2005) Integrating the proton circuit into photosynthesis: progress and challenges. *Plant, Cell Environ* 28:97–109.

35. Avenson TJ, Cruz JA, Kanazawa A, Kramer DM (2005) Regulating the proton budget of higher plant photosynthesis. *Proc Natl Acad Sci USA* 102:9709–13.

36. Kramer DM, Cruz JA, Kanazawa A (2003) Balancing the central roles of the thylakoid proton gradient. *Trends Plant Sci* 8:27–32.

37. Zhang R et al. (2009) Moderate heat stress reduces the pH component of the transthylakoid proton motive force in light-adapted, intact tobacco leaves. *Plant Cell Environ* 32:1538–47.

38. Murchie EH, Niyogi KK (2011) Manipulation of photoprotection to improve plant photosynthesis. *Plant Physiol* 155:86–92.

39. Allen J (2002) Photosynthesis of ATP-electrons, proton pumps, rotors, and poise. *Cell* 110:273–6.

40. Backhausen JE, Kitzmann C, Scheibe R (1994) Competition between electron acceptors in photosynthesis: Regulation of the malate valve during CO_2 fixation and nitrite reduction. *Photosynth Res* 42:75–86.

41. Scheibe R (2004) Malate valves to balance cellular energy supply. *Physiol Plant* 120:21–26.

42. Fridlyand LE, Backhausen JE, Scheibe R (1998) Flux control of the malate valve in leaf cells. *Arch Biochem Biophys* 349:290–8.

43. Scheibe R, Backhausen JE, Emmerlich V, Holtgrefe S (2005) Strategies to maintain redox homeostasis during photosynthesis under changing conditions. *J Exp Bot* 56:1481–9.

44. Hebbelmann I et al. (2012) Multiple strategies to prevent oxidative stress in Arabidopsis plants lacking the malate valve enzyme NADP-malate dehydrogenase. *J Exp Bot* 63:1445–59.

45. Asada K (2006) Production and scavenging of reactive oxygen species in chloroplasts and their functions. *Plant Physiol* 141:391–396.

46. Asada K (2000) The water-water cycle as alternative photon and electron sinks. *Philos Trans R Soc Lond B Biol Sci* 355:1419–31.

47. Robinson JM (1988) Does O2 photoreduction occur within chloroplasts in vivo? *Physiol Plant* 72:666–80.

48. Asada K (1999) The water-water cycle in chloroplasts: scavenging of active oxygens and dissipation of excess photons. *Annu Rev Plant Physiol Plant Mol Biol* 50:601–639.

49. Driever SM, Baker NR (2011) The water-water cycle in leaves is not a major alternative electron sink for dissipation of excess excitation energy when CO_2 assimilation is restricted. *Plant Cell Environ* 34:837–46.

50. Badger MR, von Caemmerer S, Ruuska S, Nakano H (2000) Electron flow to oxygen in higher plants and algae: rates and control of direct photoreduction (Mehler reaction) and rubisco oxygenase. *Philos Trans R Soc Lond B Biol Sci* 355:1433–46.

51. Ruuska SA, Badger MR, Andrews TJ, von Caemmerer S (2000) Photosynthetic electron sinks in transgenic tobacco with reduced amounts of Rubisco: little evidence for significant Mehler reaction. *J Exp Bot* 51 Spec No:357–68.

52. Clarke JE, Johnson GN (2001) In vivo temperature dependence of cyclic and pseudocyclic electron transport in barley. *Planta* 212:808–16.

53. Heber U (2002) Irrungen, Wirrungen? The Mehler reaction in relation to cyclic electron transport in C3 plants. *Photosynth Res* 73:223–31.

54. Proctor MCF, Smirnoff N (2011) Ecophysiology of photosynthesis in bryophytes: major roles for oxygen photoreduction and non-photochemical quenching? *Physiol Plant* 141:130–40.

55. Makino A, Miyake C, Yokota A (2002) Physiological functions of the water-water cycle (Mehler reaction) and the cyclic electron flow around PSI in rice leaves. *Plant Cell Physiol* 43:1017–26.

56. Ort DR, Baker NR (2002) A photoprotective role for O_2 as an alternative electron sink in photosynthesis? *Curr Opin Plant Biol* 5:193–8.

57. Joët T et al. (2002) Involvement of a plastid terminal oxidase in plastoquinone oxidation as evidenced by expression of the *Arabidopsis thaliana* enzyme in tobacco. *J Biol Chem* 277:31623–30.

58. Aluru MR, Yu F, Fu A, Rodermel S (2006) Arabidopsis variegation mutants: new insights into chloroplast biogenesis. *J Exp Bot* 57:1871–81.

59. Rumeau D, Peltier G, Cournac L (2007) Chlororespiration and cyclic electron flow around PSI during photosynthesis and plant stress response. *Plant Cell Environ* 30:1041–51.

60. Laureau C et al. (2013) Plastid terminal oxidase (PTOX) has the potential to act as a safety valve for excess excitation energy in the alpine plant species Ranunculus glacialis L. *Plant Cell Environ*:1296–1310.

61. Trouillard M et al. (2012) Kinetic properties and physiological role of the plastoquinone terminal oxidase (PTOX) in a vascular plant. *Biochim Biophys Acta* 1817:2140–8.

62. Lilley RM, Fitzgerald MP, Rienits KG, Walker DA (1975) Criteria of intactness and the photosynthetic activity of spinach chloroplast preparations. *New Phytol* 75:1–10.

63. Stitt M, Lilley RM, Heldt HW (1982) Adenine nucleotide levels in the cytosol, chloroplasts, and mitochondria of wheat leaf protoplasts. *Plant Physiol* 70:971–7.

64. Joliot P, Joliot A (2006) Cyclic electron flow in C3 plants. *Biochim Biophys Acta* 1757:362–8.

65. Johnson GN (2011) Physiology of PSI cyclic electron transport in higher plants. *Biochim Biophys Acta* 1807:384–9.

66. Joliot P, Johnson GN (2011) Regulation of cyclic and linear electron flow in higher plants. *Proc Natl Acad Sci USA* 108:13317–22.

67. Harbinson J, Genty B, Baker NR (1989) Relationship between the Quantum Efficiencies of Photosystems I and II in Pea Leaves. *Plant Physiol* 90:1029–34.

68. Fan D-Y et al. (2007) Quantification of cyclic electron flow around Photosystem I in spinach leaves during photosynthetic induction. *Photosynth Res* 94:347–57.

69. Livingston AK, Cruz JA, Kohzuma K, Dhingra A, Kramer DM (2010) An *Arabidopsis* mutant with high cyclic electron flow around photosystem I (*hcef*) involving the NADPH dehydrogenase complex. *Plant Cell* 22:221–33.

70. Livingston AK, Kanazawa A, Cruz JA, Kramer DM (2010) Regulation of cyclic electron flow in C_3 plants: differential effects of limiting photosynthesis at ribulose-1,5-bisphosphate carboxylase/oxygenase and glyceraldehyde-3-phosphate dehydrogenase. *Plant Cell Environ* 33:1779–88.

71. Jia H, Oguchi R, Hope AB, Barber J, Chow WS (2008) Differential effects of severe water stress on linear and cyclic electron fluxes through Photosystem I in spinach leaf discs in CO_2-enriched air. *Planta* 228:803–12.

72. Kohzuma K et al. (2009) The long-term responses of the photosynthetic proton circuit to drought. *Plant Cell Environ* 32:209–19.

73. Kubicki A, Funk E, Westhoff P, Steinmüller K (1996) Differential expression of plastome-encoded ndh genes in mesophyll and bundle-sheath chloroplasts of the C4 plant Sorghum bicolor indicates that the complex I-homologous NAD(P)H-plastoquinone oxidoreductase is involved in cyclic electron transport. *Planta* 199:276–281.

74. Finazzi G, Forti G (2004) Metabolic flexibility of the green alga *Chlamydomonas reinhardtii* as revealed by the link between state transitions and cyclic electron flow. *Photosynth Res* 82:327–38.

75. Joët T, Cournac L, Peltier G, Havaux M (2002) Cyclic electron flow around photosystem I in C_3 plants. In vivo control by the redox state of chloroplasts and involvement of the NADH-dehydrogenase complex. *Plant Physiol* 128:760–9.

76. Joliot P, Béal D, Joliot A (2004) Cyclic electron flow under saturating excitation of dark-adapted Arabidopsis leaves. *Biochim Biophys Acta* 1656:166–76.

77. Golding AJ, Finazzi G, Johnson GN (2004) Reduction of the thylakoid electron transport chain by stromal reductants--evidence for activation of cyclic electron transport upon dark adaptation or under drought. *Planta* 220:356–63.

78. Cruz JA et al. (2005) Plasticity in light reactions of photosynthesis for energy production and photoprotection. *J Exp Bot* 56:395–406.

79. Gotoh E, Matsumoto M, Ogawa K, Kobayashi Y, Tsuyama M (2010) A qualitative analysis of the regulation of cyclic electron flow around photosystem I from the post-illumination chlorophyll fluorescence transient in Arabidopsis: a new platform for the in vivo investigation of the chloroplast redox state. *Photosynth Res* 103:111–23.

80. Maiwald D et al. (2003) Knock-out of the genes coding for the Rieske protein and the ATP-synthase δ-subunit of Arabidopsis. Effects on photosynthesis, thylakoid protein composition, and nuclear chloroplast gene expression. *Plant Physiol* 133:191–202.

81. Walters RG, Ibrahim DG, Horton P, Kruger NJ (2004) A mutant of Arabidopsis lacking the triose-phosphate/ phosphate translocator reveals metabolic regulation of starch breakdown in the light. *Plant Physiol* 135:891–906.

82. Munekage Y et al. (2002) PGR5 is involved in cyclic electron flow around photosystem I and is essential for photoprotection in *Arabidopsis*. *Cell* 110:361–371.

83. DalCorso G et al. (2008) A complex containing PGRL1 and PGR5 is involved in the switch between linear and cyclic electron flow in Arabidopsis. *Cell* 132:273–85.

84. Burrows PA, Sazanov LA, Svab Z, Maliga P, Nixon PJ (1998) Identification of a functional respiratory complex in chloroplasts through analysis of tobacco mutants containing disrupted plastid ndh genes. *EMBO J* 17:868–76.

85. Sazanov LA, Burrows PA, Nixon PJ (1998) The plastid ndh genes code for an NADH-specific dehydrogenase: isolation of a complex I analogue from pea thylakoid membranes. *Proc Natl Acad Sci USA* 95:1319–24.

86. Desplats C et al. (2009) Characterization of Nda2, a plastoquinone-reducing type II NAD(P)H dehydrogenase in *Chlamydomonas* chloroplasts. *J Biol Chem* 284:4148–57.

87. Munekage Y, Hashimoto M, Miyake C (2004) Cyclic electron flow around photosystem I is essential for photosynthesis. *Nature* 700:0–3.

88. Hosler JP, Yocum CF (1987) Regulation of cyclic photophosphorylation during ferredoxin-mediated electron transport. *Plant Physiol* 83:965–969.

89. Scheller HV (1996) In vitro cyclic electron transport in barley thylakoids follows two independent pathways. *Plant Physiol* 110:187–194.

90. Ducruet J-M, Roman M, Havaux M, Janda T, Gallais A (2005) Cyclic electron flow around PSI monitored by afterglow luminescence in leaves of maize inbred lines (Zea mays L.): correlation with chilling tolerance. *Planta* 221:567–79.

91. Takabayashi A, Kishine M, Asada K, Endo T, Sato F (2005) Differential use of two cyclic electron flows around photosystem I for driving CO_2-concentration mechanism in C_4 photosynthesis. *Proc Natl Acad Sci USA* 102:16898–903.

92. Iwai M et al. (2010) Isolation of the elusive supercomplex that drives cyclic electron flow in photosynthesis. *Nature* 464:1210–3.

93. Martín M, Sabater B (2010) Plastid *ndh* genes in plant evolution. *Plant Physiol Biochem* 48:636–45.

94. Suorsa M, Sirpiö S, Aro E-M (2009) Towards characterization of the chloroplast NAD(P)H dehydrogenase complex. *Mol Plant* 2:1127–40.

95. Peng L, Fukao Y, Fujiwara M, Takami T, Shikanai T (2009) Efficient operation of NAD(P)H dehydrogenase requires supercomplex formation with photosystem I via minor LHCI in *Arabidopsis*. *Plant Cell* 21:3623–40.

96. Casano LM, Lascano HR, Martín M, Sabater B (2004) Topology of the plastid Ndh complex and its NDH-F subunit in thylakoid membranes. *Biochem J* 382:145–55.

97. Efremov RG, Sazanov LA (2011) Structure of the membrane domain of respiratory complex I. *Nature* 476:414–20.

98. Efremov RG, Baradaran R, Sazanov LA (2010) The architecture of respiratory complex I. *Nature* 465:441–5.

99. Casano LM, Martín M, Sabater B (2001) Hydrogen peroxide mediates the induction of chloroplastic Ndh complex under photooxidative stress in barley. *Plant Physiol* 125:1450–8.

100. Horváth EM et al. (2000) Targeted inactivation of the plastid *ndhB* gene in tobacco results in an enhanced sensitivity of photosynthesis to moderate stomatal closure. *Plant Physiol* 123:1337–50.

101. Li X-G, Duan W, Meng Q-W, Zou Q, Zhao S-J (2004) The function of chloroplastic NAD(P)H dehydrogenase in tobacco during chilling stress under low irradiance. *Plant Cell Physiol* 45:103–8.

102. Lascano HR, Casano LM, Martín M, Sabater B (2003) The activity of the chloroplastic Ndh complex is regulated by phosphorylation of the NDH-F subunit. *Plant Physiol* 132:256–62.

103. Gambarova NG (2008) Activity of photochemical reactions and accumulation of hydrogen peroxide in chloroplasts under stress conditions. *Russ Agric Sci* 34:149–151.

104. Livingston AK (2010) *Redefining cyclic electron flow around photosystem I (CEF1): the induction, pathway, and role of CEF1 in C3 plants* (Ph.D. Thesis. Washington State University, ProQuest Dissertations and Theses Accession No. 759377145)

105. Maul JE et al. (2002) The *Chlamydomonas reinhardtii* plastid chromosome: islands of genes in a sea of repeats. *Plant Cell* 14:2659–2679.

106. Finazzi G et al. (2002) Involvement of state transitions in the switch between linear and cyclic electron flow in *Chlamydomonas reinhardtii*. *EMBO Rep* 3:280–5.

107. Depège N, Bellafiore S, Rochaix J-D (2003) Role of chloroplast protein kinase Stt7 in LHCII phosphorylation and state transition in Chlamydomonas. *Science* 299:1572–5.

108. Bellafiore S, Barneche F, Peltier G, Rochaix J-D (2005) State transitions and light adaptation require chloroplast thylakoid protein kinase STN7. *Nature* 433:892–5.

109. Joliot P, Joliot A (2002) Cyclic electron transfer in plant leaf. *Proc Natl Acad Sci USA* 99:10209–14.

110. Hasan SS, Yamashita E, Baniulis D, Cramer WAc(2013) Quinone-dependent proton transfer pathways in the photosynthetic cytochrome b_6f complex. *Proc Natl Acad Sci USA* 110:4297–302.

111. Breyton C, Nandha B, Johnson GN, Joliot P, Finazzi G (2006) Redox modulation of cyclic electron flow around photosystem I in C3 plants. *Biochemistry* 45:13465–75.

112. Bendall DS, Manasse RS (1995) Cyclic photophosphorylation and electron transport. *Biochim Biophys Acta* 8:23–38.

113. Hertle AP et al. (2013) PGRL1 is the elusive ferredoxin-plastoquinone reductase in photosynthetic cyclic electron flow. *Mol Cell* 49:511–23.

114. Suorsa M et al. (2012) Proton Gradient Regulation 5 is essential for proper acclimation of Arabidopsis photosystem I to naturally and artificially fluctuating light conditions. *Plant Cell* 24:2934–48.

115. Cleland R, Bendall D (1992) Photosystem I cyclic electron transport: measurement of ferredoxin-plastoquinone reductase activity. *Photosynth Res* 2:409–418.

116. Jans F et al. (2008) A type II NAD(P)H dehydrogenase mediates light-independent plastoquinone reduction in the chloroplast of Chlamydomonas. *Proc Natl Acad Sci USA* 105:20546–51.

117. Mignolet E, Lecler R, Ghysels B, Remacle C, Franck F (2012) Function of the chloroplastic NAD(P)H dehydrogenase Nda2 for H_2 photoproduction in sulphur-deprived *Chlamydomonas reinhardtii*. *J Biotechnol* 162:81–8.

118. Cardol P et al. (2009) Impaired respiration discloses the physiological significance of state transitions in Chlamydomonas. *Proc Natl Acad Sci USA* 106:15979–84.

119. Takahashi H, Clowez S, Wollman F-A, Vallon O, Rappaport F (2013) Cyclic electron flow is redox-controlled but independent of state transition. *Nat Commun* 4:1954.

120. Lucker B, Kramer DM (2013) Regulation of cyclic electron flow in *Chlamydomonas reinhardtii* under fluctuating carbon availability. *Photosynth Res* 117:449–59.

121. Klughammer C, Schreiber U (1994) An improved method, using saturating light pulses, for the determination of photosystem I quantum yield via $P700^{+}$-absorbance changes at 830 nm. *Planta* 192:261–8

122. Bolwell GP et al. (2002) The apoplastic oxidative burst in response to biotic stress in plants: a three-component system. *J Exp Bot* 53:1367–76.

123. Kar RK (2011) Plant responses to water stress: role of reactive oxygen species. *Plant Signal Behav* 6:1741–5.

124. Huang G-T et al. (2012) Signal transduction during cold, salt, and drought stresses in plants. *Mol Biol Rep* 39:969–87.

125. Kaiser W (1979) Reversible inhibition of the Calvin cycle and activation of oxidative pentose phosphate cycle in isolated intact chloroplasts by hydrogen peroxide. *Planta* 382:377–382.

126. Takizawa K, Kanazawa A, Kramer DM (2008) Depletion of stromal P_i induces high 'energy-dependent' antenna exciton quenching (q_E) by decreasing proton conductivity at CF_O-CF_1 ATP synthase. *Plant Cell Environ* 31:235–43.

127. Ort DR, Oxborough K (1992) In situ regulation of chloroplast coupling factor activity. *Annu Rev Plant Physiol Plant Mol Biol* 43:269–291.

128. Kohzuma K, Bosco CD, Meurer J, Kramer DM (2013) Light- and metabolism-related regulation of the chloroplast ATPsynthase has distinct mechanisms and functions. *J Biol Chem* 288:13156-63.

129. Kramer DM, Crofts AR (1989) Activation of the chloroplast ATPase measured by the electrochromic change in leaves of intact plants. *Biochim Biophys Acta* 976:28–41.

130. Kramer DM et al. (1990) Regulation of coupling factor in field-grown sunflower: A Redox model relating coupling factor activity to the activities of other thioredoxin-dependent chloroplast enzymes. *Photosynth Res* 26:213–22.

131. Wu G, Ortiz-flores G, Ortiz-Lopez A, Ort DR (2007) A point mutation in atpC1 raises the redox potential of the Arabidopsis chloroplast ATP synthase γ-subunit regulatory disulfide above the range of thioredoxin modulation.

132. Socias FX, Medrano H, Sharkey TD (1993) Feedback limitation of photosynthesis of Phaseolus vulgaris L grown in elevated CO_2. *Plant, Cell Environ* 16:81–86.

133. Paul MJ, Foyer CH (2001) Sink regulation of photosynthesis. *J Exp Bot* 52:1383–400.

134. Kiirats O, Cruz JA, Edwards GE, Kramer DM (2009) Feedback limitation of photosynthesis at high CO_2 acts by modulating the activity of the chloroplast ATP synthase. *Funct Plant Biol* 36:893.

135. De Boer AH (2002) Plant 14-3-3 proteins assist ion channels and pumps. *Biochem Soc Trans* 30:416–21.

136. Del Riego G, Casano LM, Martín M, Sabater B (2006) Multiple phosphorylation sites in the beta subunit of thylakoid ATP synthase. *Photosynth Res* 89:11–8.

137. Reiland S et al. (2009) Large-scale Arabidopsis phosphoproteome profiling reveals novel chloroplast kinase substrates and phosphorylation networks. *Plant Physiol* 150:889–903.

138. Huber SC (2007) Exploring the role of protein phosphorylation in plants: from signalling to metabolism. *Biochem Soc Trans* 35:28–32.

139. Cruz JA, Sacksteder CA, Kanazawa A, Kramer DM (2001) Contribution of electric field ($\Delta\psi$) to steady-state transthylakoid proton motive force (*pmf*) in vitro and in vivo. control of *pmf* parsing into $\Delta\psi$ and ΔpH by ionic strength. *Biochemistry* 40:1226–37.

140. Finazzi G et al. (2006) Nonphotochemical quenching of chlorophyll fluorescence in *Chlamydomonas reinhardtii*. *Biochemistry* 45:1490–8.

141. Nicholls DG, Ferguson SJ (2002) *Bioenergetics 3*. (Academic Press, London) pp 57–87.

142. Schönknecht G, Hedrich R, Junge W, Raschke K (1988) A voltage-dependent chloride channel in the photosynthetic membrane of a higher plant. *Nature* 336:589–592.

143. Pottosin II, Schönknecht G (1996) Ion channel permeable for divalent and monovalent cations in native spinach thylakoid membranes. *J Membr Biol* 152:223–33.

144. Enz C, Steinkamp T, Wagner R (1993) Ion channels in the thylakoid membrane (a patch-clamp study). *Biochim Biophys Acta* 1143:67–76.

145. Zanetti M et al. (2010) A novel potassium channel in photosynthetic cyanobacteria. *PLoS One* 5:e10118.

146. Checchetto V et al. (2012) Thylakoid potassium channel is required for efficient photosynthesis in cyanobacteria. *Proc Natl Acad Sci USA* 109:11043–8.

147. Carraretto L et al. (2013) A thylakoid-located two-pore K^+ channel controls photosynthetic light utilization in plants. *Science* 342:114–8.

148. Ioannidis NE, Cruz JA, Kotzabasis K, Kramer DM (2012) Evidence that putrescine modulates the higher plant photosynthetic proton circuit. *PLoS One* 7:e29864.

149. Zaks J, Amarnath K, Kramer DM, Niyogi KK, Fleming GR (2012) A kinetic model of rapidly reversible nonphotochemical quenching. *Proc Natl Acad Sci USA* 109:15757–62.

150. Harbinson J (2012) Modeling the protection of photosynthesis. *Proc Natl Acad Sci USA* 109:15533–4.

151. Houille-Vernes L, Rappaport F, Wollman F, Alric J, Johnson X (2011) Plastid terminal oxidase 2 (PTOX2) is the major oxidase involved in chlororespiration in Chlamydomonas. *Proc Natl Acad Sci USA* 108:20820–5.

152. Johnson X et al. (2014) Proton Gradient Regulation 5-mediated cyclic electron flow under ATP- or redox-limited conditions: a Study of Δ*ATPase pgr5* and Δ*rbcL pgr5* mutants in the green alga *Chlamydomonas reinhardtii*. *Plant Physiol* 165:438–52.

153. Alric J (2014) Redox and ATP control of photosynthetic cyclic electron flow in *Chlamydomonas reinhardtii*: (II) Involvement of the PGR5-PGRL1 pathway under anaerobic conditions. *Biochim Biophys Acta* 1837:825–834.

154. Terashima M et al. (2012) Calcium-dependent regulation of cyclic photosynthetic electron transfer by a CAS, ANR1, and PGRL1 complex. *Proc Natl Acad Sci USA* 109:17717–22.

155. Takahashi H, Clowez S, Wollman F-A, Vallon O, Rappaport F (2013) Cyclic electron flow is redox-controlled but independent of state transition. *Nat Commun* 4:1954.

156. Rottenberg H, Moreno-Sanchez R (1993) The proton pumping activity of H^+-ATPases: an improved fluorescence assay. *Biochim Biophys Acta* 1183:161–70.

157. Takahashi S, Milward SE, Fan D-Y, Chow WS, Badger MR (2009) How does cyclic electron flow alleviate photoinhibition in Arabidopsis? *Plant Physiol* 149:1560–7.

158. Jocelyn PC (1967) The standard redox potential of cysteine-cystine from the thiol-disulphide exchange reaction with glutathione and lipoic acid. *Eur J Biochem* 2:327–31.

159. Åslund F, Berndt KD, Chem JB, Holmgren A (1997) Redox potentials of glutaredoxins and other thiol-disulfide oxidoreductases of the thioredoxin superfamily determined by direct protein-protein redox equilibria. *J Biol Chem* 272:30780–6

160. Schürmann P, Buchanan BB (2008) The ferredoxin/thioredoxin system of oxygenic photosynthesis. *Antioxid Redox Signal* 10:1235–74.

161. Johnson GN (2003) Thiol regulation of the thylakoid electron transport chain--a missing link in the regulation of photosynthesis? *Biochemistry* 42:3040–4.

162. Wu G, Ort DR (2008) Mutation in the cysteine bridge domain of the γ-subunit affects light regulation of the ATP synthase but not photosynthesis or growth in Arabidopsis. *Photosynth Res* 97:185–193.

163. Courteille A et al. (2013) Thioredoxin m4 controls photosynthetic alternative electron pathways in Arabidopsis. *Plant Physiol* 161:508–20.

164. Nakano Y, Asada K (1987) Purification of ascorbate peroxidase in spinach chloroplasts; its inactivation in ascorbate-depleted medium and reactivation by monodehydroascorbate radical. *Plant Cell Physiol* 28:131–140.

165. Seigneurin-Berny D, Salvi D, Joyard J, Rolland N (2008) Purification of intact chloroplasts from Arabidopsis and spinach leaves by isopycnic centrifugation. *Curr Protoc Cell Biol* Chapter 3:Unit 3.30.

166. Hall C et al. (2013) Photosyntheric measurements with the Idea Spec: An Integrated Diode Emitter Array Spectrophotometer/Fluorometer. *Photosynthesis Research for Food, Fuel and Future*, eds Kuang T, Lu C, Zhang L (Zhejiang University Press, Hangzhou; Springer, Heidelberg) pp 184-188.

167. Yamamoto H, Peng L, Fukao Y, Shikanai T (2011) An Src homology 3 domain-like fold protein forms a ferredoxin binding site for the chloroplast NADH dehydrogenase-like complex in Arabidopsis. *Plant Cell* 23:1480–93.

168. Zhang H, Whitelegge JP, Cramer WA (2001) Ferredoxin:$NADP^+$ oxidoreductase is a subunit of the chloroplast cytochrome b_6f complex. *J Biol Chem* 276:38159–65.

169. Havaux M, Rumeau D, Ducruet J-M (2005) Probing the FQR and NDH activities involved in cyclic electron transport around Photosystem I by the "afterglow" luminescence. *Biochim Biophys Acta* 1709:203–13.

170. Traverso JA, Pulido A, Rodríguez-García MI, Alché JD (2013) Thiol-based redox regulation in sexual plant reproduction : new insights and perspectives. *Front Plant Sci* 4:1–14.

171. O'Brien JA, Daudi A, Butt VS, Bolwell GP (2012) Reactive oxygen species and their role in plant defence and cell wall metabolism. *Planta* 236:765–79.

172. Karpiński S, Szechyńska-Hebda M, Wituszyńska W, Burdiak P (2013) Light acclimation, retrograde signalling, cell death and immune defences in plants. *Plant Cell Environ* 36:736–44.

173. Lushchak VI (2011) Adaptive response to oxidative stress: bacteria, fungi, plants and animals. *Comp Biochem Physiol C Toxicol Pharmacol* 153:175–90.

174. Buchanan BB, Balmer Y (2005) Redox regulation: a broadening horizon. *Annu Rev Plant Biol* 56:187–220.

175. Hancock J et al. (2006) Doing the unexpected: proteins involved in hydrogen peroxide perception. *J Exp Bot* 57:1711–8.

176. Fahnenstich H, Scarpeci TE, Valle EM, Flügge U-I, Maurino VG (2008) Generation of hydrogen peroxide in chloroplasts of Arabidopsis overexpressing glycolate oxidase as an inducible system to study oxidative stress. *Plant Physiol* 148:719–29.

177. Balazadeh S, Jaspert N, Arif M, Mueller-Roeber B, Maurino VG (2012) Expression of ROS-responsive genes and transcription factors after metabolic formation of H_2O_2 in chloroplasts. *Front Plant Sci* 3:234.

178. Sacksteder CA, Kramer DM (2000) Dark-interval relaxation kinetics (DIRK) of absorbance changes as a quantitative probe of steady-state electron transfer. *Photosynth Res* 66:145–58.

179. Baker NR, Harbinson J, Kramer DM (2007) Determining the limitations and regulation of photosynthetic energy transduction in leaves. *Plant Cell Environ* 30:1107–25.

180. Shikanai T et al. (1998) Directed disruption of the tobacco ndhB gene impairs cyclic electron flow around photosystem I. *Proc Natl Acad Sci USA* 95:9705–9.

181. Brooks A, Farquhar GD (1985) Effect of temperature on the CO2/O2 specificity of ribulose-1,5-bisphosphate carboxylase/oxygenase and the rate of respiration in the light. *Planta* 165:397–406.

182. Sharkey TD (1988) Estimating the rate of photorespiration in leaves. *Physiol Plant* 73:147–152.

183. Hashimoto M, Endo T, Peltier G, Tasaka M, Shikanai T (2003) A nucleus-encoded factor, CRR2, is essential for the expression of chloroplast ndhB in Arabidopsis. *Plant J* 36:541–549.

184. Cruz de Carvalho MH (2008) Drought stress and reactive oxygen species. *Plant Signal Behav* 3:156–165.

185. Ma X, Browse J (2006) Altered rates of protein transport in Arabidopsis mutants deficient in chloroplast membrane unsaturation. *Phytochemistry* 67:1629–36.

186. Conte L, Trumpower BL, Zara V (2011) Bcs1p can rescue a large and productive cytochrome bc1 complex assembly intermediate in the inner membrane of yeast mitochondria. *Biochim Biophys Acta* 1813:91–101.

187. Genty B, Briantais J-M, Baker NR (1989) The relationship between the quantum yield of photosynthetic electron transport and quenching of chlorophyll fluorescence. *Biochim Biophys Acta - Gen Subj* 990:87–92.

188. Edwards G, Baker N (1993) Can CO2 assimilation in maize leaves be predicted accurately from chlorophyll fluorescence analysis? *Photosynth Res* 37:89–102.

189. Oxborough K, Horton P (1987) Characterisation of the effects of Antimycin A upon high energy state quenching of chlorophyll fluorescence (qE) in spinach and pea chloroplasts. 128:119–127.

190. Hope AB, Valente P, Matthews DB (1994) Effects of pH on the kinetics of redox reactions in and around the cytochromebf complex in an isolated system. *Photosynth Res* 42:111–20.

191. Huang W, Yang S-J, Zhang S-B, Zhang J-L, Cao K-F (2012) Cyclic electron flow plays an important role in photoprotection for the resurrection plant Paraboea rufescens under drought stress. *Planta* 235:819–28.

192. Huang W, Zhang S-B, Cao K-F (2010) Stimulation of cyclic electron flow during recovery after chilling-induced photoinhibition of PSII. *Plant Cell Physiol* 51:1922–8.

193. Dai Z, Ku MB, Edwards G (1996) Oxygen sensitivity of photosynthesis and photorespiration in different photosynthetic types in the genus Flaveria. *Planta* 198:563–571.

194. Krause GH, Weis E (1984) Chlorophyll fluorescence as a tool in plant physiology : II. Interpretation of fluorescence signals. *Photosynth Res* 5:139–57.

195. Karcher D, Bock R (2009) Identification of the chloroplast adenosine-to-inosine tRNA editing enzyme. *RNA* 15:1251–7.

196. Delannoy E et al. (2009) Arabidopsis tRNA adenosine deaminase arginine edits the wobble nucleotide of chloroplast $tRNA^{Arg}$(ACG) and is essential for efficient chloroplast translation. *Plant Cell* 21:2058–71.

197. Tiller N et al. (2012) The plastid-specific ribosomal proteins of Arabidopsis thaliana can be divided into non-essential proteins and genuine ribosomal proteins. *Plant J* 69:302–16.

198. Lundin B et al. (2008) Towards understanding the functional difference between the two PsbO isoforms in Arabidopsis thaliana--insights from phenotypic analyses of *psbo* knockout mutants. *Photosynth Res* 98:405–14.

199. Suorsa M et al. (2006) PsbR, a missing link in the assembly of the oxygen-evolving complex of plant photosystem II. *J Biol Chem* 281:145–50.

200. Mullet JE, Burke JJ, Arntzen CJ (1980) A developmental study of photosystem I peripheral chlorophyll proteins. *Plant Physiol* 65:823–7.

201. Boynton JE et al. (1988) Chloroplast transformation in Chlamydomonas with high velocity microprojectiles. *Science* 240:1534–8.

202. De Vitry C, Vallon O (1999) Mutants of Chlamydomonas: tools to study thylakoid membrane structure, function and biogenesis. *Biochimie* 81:631–43.

203. Lyska D, Meierhoff K, Westhoff P (2013) How to build functional thylakoid membranes: from plastid transcription to protein complex assembly. *Planta* 237:413–28.

204. Komenda J, Sobotka R, Nixon PJ (2012) Assembling and maintaining the Photosystem II complex in chloroplasts and cyanobacteria. *Curr Opin Plant Biol* 15:245–51.

205. Sato S (1999) Complete structure of the chloroplast genome of *Arabidopsis thaliana*. 290:283–290.

206. Weis E (1985) Chlorophyll fluorescence at 77K in intact leaces: characterization of a technique to eliminate artifacts related to self-absorption. *Photosynth Res* 6:73–86.

207. Idle DB, Proctor CW (1983) An integrating sphere leaf chamber. *Plant, Cell Environ* 6:437–439.

208. Konieczny A, Ausubel FM (1993) A procedure for mapping Arabidopsis mutations using co-dominant ecotype-specific PCR-based markers. *Plant J* 4:403–10.

209. Eng JK, McCormack AL, Yates JR (1994) An approach to correlate tandem mass spectral data of peptides with amino acid sequences in a protein database. *J Am Soc Mass Spectrom* 5:976–89.

210. Friedrich T (2014) On the mechanism of respiratory complex I. *J Bioenerg Biomembr* 46:255–68.

211. Wikström M, Hummer G (2012) Stoichiometry of proton translocation by respiratory complex I and its mechanistic implications. *Proc Natl Acad Sci USA* 109:4431–6.

212. Fu A et al. (2012) Alternative oxidases (AOX1a and AOX2) can functionally substitute for plastid terminal oxidase in Arabidopsis chloroplasts. *Plant Cell* 24:1579–95.

213. Rumeau D, Peltier G (2005) New Subunits NDH-M , -N , and -O , encoded by nuclear genes, are essential for plastid ndh complex functioning in higher plants. 17:219–232.

214. Kaila VRI, Wikström M, Hummer G (2014) Electrostatics, hydration, and proton transfer dynamics in the membrane domain of respiratory complex I. *Proc Natl Acad Sci USA* 111:6988–93.

215. Zandueta-Criado A, Bock R (2004) Surprising features of plastid *ndhD* transcripts: addition of non-encoded nucleotides and polysome association of mRNAs with an unedited start codon. *Nucleic Acids Res* 32:542–50.

216. Masselon C et al. (2005) Targeted comparative proteomics by liquid chromatography-tandem Fourier ion cyclotron resonance mass spectrometry. *Anal Chem* 77:400–6.

217. Qian W et al. (2005) Probability-based evaluation of peptide and protein identifications from tandem mass spectrometry and SEQUEST analysis: the human proteome. *J Proteome Res* 4:53–62.

218. Livesay EA et al. (2008) Fully automated four-column capillary LC-MS system for maximizing throughput in proteomic analyses. *Anal Chem* 80:294–302.

219. Smith RD et al. (2002) An accurate mass tag strategy for quantitative and high-throughput proteome measurements. *Proteomics* 2:513–23.

220. Kelly RT et al. (2006) Chemically etched open tubular and monolithic emitters for nanoelectrospray ionization mass spectrometry. *Anal Chem* 78:7796–801.

221. Jaitly N et al. (2006) Robust algorithm for alignment of liquid chromatography-mass spectrometry analyses in an accurate mass and time tag data analysis pipeline. *Anal Chem* 78:7397–409.

222. Monroe ME et al. (2007) VIPER: an advanced software package to support high-throughput LC-MS peptide identification. *Bioinformatics* 23:2021–3.

223. Li XP et al. (2000) A pigment-binding protein essential for regulation of photosynthetic light harvesting. *Nature* 403:391–5.

224. Walter A, Studer B, Kölliker R (2012) Advanced phenotyping offers opportunities for improved breeding of forage and turf species. *Ann Bot* 110:1271–9.

225. Harbinson J, Prinzenberg AE, Kruijer W, Aarts MGM (2012) High throughput screening with chlorophyll fluorescence imaging and its use in crop improvement. *Curr Opin Biotechnol* 23:221–6.

226. Rousseau C et al. (2013) High throughput quantitative phenotyping of plant resistance using chlorophyll fluorescence image analysis. *Plant Methods* 9:17.

227. Murchie EH, Lawson T (2013) Chlorophyll fluorescence analysis: a guide to good practice and understanding some new applications. *J Exp Bot* 64:3983–98.

228. Loriaux SD et al. (2013) Closing in on maximum yield of chlorophyll fluorescence using a single multiphase flash of sub-saturating intensity. *Plant Cell Environ* 36:1755–70.

229. Blankenship R (2002) *Molecular Mechanisms of Photosynthesis* (Blackwell Science Ltd, Oxford, UK)

230. Cardol P et al. (2008) An original adaptation of photosynthesis in the marine green alga Ostreococcus. *Proc Natl Acad Sci USA* 105:7881–6.

231. Lavergne J, Trissl HW (1995) Theory of fluorescence induction in photosystem II: derivation of analytical expressions in a model including exciton-radical-pair equilibrium and restricted energy transfer between photosynthetic units. *Biophys J* 68:2474–92.

232. Genty B, Wonders J, Baker NR (1990) Non-photochemical quenching of F_o in leaves is emission wavelength dependent: consequences for quenching analysis and its interpretation. *Photosynth Res* 26:133–9.